UNIVERSITY OF CALIFORNIA,
IRVINE

The Molecular Basis for Restoring Function to Oncogenic p53 Mutants

DISSERTATION

submitted in partial satisfaction of the requirements
for the degree of

DOCTOR OF PHILOSOPHY

in Molecular Biology and Biochemistry

by

Bradley Dale Wallentine

Dissertation Committee:
Professor Hartmut Luecke, Chair
Professor Donald Senear
Professor Melanie Cocco
Professor Celia Goulding

2016

DEDICATION

To

My amazing parents and loving wife

For all of the opportunities and support they have given me

Everything I have been able to accomplish is because

They made it possible

And fun

TABLE OF CONTENTS

LIST OF FIGURES

LIST OF TABLES

ACKNOWLEDGMENTS

I would like to sincerely thank my thesis advisor, Dr. Hartmut "Hudel" Luecke. He has been such a great mentor, allowing me freedom to take this project in the direction I deemed important while also providing guidance when I needed help. His trust in me has allowed me to grow immensely into a motivated, independent researcher. I will be forever grateful for his mentoring and the opportunities afforded to me in his laboratory.

I owe a large thank you to all of our collaborators over these years. None of this work would have been possible without all of their hard work. Our collaborators are many and the contribution of each laboratory is noted throughout the thesis story.

I also appreciate the support from the numerous resources I've been fortunate enough to have through my graduate work. First, I'd like to thank the National Cancer Institute Developmental Therapeutics Program. Their virtual and chemical screening libraries made our chemical screens possible. They were also a great resource for obtaining new chemicals and cancer cells for our research. I would also like to thank my training grant sources including the UCI Medical Scientist Training Program, the UCI Cancer Research Institute, the UCI Institute for Clinical and Translational Science, and the National Cancer Institute. Last, I am very grateful to the national synchrotrons the Lawrence Berkeley National Lab and the Stanford Syncrotron Radiation Laboratory for granting us access and assisting us in our collection of crystal diffraction data.

CURRICULUM VITAE

Bradley Dale Wallentine

2009	B.A. in Biology, minors in Chemistry, Biomedical Engineering, and Spanish, University of Texas at Austin, Austin, Texas
2009-2010	Research/Teaching Assistant, University of Texas at Austin
2010-2019	M.D., University of California, Irvine
2011-2016	Ph.D. in Molecular Biology and Biochemistry, University of California, Irvine

FIELD OF STUDY

Structural Biology, Cancer, and Drug Discovery

PUBLICATIONS

Wassman, C.D., Baronio, R., Demir, Ö., Wallentine, B.D., Chen, C.-K., Hall, L.V., Salehi, F., Lin, D.-W., Chung, B.P., Hatfield G.W., Chamberlin, A.R., Luecke, H., Lathrop, R.H., Kaiser, P., Amaro, R.E. " Computational Identification of a Transiently Open L1/S3 Pocket for p53 Cancer Mutant Reactivation" (2013) *Nature Communications* 4, article number 1407.

Wallentine, B.D., Wang, Y., Tretyachenko-Ladokhina, V., Tan, M., Senear, D.F., Luecke, H. "Crystal structures of oncogenic, suppressor, and rescued p53 core domain variants: Mechanisms of mutant p53 rescue" (2013) *Acta Cryst. D* 69, 2146-2156.

FELLOWSHIPS

2013	Cancer Research Institute Fellow (T32), University of California Irvine
2014 – 2015	Institute for Clinical and Translational Science Fellow (TL1), University of California, Irvine
2015 – 2018	NRSA MD/PhD Fellow (F30), National Cancer Institute, University of California, Irvine

PATENT APPLICATION

US20150307519 A1; Inventors: Hartmut Luecke, Brad Wallentine, Chiung-Kuang Chen, Roberta Baronio, Peter Kaiser; Title: Small molecules for restoring function to p53 cancer mutants

ABSTRACT OF THE DISSERTATION

The Molecular Basis for Restoring Function to Oncogenic p53 Mutants

By

Bradley Dale Wallentine

Doctor of Philosophy in Structural Biology, Biochemistry, and Biophysics

University of California, Irvine, 2016

Professor Christopher Hughes, Chair

The tumor suppressor *p53* is the most commonly mutated gene in cancers, with approximately half of all tumors containing a *p53* mutation. p53 normally functions to moderate cell growth, incite DNA repair, and induce apoptosis in response to cellular stresses. Mutation of *p53* gene leads to the p53 protein losing its tumor suppressor activity within the cell. Despite being the most commonly mutated gene in cancer, there are currently no drugs in the clinic able to target p53 and restore its function as a tumor suppressor. This thesis work encompasses the use of structural and biophysical techniques to understand the molecular basis for restoring function to oncogenic p53 mutants. First, I helped solve the X-ray crystal structures of oncogenic and rescue mutations in p53 in order to better understand possible molecular mechanisms for restoring function to mutant p53 (Chapter 2). Next working with our collaborators, I helped establish that a small molecule that is able to restore activity to mutant p53 would likely act by thermodynamically stabilizing the p53 structure (Chapter 3). Last, I discovered a small molecule which greatly stabilizes mutant p53, causes cancer cells containing mutant p53 to undergo massive cell death, and is continuing to show great promise as a p53 reactivating pharmacophore (Chapter 4).

CHAPTER 1: INTRODUCTION

The *tumor suppressor p53* is the most frequently mutated gene in human cancers, with mutations in this gene occurring in approximately 50% of cancers across all organ systems[1,2-4]. The most common forms of cancers, bladder, breast, colorectal, lung, prostate, and uterine, all have significantly high mutation rates in the *p53* gene (Fig 1.1). Cancers having the highest prevalence of *p53* mutations include ovarian (90%), lung (60%), and colorectal (60%)[3-5]. For reference, the second most commonly mutated gene in cancer, *PIK3CA*, has an average mutation rate of 10% to 15% across all cancer types[3-5] while the well-known cancer gene, *BRCA1*, has an average mutation rate of 2% to 5% across all cancer types[3-5].

In healthy cells, p53 protein functions as a multi-domain, tetrameric transcription factor, controlling genes important for cell-cycle regulation, DNA repair, and apoptosis. The p53 protein contains 393 amino acids with an approximate molecular weight of 44 kDa. The p53 protein becomes activated when the cell comes under stress including DNA damage, nutrient depletion, oxidative stress, and oncogene activation[6]. This activation is elicited through posttranslational modifications of p53 by various stress-sensing proteins within the cell[7]. The canonical role of activated p53 is that of a transcription factor which binds to promoters to regulate expression of genes controlling DNA repair, growth, senescence, apoptosis, and metabolism[6]. In general, p53 upregulates expression of proteins to promote DNA repair, cell cycle arrest, senescence, and apoptosis, while downregulating genes which promote cellular growth. More recently, it has been reported that activated

p53 exits in the nucleus to interact with Bcl2 family proteins at the outer mitochondrial membrane to promote apoptosis[8].

Mutations in the *p53* gene cause the p53 protein to lose its function within the cell. Loss of the tumor suppressor functions of the p53 protein as a result of mutation is a significant step in the oncogenic process. Not only do mutations in *p53* facilitate carcinogenesis, but tumor cells containing *p53* mutations are typically more resistant to traditional cancer therapies[9,10]. Malignant cells with *p53* cancer mutations continue to express these mutant p53 proteins which accumulate within the cell[11].

Almost three-fourths of *p53* mutations lead to single amino-acid substitutions (Fig. 1.2), with 92.5% of these substitutions occurring within the DNA-binding domain of p53 (p53DBD)[1]. The p53DBD, which constitutes about half of the protein, is responsible for sequence-specific binding to the DNA regulatory regions of genes to control their transcription (Fig. 1.3)[12] and interactions with protein binding partners at the mitochondrial membrane to promote apoptosis[13,14]. Missense mutations in the p53DBD fall into two categories: (1) *DNA contact mutations* create substitutions at residues that make direct contact with DNA, causing a significant reduction in the capacity for binding regulatory regions of genes. DNA contact residue substitutions account for approximately 20% of p53DBD missense mutations[1]. (2) *Conformational mutations* comprise 80% of p53DBD missense mutations[1]. These mutations disrupt the function of the protein by perturbing structural features and destabilizing the domain. The wild-type (WT) p53DBD is only marginally stable at physiological temperature with a melting temperature (T_m) of 36 to 44 °C depending on experimental approach[15-17], so even minor destabilization can have detrimental effects on the protein's ability to carry out its native function within the cell.

Because of the extraordinarily high incidence of *p53* mutations in human cancers, p53 is one of the most attractive targets for novel anticancer therapies. Studies continue to show that reintroduction of $p53^{WT}$ into mutant p53 malignant cell lines and tumors induces high rates of cell cycle arrest and apoptosis[18,19]. Reintroducing functional p53 also sensitizes tumors to traditional chemotherapies[20-22], providing a proof-of-principle that restoring p53 activity in a patient's cancer cells could reduce or eliminate their cancer. A very promising approach for reinstating p53 tumor suppressor function, given cancer cells with *p53* mutations continue to express full-length p53 proteins with a single amino acid alteration, entails a pharmaceutical that can restore wild-type function to mutant p53 proteins. A pharmaceutical which can specifically bind and reactivate mutant p53 would have the advantage of reduced side effects against healthy cells as well as being broadly applicable to a large number of cancers, based on the fact that p53 is mutated in a large number of cancer types.

Several small molecules have been identified which have been presumed to restore the function of mutant p53 including CP-31398, PRIMA-1, MIRA-1, STIMA-1, and APR-246[23-28], though these previously discovered molecules have fallen short of their expected potentials. Most of them were discovered using a mutant p53 cell-based assay and later discovered that the small molecules do not actually directly bind p53 (CP-31398)[29] or interact with p53 through nonspecific alkylation (PRIMA-1, MIRA-1, STIMA-1, and APR-246)[25,26,30]. Despite its nonspecific binding, APR-246 underwent phase I/II clinical trials in hematological and prostate cancers (NCT02098343)[31] but "the increase in p53 activity [observed in patients during this trial] did not appear to correlate with p53 mutational status and further assessment of APR-246 needs to be made to assess its ability as a mutant

[p53] reactivator"[32]. For a p53-reactivating small molecule to be successfully developed from benchtop discovery to use as a targeted clinical therapy, a thorough understanding of the molecular interactions and reactivation mechanism is essential.

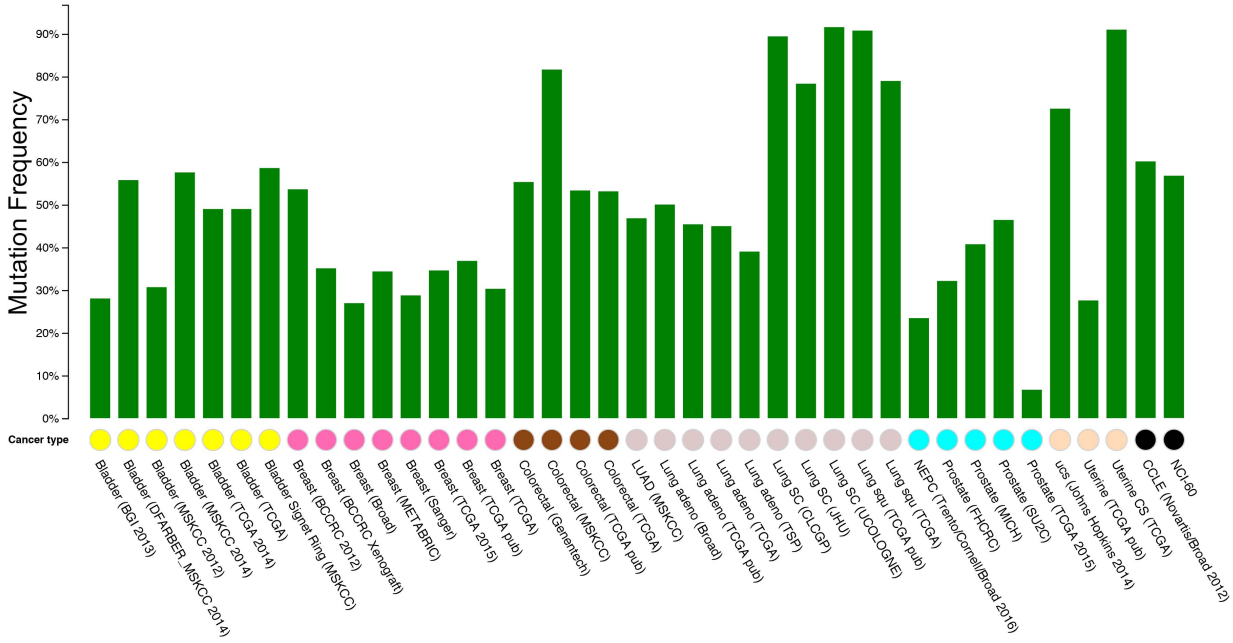

Figure 1.1. *p53* mutation rates in the most common forms of cancer. cBioPortal[3,4] contains mutation data from 146 studies from various research groups based on genome-wide mutation analysis on tumor samples from cancer patients. The rate of mutation in the *p53* gene was evaluated in the most common forms of cancer (including bladder, breast, colorectal, lung, prostate, and uterine cancers). Each bar (green) indicates the number of tumor samples with a mutation in the *p53* gene divided by the total number of tumor samples analyzed within the particular study. Cancers types are grouped together. Also included in the evaluation are the mutation results from the Cancer Cell Line Encyclopedia study[33] (which includes mutation results of 947 cancer cell lines from 36 different cancer types) and the NCI60 Cancer Cell Line study[34] (which includes mutation results for the 60 cancer cells frequently tested by the National Cancer Institute for efficacy of potential cancer therapies). p53 has mutation rate of approximately 40% to 50% across these common cancer types.

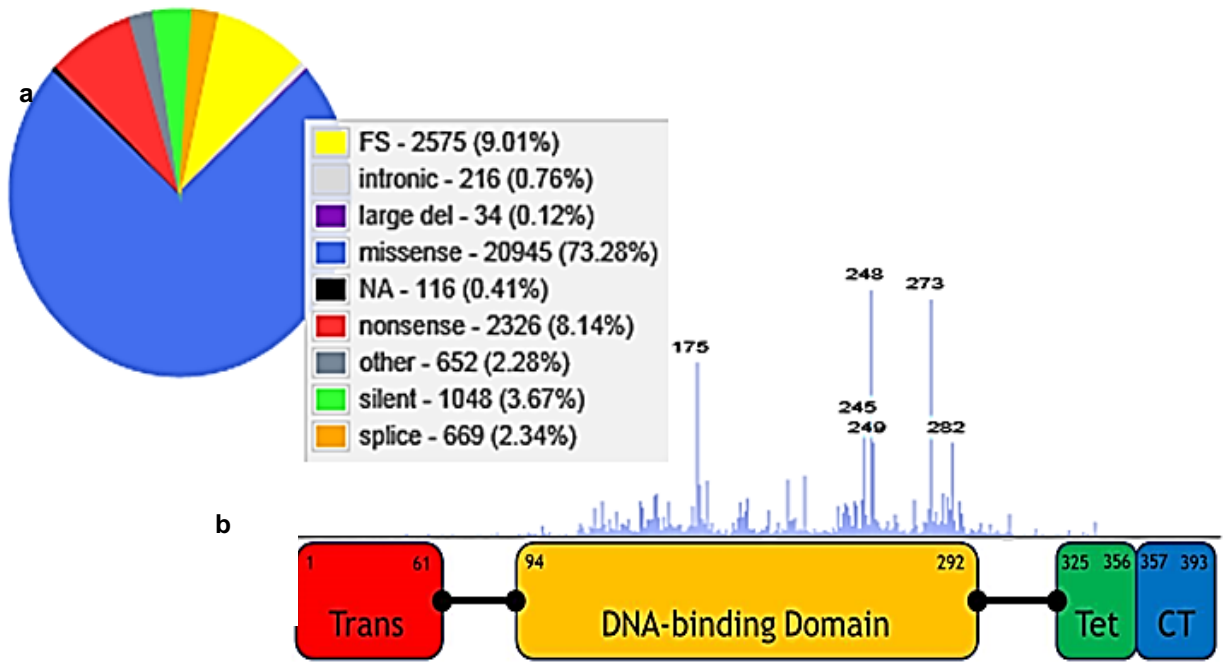

Figure 1.2. *p53* mutations by type and location within gene. (a) Distribution of *p53* somatic mutations in human cancer by mutation type[1]. FS: frameshift. (b) Histogram plot of *p53* missense mutations at each codon mapped onto the transactivation (Trans), DNA-binding, tetramerization (Tet), and C-terminal (CT) domains of the protein[1,2]. Numbers indicate the first and last residues of each domain.

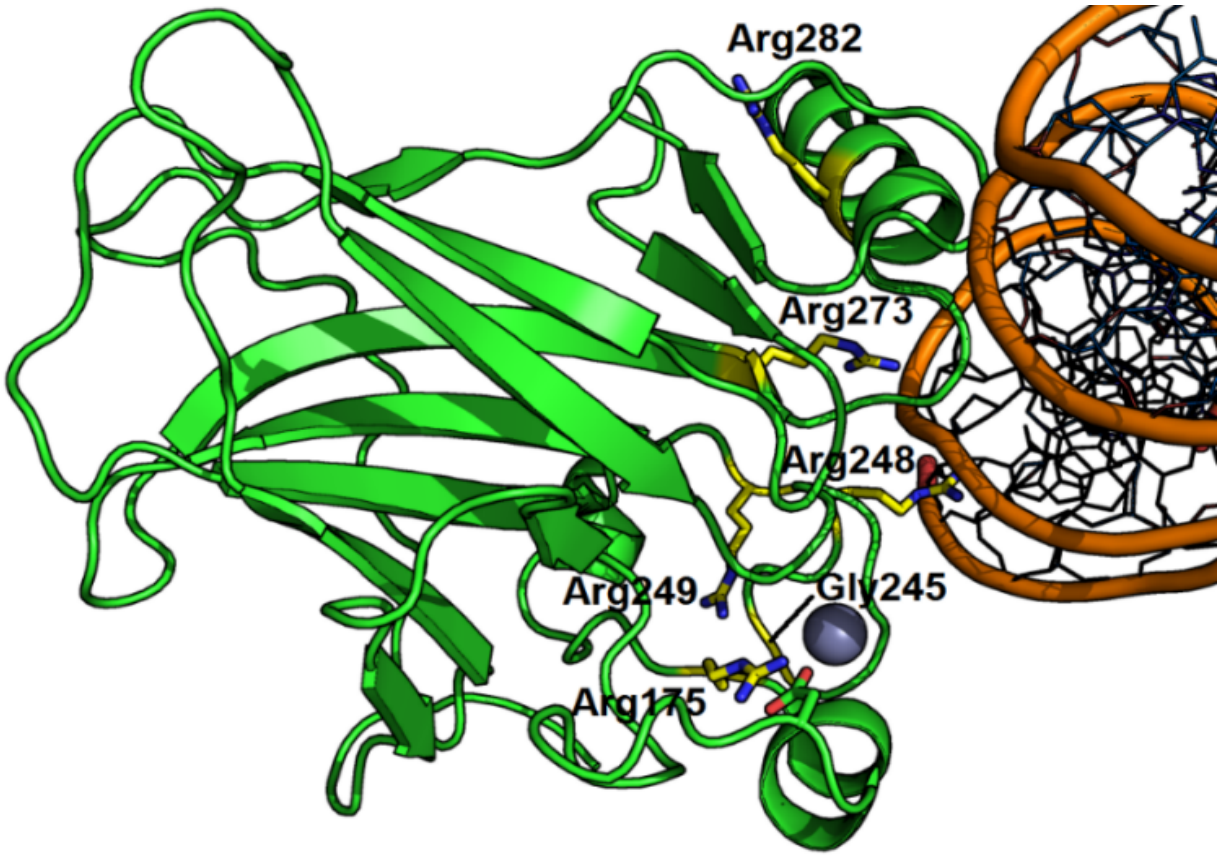

Figure 1.3. Structural depiction of p53 hotspot missense mutations. Cartoon representation of p53DBD (green) bound to DNA (orange) [PDB: 3KMD] highlighting the six most frequently mutated amino acids in human cancer (yellow, stick) and coordinated zinc (gray, sphere). *DNA-contact* mutation sites: Arg248 and Arg273. *Conformational* mutation sites: Arg175, Gly245, Arg249, and Arg282. The salt-bridge partner of Arg175, Asp184 (green, stick), is also indicated.

CHAPTER 2: STRUCTURES OF ONCOGENIC AND RESCUED p53

Previously published in *Acta Crystallographica Section D* in 2013 as: Wallentine, B.D., Wang, Y., Tretyachenko-Ladokhina, V., Tan, M., Senear, D.F., Luecke, H. "Crystal structures of oncogenic, suppressor, and rescued p53 core domain variants: Mechanisms of mutant p53 rescue" (2013) *Acta Cryst. D* 69, 2146-2156.

ABSTRACT

To gain insights into the mechanisms by which certain second-site suppressor mutations rescue the function of a significant number of cancer mutations of the tumor suppressor protein p53 we have determined X-ray crystallographic structures of four p53 core domain variants. These include an oncogenic mutant, V157F, two single-site suppressor mutants, N235K and N239Y, and the rescued cancer mutant, V157F/N235K/N239Y. The V157F mutation substitutes a smaller hydrophobic valine with a larger hydrophobic phenylalanine within strand S4 of the hydrophobic core. The structure of this cancer mutant indicates no gross structural changes in the overall fold of the p53 core domain, only minor rearrangements of side chains within the hydrophobic core of the protein. Based on biochemical analysis, these small local perturbations induce instability in the protein, increasing the free energy by 3.6 kcal/mol. Further biochemical evidence shows that each suppressor mutation, N235K or N239Y, acts individually to restore thermodynamic stability to V157F and that both together are more effective than either alone. All rescued mutants were found to have wild-type DNA-binding activity when assessed at a permissive temperature, thus pointing to thermodynamic stability as the critical underlying variable. Interestingly, thermodynamic analysis shows that while N239Y demonstrates stabilization of the wild-type p53 core domain, N235K does not. These

observations suggest distinct structural mechanisms of rescue. A new salt bridge between Lys235 and Glu198, found in both the N235K and rescued cancer mutant structures, suggests a rescue mechanism that relies on stabilizing the ß-sandwich scaffold. On the other hand, the substitution N239Y creates an advantageous hydrophobic contact between the aromatic ring of this tyrosine and adjacent Leu137. Surprisingly, the rescued cancer mutant shows much larger structural deviations than the cancer mutant alone when compared to wild-type p53. These suppressor mutations appear to rescue p53 function by creating novel intradomain interactions that stabilize the core domain, allowing compensation for this destabilizing mutation.

INTRODUCTION

Considerable efforts are being made to design pharmaceuticals which can restore normal cellular functions to these mutated p53 proteins. To understand how these pharmaceuticals could be designed, researchers began by using a systematic genetic approach. This approach screens for novel point mutations, known as second-site suppressor mutations or rescue mutations, in the *p53* gene which restore wild-type function to a previously nonfunctional p53 mutant[35]. In correspondence with the two categories of p53 DNA-binding domain (DBD) cancer mutations, two rationally designed suppressor mutation classes have emerged: (i) mutations that provide additional contacts to bind DNA; and (ii) mutations that compensate local or overall structural disruptions. An example of the first class of suppressor mutations is T284R, which restores native-like DNA-binding affinity to DNA contact mutants R273C and R273H by providing a new DNA contact[36]. The second category is illustrated by the structure of the H168R/R249S mutant. It reveals a mechanism whereby the introduction of a guanidinium via Arg168 mimics the

function of Arg249 which is lost in the R249S cancer mutant, thereby limiting structural distortion of the DNA binding surface[37]. However, due to the large number of cancer mutations, screening for specific suppressor variants to correct the defect caused by each cancer mutant individually appears impractical. Stabilizing second-site suppressor mutations in the second class which compensate for overall structural disruptions hold the promise of more broadly effective rescue mechanisms, with a single second-site suppressor mutation able to rescue the effects of several destabilizing missense mutations. Second-site suppressor mutations known to rescue multiple oncogenic mutations are known as *global suppressor mutation.*

With the idea of using these second-site suppressor mutations to design pharmaceuticals which can restore function to a variety of p53 mutants, understanding global suppressor mutations has become particularly lucrative. Specific mutations at positions 235, 239 and 240 have been identified from such screens as potential global suppressors[38]. These mutations, alone or in combination, are capable of restoring function to 13 of 30 of the most common p53 cancer mutants[35,38,39]. Substitutions at two positions, Lys235 and Tyr239, are particularly effective in restoring function to ß-sandwich cancer mutants. In combination with other second-site suppressor mutations, N235K is able to restore function to six of the seven most common ß-sandwich mutants studied[38]. N239Y is able to rescue three of these seven β-sandwich mutations when acting alone, and five when combined with other second-site suppressor mutations[38]. Because most β-sandwich mutations belong to the destabilizing category of cancer mutants studied so far, it is expected that both N235K and N239Y may enhance the thermodynamic stability of the

p53DBD. Indeed, previous thermodynamic studies have revealed that N239Y enhances stability by more than one kcal/mol[40,41].

Currently, no crystal structure of a β-sandwich mutant exists without additional stabilizing mutations. It is important to study the structural effects of these β-sandwich mutations and how they lead to instability of the p53DBD. Additionally, no literature has addressed the structural basis of the N235K rescue mechanism. The structural effects of the N239Y suppressor mutation have been previously studied in the context of M133L/V203A/N239Y/N268D (PDB code 1UOL), referred to as *thermostable mutant* or *T*-p53 in the following text, which forms a hyper-stabile core[42]. It is interesting to examine the individual structural effects of N239Y independently from the other three mutations of this thermostable mutant.

These considerations motivated our analysis of the oncogenic mutation V157F and the rescue mechanisms of N235K and N239Y. To this end, we have conducted thermodynamic and biochemical analyses of the oncogenic V157F mutant, one of the most strongly destabilized β-sandwich cancer mutants, the second-site suppressor mutants N235K and N239Y, and the rescue of V157F by N235K/N239Y. We found that N235K is an effective stabilizer of V157F, despite having almost no effect on the thermodynamic stability of the wild-type p53DBD. N239Y stabilizes both V157F and wild-type p53 to a similar degree. Furthermore, we determined and analyzed the crystal structures of four p53 variants: the oncogenic mutant, V157F, the two suppressor mutants, N235K and N239Y, and the oncogenic mutant in conjunction with both suppressor mutations, V157F/N235K/N239Y, referred to as the *rescued cancer mutant* in the following text. By comparing these mutant structures to that of wild-type p53[12,43], we find that both of these suppressor mutations

create novel residue interactions that stabilize the native p53 structure[12,43]. These findings enhance our understanding of global suppressor motifs and afford valuable knowledge as p53 rescue is beginning to move towards providing clinical value [31].

RESULTS

Equilibrium properties of p53 cancer, rescued and suppressor mutants

As a first step to delineate the rescue mechanism mediated by suppressor mutations N235K and N239Y, the laboratory of Dr. D. F. Senear (Department of Molecular Biology and Biochemistry, University of California, Irvine) conducted a thermodynamic analysis of their rescue of the V157F cancer mutation. Though one of the most strongly destabilized β-sandwich p53 cancer mutants, in yeast assays wild-type function of V157F is restored by either N235K or by N239Y alone, as well as both together[38,44]. Stability was assessed using urea-induced unfolding at 10 °C, a permissive temperature at which even severely destabilized cancer mutants such as V157F are predominantly folded[45].

Unfolding titrations for the wild-type p53DBD, the cancer mutant, both suppressor mutants and two rescued cancer mutants are shown (Fig. 2.1). Parameters obtained by analysis of these data using eq. 1 as described below are listed (Table 2.1). The urea concentration at the midpoints of the unfolding transitions varies substantially, from 3.3 to 1.9 M urea, indicating widely varying stability. However, the slopes of the transitions, obtained independently, do not vary. This feature is in accord with all previous reports and the weighted mean value of the slope obtained from these six p53 variants, 2.97 ± 0.14 $kcal \cdot mol^{-1} \cdot M^{-1}$, is in the middle of the range of previous reports[15,41,45,46]. Based on this, we have used the average slope to calculate the free energy change for folding in the absence

of urea ($\Delta G_{D-N}^{H_2O}$) and the difference for each variant compared to the wild-type p53DBD ($\Delta\Delta G_{D-N}$).

The results by members of the Dr. Senear laboratory obtained for wild-type p53, -9.5 kcal/mol, and the V157F cancer mutant, -5.9 kcal/mol, are indistinguishable from what others reported previously[45]. Results for N239Y are also similar to those reported previously, although they find a somewhat smaller net stabilization of -0.9 kcal/mol versus either -1.2 or -1.5 kcal/mol[41,46]. Perhaps more significant, the net stabilization is the same, whether the N239Y suppressor mutation is introduced into the V157F/N235K variant, or whether it is introduced into the wild-type p53 variant, consistent with previous reports of additive effects. In contrast to this behavior, the N235K suppressor mutation yields a negligible net stabilization of the wild-type p53DBD, whereas this substitution results in robust stabilization of the cancer mutant, V157F (-1.32 kcal/mol, Table 2.1). Together, N239Y and N235K reduce the destabilization of V157F to only 1.36 kcal/mol, which is well below the threshold associated with loss of function[45].

Binding by each of the p53 variants to its specific site in the *gadd45* promoter was assayed by members of the Dr. Senear laboratory to assess the functional properties of each of the folded structures. Typical results of these experiments are presented for the N235K suppressor mutant (Fig. 2.2). The gel image in the inset documents the formation of a prominent mobility-shifted band as a function of p53 concentration, followed by a short ladder of lower mobility bands. Full-length p53 is tetrameric, and the tetramer is the basic DNA-binding unit[47-49]. Similarly, the p53DBD, which is monomeric in solution, binds in a cooperative fashion to form a tetramer as the DNA-bound form[50,51]. Consistent with these

findings, when the fraction of unbound DNA in our experiments was analyzed by members of the Dr. Senear laboratory as a function of p53 concentration using a Hill model, values of the Hill coefficient ranging from 3 to 3.7 were routinely obtained. Based on this finding, analysis of the specific binding assumed strictly concerted binding of monomers to form DNA-bound tetramers as described in the Methods section. The ladder of lower mobility bands indicates higher order species, presumably a consequence of additional, electrostatically-mediated non-specific binding as described previously[51]. These bands were combined and analyzed using a single, average integral stoichiometry. In all cases, the best fit was obtained with N=6, leading to the binding isotherm (eq. 3) described in the Methods section.

Results of the analysis of p53 variants shown in Table 2.1 indicate a per-subunit free energy change for binding of -8 kcal/mol under these conditions, which corresponds to approximately 1 μM affinity. The non-specific complexes form with an approximately 1 kcal/mol smaller per-subunit free energy change. More significant, the DNA-binding properties of all variants, suppressor and rescued cancer studied here, are indistinguishable from those of the wild-type p53DBD at a permissive temperature at which all variants are fully folded.

Overall structures of p53 mutants

A previous graduate student in the lab, Dr. Ying Wang crystallized and collected diffraction data for V157F, N235K, N239Y, and V157F/N235K/N239Y. The crystals of V157F, N235K and N239Y are isomorphous to the DNA-free wild-type p53 crystals, spacegroup $P2_1$ (PDB code 2OCJ)[43]. All four molecules in the asymmetric unit are

structurally similar, with low root mean square (rms) deviations for the superposition of the backbone atoms. V157F suffered from significant hemihedral crystallographic twinning, with a twin fraction of 0.12 and twin operator h,-k,-l. In identifying this twinning, I accounted for the twinning during subsequent refinement. The crystals of the rescued cancer mutant, V157F/N235K/N236Y, formed in a new spacegroup, $P2_12_12$, with one molecule in the asymmetric unit.

Since all mutant crystals were grown at 4 °C, a permissive temperature at which all mutants are expected to be fully folded, it is not surprising that the overall fold of these four p53 variants resembles that of the typical wild-type p53DBD (Fig. 2.3a)[12,43]: two twisted anti-parallel β-sheets pack together, forming a β-sandwich as a hydrophobic core. Compared with the β-sheet composed of strands S4, S6, S7, S9, and S10, the β-sheet composed of the remaining four strands, S1, S3, S5, and S8, have fewer hydrogen bonds and is more loosely packed. The DNA-binding region includes two large loops, L2 and L3, and a loop-sheet-helix motif, comprising loop L1, the S2-S2' hairpin, the C-terminal residues of strand S10, and helix H2. A zinc ion is bound in a tetrahedral-coordinated complex with the side chains of Cys176, His179, Cys238 and Cys242, stabilizing loops L2 and L3. The cancer mutation Phe157 is located within strand S4 in the hydrophobic core, while the suppressor mutations Lys235 and Tyr239 are in strand S8 and loop L3, respectively. As expected from evaluation of previous p53DBD structures, both suppressor mutations are far from the cancer mutation. The distances between the Cα atoms of Phe157 and both Lys235 and Tyr239 are 15.2 Å and 23.8 Å, respectively (Fig. 2.3a). Because of these distances, it is highly unlikely that a direct structural compensation can account for their mechanisms of rescue.

Although no significant perturbation occurs in the overall fold of p53 mutants, there exist local structural deviations among different p53 mutant structures. The rms deviations between various human p53DBD structures are summarized (Table 2.2). The second column compares the different p53 structures to that of DNA-bound wild-type p53 (PDB code 1TSR, chain B) [12]. In most cases, the rms deviation is approximately 0.75 Å, including a 0.76 Å deviation by V157F. The rescued cancer mutant (V157F/N235K/N239K) shows the highest rms deviation, 0.81 Å. When compared with the DNA-free p53 wild-type structure, the rescued cancer mutant stands out with the largest rms deviation as well, 0.87 Å, whereas the cancer mutant V157F and the two suppressor mutants, N235K and N239Y, display significantly smaller deviations, 0.24 Å, 0.23 Å and 0.20 Å, respectively (third column). Similar results are also found with superposition of other p53 structures (columns 4 to 6 and 8 to 13). In all cases, the largest rms deviation results from superposition of the rescued cancer mutant structure with either the DNA-free or the DNA-bound p53 structures. Therefore, somewhat surprisingly, the largest structural changes are observed for the rescued cancer mutant, and not, as one might naively have presumed, for the cancer mutant.

To identify specific regions of structural deviations in the rescued cancer mutant, we compared this structure with that of wild-type DNA-free p53 (PDB code 2OCJ, chain B) and DNA-bound p53 (PDB code 1TSR, chain B) (Fig. 2.3b). The β-sandwich remains largely intact, with little backbone variability between the rescued cancer mutant and these two wild-type structures. The largest deviations occur in loops L1 and L2, both located on the DNA-binding surface. The loop L1 structures of the rescued cancer mutant and both DNA-free and DNA-bound wild-type p53 structures are mutually distinct. The largest deviation

is at Ser121 for which the Cα atom of the rescued cancer mutant is displaced by 1.8 Å and by 3.2 Å from the DNA-free and DNA-bound wild-type structures, respectively. Overall, the structure of loop L1 in the rescued cancer mutant is midway between that of DNA-free and DNA-bound wild type, which themselves vary by 5.0 Å at Ser121, though it more closely resembles L1 of DNA-free wild type. Although not involved in direct contacts with target DNA, loop L2 is near the DNA-binding surface. The Cα of Ser183 in loop L2 of the rescued cancer mutant is displaced 1.9 Å compared to the DNA-free structure and 3.1 Å compared to the DNA-bound structure. Again, loop L2 of the rescued cancer mutant is between that of the DNA-free and DNA-bound loops, but more closely resembling that of DNA-free wild type. Significant conformational changes are also detected in all turn regions opposite the DNA-binding surface, including turns S3/S4, S7/S8, and S9/S10.

Local structural changes at mutation sites

The V157F cancer mutation induces a significant local conformational change at Ile232, whose C_δ and $C_{\gamma 1}$ are displaced by a rotation around χ_1 (from the 60% rotamer with a χ_1 of -66° to the 2% rotamer with a χ_1 of -169°, Fig. 2.4) to accommodate the large hydrophobic benzyl moiety of Phe157. Surprisingly, this local re-packing of the hydrophobic core results in only minor longer-range structural changes as indicated by the small rms deviation (0.24 Å) between the backbone atom alignment of the V157F mutant compared with DNA-free p53 structures. In contrast, the aromatic ring of Phe157 in the rescued cancer mutant is accommodated by significant structural changes in several neighboring residues (Fig. 2.4). The Tyr220 side chain is pushed away from the center of hydrophobic core with its hydroxyl group displaced by 2.8 Å compared to wild type. The side chain of Leu145 shows

more moderate rotation and shift. Additionally, Val218 and Tyr234 undergo conformational changes.

It is striking that the orientations of the phenyl group of Phe157 in the cancer mutant and the rescued cancer mutant are quite distinct, essentially projecting in opposite directions. In the V157F cancer mutant the phenyl group is oriented toward the interior of the hydrophobic core where it is sandwiched between the side chains of Leu145 and Val218 (13% rotamer with a χ_1 of +59°, although molecules C & D do show partial occupancy for the "rescued" rotamer as well), while in the rescued cancer mutant Phe157 points toward the edge of the β-sandwich where it is sandwiched between Leu145 and Leu257 (44% rotamer with a χ_1 of -64°). Being buried within the hydrophobic core, the nearest ordered water molecule from wild-type Val157 is at a distance of 4.4 Å. In the V157F structure, the large phenylalanine protrudes across the β-sandwich through strands S7 and S8, toward the surrounding hydration shell. This protrusion causes the Cα of Phe157 to come within 3.4 Å of an ordered water molecule. This solvent protrusion of Phe157 is only partially retained in the rescued cancer mutant structure with the Cα within 3.9 Å of an ordered water molecule, having the varied ring orientation and contact with a non-analogous water molecule.

In the wild-type p53 structure, a hydrogen bond exists between Asn235, in strand S8, and Glu198, in strand S5, on the solvated surface of the β-sandwich (Fig. 2.5a). However, in the N235K suppressor mutant, the substituted Lys235 forms a 3.7 Å salt bridge with Glu198, which also contacts Thr140 in the turn between S2' and S3 via a hydrogen bond. This network establishes a strong connection between S5, S8 and the transition of the β-sandwich into the DNA-binding surface. A similar network of interactions occurs in the

rescued cancer mutant. However, the salt bridge distance between Lys235 and Glu198 is reduced to 2.9 Å in this structure and the Glu198-Thr140 hydrogen bond is lost. Taken together, these three amino acids in N235K variants form a strong network between separate strands of the β-sandwich with Glu198 at its center, and this would be expected to contribute additional stability.

The second rescue mutation, Tyr239 is located in loop L3 on the DNA-binding surface and is exposed to the solvent in the crystal lattice. The Cα atom of Tyr239 is approximately 5 Å from the sulfur atom of two zinc-coordinating residues, Cys238 and Cys242 and only 5.3 Å away from the zinc ion itself. Meanwhile, Val274 and Cys275 in helix H2, which are neighboring two important DNA backbone contacts, Arg273 and Ala276, also lie in this Tyr239 region. In the N239Y structure, as well as in the thermostable mutant (*T*-p53), a novel hydrophobic contact is created between the aromatic ring of Tyr239 and Leu137 (Fig. 2.5b) [42]. In the wild-type structure, this leucine side chain appears to be predominantly exposed to solvent. Despite this novel hydrophobic contact in the N239Y structure, Leu137 remains in a relatively similar position compared to the wild type. However, in the rescued cancer mutant, the side chain of Leu137 has shifted slightly towards Tyr239 with a C_γ-to-C_ε distance of 3.4 Å compared to 3.8 Å for N239Y alone. Extending into the solvent, the hydroxyl of the Tyr239 phenol moiety hydrogen bonds with a nearby water molecule in all structures containing this mutation, N239Y, V157F/N235K/N239Y and the thermostable mutant. Other nearby amino acids undergo only slight conformational changes. Noticeably, the side chains of Tyr239 in these three structures are arranged in the same orientation with slight shifts of the phenol groups. As is also described by Joerger *et al.*, overlaying these DNA-free N239Y variants with DNA-bound

p53 illustrates the proximity of Tyr239 to the DNA-binding interface, with the hydroxyl of the rescued cancer mutant approximately 3.5 Å from the DNA phosphodiester backbone[42].

DISCUSSION

Here, we present the biochemical and structural studies of V157F, an oncogenic p53 mutation occurring in the β-sandwich of the p53DBD, both with and without associated second-site rescue mutations, N235K and N239Y. This is the first structure of a β-sandwich cancer mutant without additional stabilizing mutations. To understand the structural effects of these deleterious mutations, particularly for those mutations expected to lead to structural and thermodynamic abnormalities, it is meaningful to study them without added stabilizing or rescue mutations, which could potentially mask their actual effects. This is especially important since there is a crystal structure of only one other p53DBD missense mutant, R249S, a local structure-perturbing mutant, which does not contain stabilizing mutations[45,52]. The mechanism of rescue by these two suppressor mutations, N235K, a novel mutation, and N239Y, which has been studied in the context of *T*-p53, are also considered.

Destabilizing mechanism of V157F mutation

Statistical analysis reveals that the mutation frequency of p53 at codon 157 represents about 1% of point mutations, where V157F contributes to 77% of missense mutations at this codon[1]. Denaturation studies show that the V157F mutation destabilizes the p53DBD 3.6 kcal/mol, and disturbances in the hydrophobic packing of the β-sandwich are visible based on the crystal structure (Fig. 2.4). The induced steric clashes in the core, which cause the rearrangement of several surrounding side chains and reduced shielding from the

solvent, likely account for this loss in stability. However only minor deviations of the protein backbone, both in this region and in the overall domain, are observed.

The crystal structures of two other deleterious mutations within the hydrophobic core, V143A (PDB code 2J1W) and F270L (PDB code 2J1Z), have been solved in the background of the thermostable p53 mutant (M133L, V203A, N239Y, and N268D)[53]. These mutations have the opposite substitution effects as V157F, as both are *large to small* mutations within the core. Both V143A and F270L create an internal cavity within the hydrophobic core. All three of these hydrophobic side chain substitutions cause similar destabilizing effects on the p53DBD, 3.5 – 4.5 kcal/mol loss in stability[45]. This indicates that the β-sandwich contains a fairly stringent organization, where increases or decreases in the mass of side chains of a single side chain, even if the substitution preserves the hydrophobicity of the core, are not well tolerated.

Structural effects of rescue mutations N235K and N239Y

Structural studies reveal the mechanism of rescue for two suppressor mutations, N235K and N239Y, which are particularly effective at rescuing β-sandwich mutations, alone and in concert. The novel N235K mutation structure presents a new salt bridge on the surface of the β-sandwich between strands S8 and S5. This additional salt bridge is able to restabilize the V157F mutant by 1.3 kcal/mol, though little stabilization is gained when this salt bridge is added to wild-type p53DBD. This is likely because V157F disrupts the packing of the hydrophobic core, and the added salt bridge is able to overcome any loss in stability of this core. The V157F mutation causes the most drastic rearrangement of the Ile232 side chain, which is located on S8, the same β-strand that contains Lys235 and the

new salt bridge in the rescued mutant. It appears that the addition of the Lys235-Glu198 interaction is able to compensate for unfavorable packing of the β-sandwich by fastening these two β-strands together. N235K shows no stability gain when added to wild-type p53DBD, which does not have an unfavorable packing of its hydrophobic core. The effects of the Lys235-Glu198 interaction salt bridge may only be apparent in variants with perturbations of their β-sandwich. The N235K suppressor mutation was originally discovered for its ability to rescue cancer mutations in combination with other second-site suppressor mutations, mostly in codon 239 and 240, based on functional p53 yeast assays[38]. These combination suppressor mutations were able to recover the function of deleterious mutations in the β-sandwich, as well as in other areas of the p53DBD. Although N235K demonstrates an ability to stabilize the V157F mutation here, it is difficult to discern if this rescue mutation has utility against mutations outside of β-sandwich destabilization.

The N239Y suppressor mutation demonstrates the capacity to add stability, approximately 1 kcal/mol, to either wild type or V157F/N235K. Utilizing the structure of this N239Y mutation, the aromatic ring of Tyr239 makes a unique hydrophobic contact with a Leu137 and its hydroxyl moiety extends to hydrogen bond with the solvent. As Leu137 is normally solvent exposed, a majority of the reduction in free energy caused by this substitution can be attributed to a gain in entropy at the protein-solvent surface, with the phenol group both protecting this leucine from solvent as well as allowing hydrogen bonding with the surrounding water. Comparing between the N239Y, rescued cancer mutant, and thermostable mutant structures, the orientation of the Tyr239 phenol moiety is very similar and a consistent distance is seen between it and Leu137, indicating a

conserved mechanism of N239Y rescue. As well, Tyr239 lies at the DNA-binding interface of the p53DBD and may be able to make favorable interactions with the phosphodiester backbone of the DNA. In particular, N239Y acts as a rescue mutation at a very distant site from the original deleterious mutation, V157F. With the ability to add stability to the p53DBD as well as rescue the function of several cancer-causing mutations, N239Y likely acts as more of a global second-site suppressor mutation[38,39]. This means that the gain in stability from Tyr239 may be able to compensate for a wide variety of deleterious mutations: stability mutations and local structural deviations alike.

Surprisingly, the overall fold of the wild-type structure more closely aligns with that of the destabilized cancer mutant, V157F, than the rescued cancer mutant structure, V157F/N235K/N239Y. This seems to indicate that the two suppressor mutations presented here do not function by simply reversing the effects of the deleterious mutation and returning the structure of the protein to a more native-like fold. Instead their introduction seems to create novel molecular interactions, which enhance the overall stability of the protein, allowing it to retain function within the cell.

Beyond second-site suppressor mutations

The goal of the field is to identify pharmaceuticals which can restore wild-type function to p53 mutants. Over the past decade, a variety of cell-based screening techniques have led to the discovery of several small molecules which appear to rescue the function of mutant p53[23,24,54]. One of these small molecules, APR-246 (PRIMA-1MET), is currently in phase I/II clinical trials[31]. Despite this, the actual binding of these small molecules to p53 and their mechanisms of rescue have remained elusive. This lack of understanding has hampered the

development of small molecules into useful pharmaceuticals in the clinic. The structures of second-site suppressor mutations are giving us the tools to understand mechanisms of counteracting oncogenic mutations in the p53DBD. By understanding how some of these rescue mutations function, particularly global suppressor mutations such as N239Y, we are beginning to understand how a pharmaceutical could function in this capacity.

MATERIALS AND METHODS

Protein purification and crystallization

The DNA sequences encoding the human p53DBD (residues 94-312) mutants V157F, N235K, N239Y and V157F/N235K/N239Y were subcloned into the pSE420 (Invitrogen) bacterial expression vector. The plasmids were transformed into the *Escherichia coli* BL21 (DE3) strain. Cells were initially grown at 30 °C to an OD_{600} of 1.2 before overnight induction with 0.5 mM IPTG (β-isopropyl-D-thiogalactoside) and 1 mM $ZnSO_4$ at 10 °C. The cells were isolated by centrifugation and sonicated in 50 mM imidazole, pH 7.2, 5 mM dithiothreitol (DTT) and protease inhibitor cocktail tablets (Roche). The supernatant was loaded onto a SP-sepharose cation exchange column (Pharmacia) and eluted with a NaCl gradient (0-600 mM). Elution fractions were diluted in 5-6 volume of buffer with 50 mM imidazole pH 7.2, 5 mM DTT, and 50 mM NaCl. Further purification was achieved by affinity chromatography using a HiTrap heparin sepharose column in 50 mM imidazole pH 7.2, 5 mM DTT with a NaCl gradient (0-600 mM). Elution fractions were dialyzed against 20 mM Tris pH 7.6, 150 mM NaCl, 10 mM DTT. Columns were kept at 4 °C. Mutant proteins were concentrated to 15mg/ml and stored at -20 °C until further use. Crystals were grown at 4 °C by using the sitting drop or hanging drop vapor diffusion technique. 2 µl protein solution

(around 5.0-7.0 mg/ml protein in 20 mM Tris pH 7.6, 150 mM NaCl, 10 mM DTT) was mixed with 2 µl reservoir buffer. The reservoir conditions were different for individual mutants as follows: (1) the V157F mutant: 25% (w/v) polyethylene glycol (PEG) 2000 monomethyl ether (MME); (2) the N235K mutant: 100 mM HEPES, 30 % (w/v) polyethylene glycol (PEG) 6000, pH 7.0; (3) the N239Y mutant: 200 mM lithium acetate, 20% (w/v) PEG 3350; (4) the V157F/N235K/N239Y mutant: 200 mM di-sodium hydrogen phosphate dehydrate (Na_2HPO_4), 20% (w/v) PEG 3350. Colorless plate-shaped crystals were obtained within a week. Crystals were flash-cooled in cryo buffer with 40% (w/v) PEG 2000 MME (monomethyl ether) for V157F crystals, 35% (w/v) PEG 6000 for N235K crystals, and 35% (w/v) PEG 3350 for N239Y and V157F/N235K/N239Y crystals.

Data collection and structure determination

Diffraction data sets of N235K and V157F/N235K/N239Y crystals were collected at 100 K on beamline 4.2.2 at the Advanced Light Source (ALS) in Berkeley, while diffraction data sets of V157F and N239Y crystals were collected at 100 K on beamlines 9-1 and 1-5 at Stanford Synchrotron Radiation Laboratory (SSRL). The data sets were indexed, integrated and further processed using the program D*TREK[55]. Data collection statistics are summarized in Table 2.3.

Since the V157F, N235K and N239Y crystals were isomorphous to our wild-type p53 crystals with very similar cell dimensions, all four molecules in the asymmetric unit of the wild-type p53 were used as the primary model for the program, rigid body refinement in CNS[43,56]. The V157F/N235K/N239Y mutant crystallized in a different space group ($P2_12_12$), and molecular replacement was carried out with the program Phaser using

molecule A of the DNA-free wild-type p53DBD as the search model [43,57]. All models were manually rebuilt into $2F_o$-F_c and F_o-F_c maps using the programs O and/or Coot [58,59]. Diffraction data were checked for twinning using POINTLESS and Xtriage [60,61]. No twinning was indicated for the N235K, N239Y, or V157F/N235K/N239Y crystals. The V157F crystal contained a twin fraction of 0.12 with the twin operator h,-k,-l. Subsequent refinement was carried out with the programs CNS and Phenix, with an h,-k,-l twin operator used during refinement for V157F with Phenix [56,61,62]. Water molecules were added to the structures using the *Waterpick* option implemented in CNS and *Update Waters* option Phenix [56,62]. The stereochemistry of the models was validated with the program PROCHECK or MolProbity and all four p53 mutant structures had excellent stereochemistry [63,64]. Details of the model refinement are presented in Table 2.3.

Figures were generated with the program Pymol (DeLano, W.L. The PyMOL Molecular Graphics System, 2002. http://www.pymol.org). Pairwise alignment of p53 structures for root mean square deviations was performed using the Secondary Structure Matching function within Coot [65].

Protein Data Bank accession codes

The atomic coordinates and structure factors for the cancer mutant (V157F), the suppressor mutants (N235K and N239Y), and the rescued cancer mutant (V157F/N235K/N239Y) have been deposited in the RCSB Protein Data Bank under the accession codes 4KVP, 4LO9, 4LOE and 4LOF, respectively.

Solute denaturation

Equilibrium unfolding of the p53DBD was monitored by intrinsic protein fluorescence as described by Fersht and colleagues [15]. Individual p53 mutant samples in 50 mM sodium phosphate buffer, pH 7.2, containing 5 mM DTT plus urea at concentrations ranging from 0 to 5.5 M were incubated overnight at 10 ºC. Fluorescence emission spectra (average of 20 scans) were recorded from 300 to 370 nm in an SLM-8100 spectrofluorimeter in 2 x 10 mm cuvettes in a Peltier-controlled cell holder at 10 ºC. Excitation was at 280 nm and the bandpass was 8 nm on both excitation and emission. Folded p53DBD generates a characteristic emission spectrum with a peak at 305 nm reflecting strong contributions from some or all of the protein's eight tyrosine residues. A long tail extending to the red reflects a weak contribution from its single tryptophan residue, probably quenched. Unfolded monomeric p53 is characterized by a decrease in 305 nm emission and appearance of a peak at around 350 nm, consistent with decreased tyrosine emission and increased tryptophan emission. An isofluorescence point at about 320 nm is indicative of a two-state unfolding transition. The date are consistent with data published previously [15].

Baseline-subtracted spectra were normalized using the isofluorescence for all variants except V157F. Aggregated p53 is characterized by broad emission with a maximum near 340 nm [45]. A small amount of this material that was present in V157F samples precluded normalization. The difference in intensity, I_{356}- I_{305}, was fitted as a function of urea concentration to eq. 1, which assumes a two-state unfolding model and a linear dependence of the fluorescence for both folded and unfolded states on urea concentration [66].

$$I_{obs} = (I_N + m_N[urea]) + (I_D + m_D[urea]) \frac{\exp(-m_{urea}([urea] - [urea]_{0.5}))/RT)}{1 + \exp(-m_{urea}([urea] - [urea]_{0.5}))/RT)}$$

eq. 1

where $I_{obs} = I_{356s} - I_{305}$, and I_N and I_U. represent the intercepts, and m_N and m_U the slopes of the pre- (native protein) and post- (unfolded protein) baselines. $[\text{urea}]_{0.5}$ is the midpoint of the transition and m_D the slope of the linear dependence of unfolding free energy (ΔG_{D-N}) on urea concentration. Data were fitted using the program Origin 7.0. Independent urea denaturations of a large number or p53 variants by others and by us (Table 2.1) have yielded very similar values of m_{urea}, suggesting that this parameter is little affected by mutation [15,41,45,46]. Given a linear dependence of ΔG_{D-N} on urea concentration, the folding stability in the absence of denaturant is approximated well by

$$\Delta G_{D-N}^{H_2O} = < m_{urea} > \cdot [urea]_{0.5}$$ eq. 2

where $<m_{\text{urea}}>$ is the average of independently determined values.

DNA binding

Site-specific binding of p53 variants was analyzed using the electrophoretic mobility-shift assay (EMSA). The DNA binding target used was a 30-basepair double-stranded oligonucleotide containing the native sequence surrounding the p53 binding site at the *gadd45* promoter. The top strand (5'-GTACAGAACATGTCTAAGCATGCTGGGGAC-3'), conjugated to Oregon green 514 via a 5' 6 carbon linker and complementary bottom strand oligonucleotides were purchased from Integrated DNA Technologies, Inc. (Coralville, IA). These were annealed to double strand as described previously [67]. Reaction mixtures (20 µl)

containing 50 nM *gadd45* DNA and p53 ranging in concentration from 0.05 to 10 μM in 10 mM PIPES, pH 6.8, 100 mM NaCl, 5 mM DTT and 1% (w/v) Ficoll 400 were incubated 20 min in a water bath at 10 °C. Bound and free *gadd45* species were separated by electrophoresis in 5% acrylamide TBE mini-gels (either pre-cast Readygels with 29:1 acrylamide:bis or hand-cast gels with 39:1 acrylamide:bis). Gels were pre-electrophoresed for 6 min at constant 200 V (ca. 10 mA per gel) prior to loading the samples with the current on at reduced voltage (25 V). Electrophoresis was at constant 100 V (ca. 11 mA per gel) for 40 min.

The wet gels were imaged using a GE Healthcare Typhoon 9400. Excitation and emission used the 488 laser and a 520 nm, 40 nm bandpass filter, respectively. The images were analyzed as described previously to determine the fraction of DNA (θ_i) in each of the electrophoretic bands [68]. Unliganded *gadd45* DNA and the specific complex (first mobility shifted band) were analyzed individually. A short ladder of lower mobility bands corresponding to higher order species that presumably represent additional non-specific interactions was poorly resolved. These were grouped together to yield θ_N. The fractions of these species are given as a function of p53 concentration by:

$$\theta_i = e^{i\cdot(Ln[p53]-\Delta G_i/RT)} \Big/ \sum_i e^{i\cdot(Ln[p53]-\Delta G_i/RT)} \qquad \text{eq. 3}$$

where i is the p53 stoichiometry in each of the complexes and ΔG_i is the free energy change per monomer for binding to form the particular complex. For the specific complex, i was set equal to 4 to account for concerted binding of p53 monomer to form tetramer-bound p53 [47]. The value of i was adjusted for the higher order complexes (θ_N). The best fit

was obtained with i=6, indicating hexamer to be the average stoichiometry of these higher order species. Thus, the summation in the denominator of eq. 3 is over i = 0, 4 & 6.

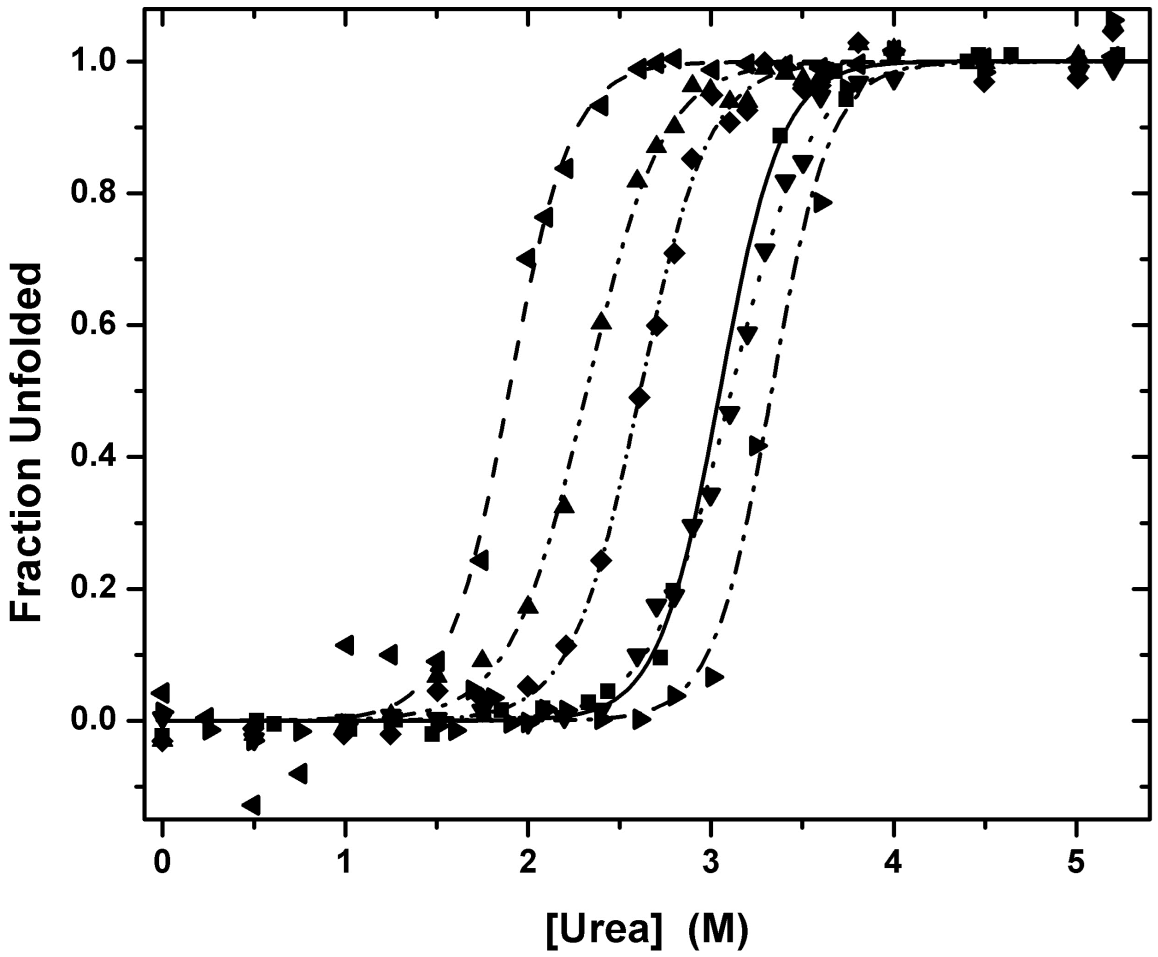

Figure 2.1. Urea-induced denaturation of wild-type and mutant p53DBD at 10 °C. Unfolding of wild-type p53 (squares) and mutants: V157F (triangles left), N235K (triangles down), N239Y (triangles right), V157F/N235K (triangles up), and V157F/N235K/N239Y (diamonds) was monitored by the difference in fluorescence intensity as described in the text. The curves indicate the fits to eq. 1. The data plotted have been transformed from fluorescence to fraction unfolded.

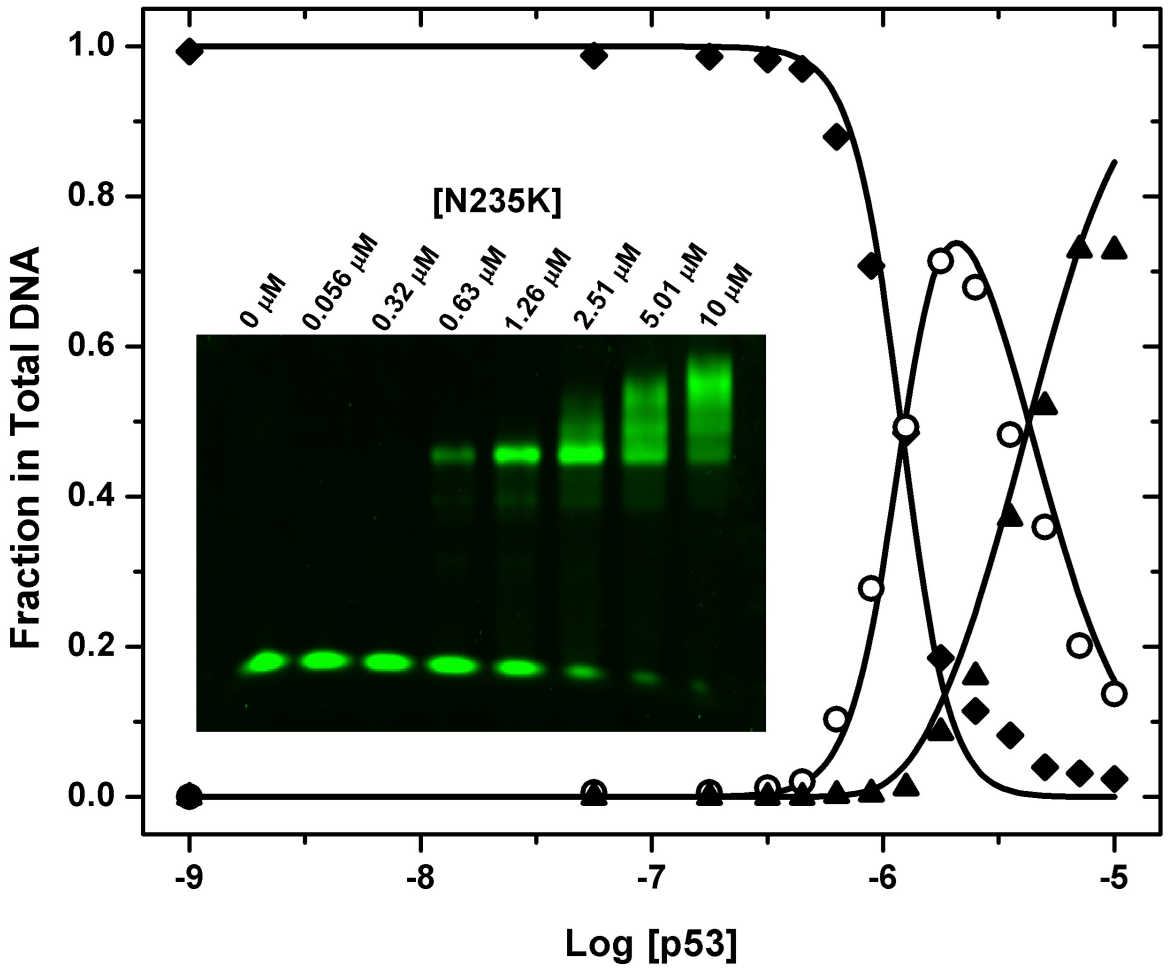

Figure 2.2. Binding of the N235K to *gadd45* DNA. Inset shows a false color image of Oregon green 514 fluorescence from one of two acrylamide gels used to separate bound from free DNA species. Concentrations of the N235K samples are indicated for each lane. Plot shows fractions of the different DNA species. Symbols are: filled diamonds, free DNA (bottom band on gel); open circles, specific p53-*gadd45* complex (first mobility-shifted band); filled triangles, higher order species (summed ladder of additional mobility-shifted bands). Solid lines indicate the fit to eq. 3. Free energy changes (per p53 monomer) for p53 binding to form the specific tetrameric species and to form higher order species are listed in Table 2.1.

Table 2.1. Equilibrium characteristics of p53 cancer, suppressor, and rescued cancer mutants.

	Folding stability							
	Fitted parameters			Calculated parameters†		DNA binding		
p53 variant	m† (kcal mol^{-1} M^{-1})	$[\text{Urea}]_{0.5}$ (kcal mol^{-1})	s‡	$\Delta G^{H_2O}_{D-N}$ (kcal mol^{-1})	$\Delta\Delta G_{D-N}$ (kcal mol^{-1})	ΔG_{spec} (kcal mol^{-1})	$\Delta G_{non\text{-}spec}$ (kcal mol^{-1})	s‡
N239Y	3.50 ± 0.29	3.33 ± 0.02	0.028	−10.4 ± 0.07	−0.88	−7.95 ± 0.056	−6.86 ± 0.008	0.082
N235K	2.61 ± 0.11	3.11 ± 0.01	0.021	−9.7 ± 0.06	−0.19	−7.66 ± 0.022	−7.03 ± 0.044	0.035
Wild type	3.35 ± 0.19	3.00 ± 0.02	0.018	−9.5 ± 0.07	–	−8.00 ± 0.021	−7.02 ± 0.021	0.035
V157F/N235K/N239Y	3.00 ± 0.20	2.61 ± 0.01	0.030	−8.2 ± 0.06	1.36	−7.99 ± 0.040	−7.04 ± 0.085	0.078
V157F/N235K	2.70 ± 0.17	2.32 ± 0.02	0.028	−7.2 ± 0.07	2.28	−8.14 ± 0.019	−7.21 ± 0.064	0.037
V157F	3.31 ± 0.42	1.90 ± 0.03	0.050	−5.9 ± 0.08	3.60	nd§	nd§	

† The weighted mean value of m for these six urea-denaturation transitions is 2.97 ± 0.14 kcal mol^{-1} M^{-1}, which is indistinguishable from the value of 3.12 ± 0.05 kcal mol^{-1} M^{-1} reported previously (Bullock *et al.*, 2000; Nikolova *et al.*, 2000). In consideration of the much larger number of p53 variants represented in the earlier value and to facilitate comparison, we have used m = 3.12 kcal mol^{-1} M^{-1} to calculate $\Delta G^{H_2O}_{D-N}$ and $\Delta\Delta G_{D\text{-}N}$ from (2) in the text. ‡ Square root of the variance of the fitted curve. The parameters from the fits to (1) were used to transform s from the fitted units of intensity to the fraction unfolded, as plotted in Fig. 1. § Not determined. The low thermal stability of this mutant precluded these measurements.

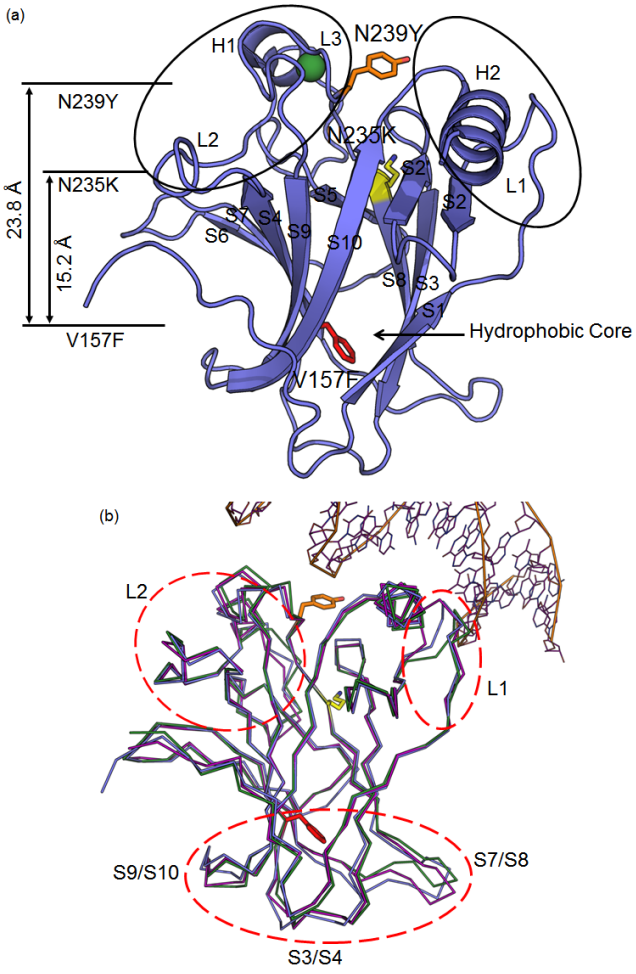

Figure 2.3. The crystal structure of the rescued cancer mutant V157F/N235K/N239Y (PDB code 4LOF). (a) Cartoon representation of the rescued cancer mutant. The β-sandwich scaffold with its hydrophobic core supports the DNA-binding surface including two large loop regions (circled by two black ellipses). The coordinated zinc ion is highlighted as a green sphere. The oncogenic mutation Phe157 (red), and two suppressor mutations Lys235 (yellow) and Tyr239 (orange) were mapped as stick models in the overall structure. The three mutations are spatially separated as indicated. (b) Backbone atom alignment of the rescued cancer mutant V157F/N235K/N239Y (blue) with DNA-free wild-type p53 (PDB code 2OCJ, Chain B, green) and DNA-bound wild-type p53 in complex with the consensus DNA (PDB code 1TSR, Chain B, purple). Dotted red ellipses indicate the regions of significant structural deviations. The cancer mutation Phe157 (red), and two suppressor mutations Lys235 (yellow) and Tyr239 (orange) are mapped as sphere models.

Table 2.2. Pairwise root-mean-square (rms) deviations (in Å) of different human p53DBD structures (values related to the rescued cancer mutant V157F/N235K/N239Y are highlighted in bold)

	1tsr_*B*, DNA-bound	2ocj_*B*, DNA-free	4kvp_*B*, V157F	4lo9_*B*, N235K	4loe_*B* N239Y	4lof, V157F/ N235K/ N239Y	1uol_*B*, M133L/ V203A/ N239Y /N268D	2bim_*B*, T-p53c, R273H	2bin, T-p53c, H168R	2bio, T-p53c, R249S	2bip, T-p53c, H168R/ R249S	2biq, T-p53c, T123A/ H168R/ R249S
1tsr_*B*, DNA-bound		0.76	0.76	0.73	0.76	**0.81**	0.71	0.73	0.62	0.75	0.79	0.79
2ocj_*B*, DNA-free	0.76		0.24	0.23	0.20	**0.87**	0.46	0.47	0.50	0.78	0.60	0.56
4kvp_*B*, V157F	0.76	0.24		0.28	0.27	**0.88**	0.46	0.46	0.51	0.82	0.63	0.58
4lo9_*B*, N235K	0.73	0.23	0.28		0.26	**0.86**	0.44	0.46	0.51	0.64	0.62	0.56
4loe_*B* N239Y	0.76	0.20	0.27	0.26		**0.88**	0.46	0.48	0.48	0.75	0.58	0.53
4lof, V157F/N235K/N239Y	**0.81**	**0.87**	**0.88**	**0.86**	**0.88**		**0.74**	**0.77**	**0.82**	**0.89**	**0.95**	**0.90**
1uol_*B*, M133L/V203A/N239Y/N268D	0.71	0.46	0.46	0.44	0.46	**0.74**		0.15	0.45	0.74	0.61	0.53
2bim_*B*, T-p53c, R273H	0.73	0.47	0.46	0.46	0.48	**0.77**	0.15		0.47	0.77	0.61	0.54
2bin, T-p53c, H168R	0.62	0.50	0.51	0.51	0.48	**0.82**	0.45	0.47		0.60	0.38	0.43
2bio, T-p53c, R249S	0.75	0.78	0.82	0.64	0.75	**0.89**	0.74	0.77	0.60		0.70	0.71
2bip, T-p53c, H168R/R249S	0.79	0.60	0.63	0.62	0.58	**0.95**	0.61	0.61	0.38	0.70		0.21
2biq, T-p53c, T123A/H168R/R249S	0.79	0.56	0.58	0.56	0.53	**0.90**	0.53	0.54	0.43	0.71	0.21	

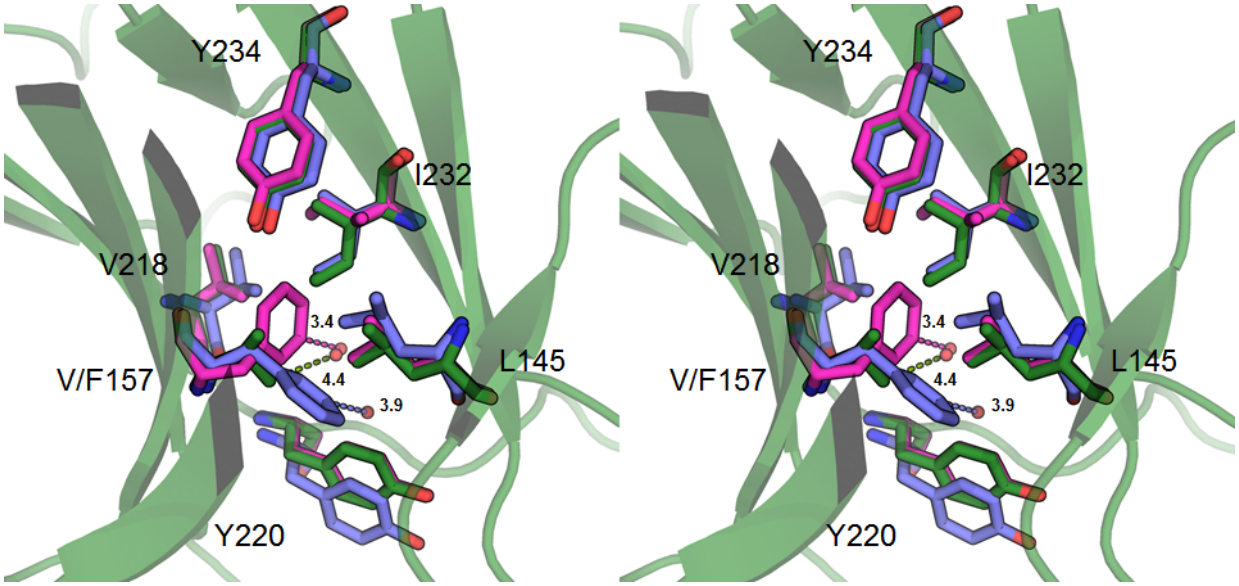

Figure 2.4. Structural effects of the cancer mutation V157F and its rescue. Stereoview of the mutation site with the backbone atom alignment of the V157F cancer mutant (Chain B, magenta), the rescued cancer mutant V157F/N235K/N239Y (blue) and the DNA-free wild-type p53DBD (PDB code 2OCJ, Chain B, green). Cartoon representation of DNA-free wild-type p53DBD backbone is displayed for reference. Ordered water molecules are shown as red spheres with distances to protein atoms indicated by dashed lines of color corresponding to respective p53 variant.

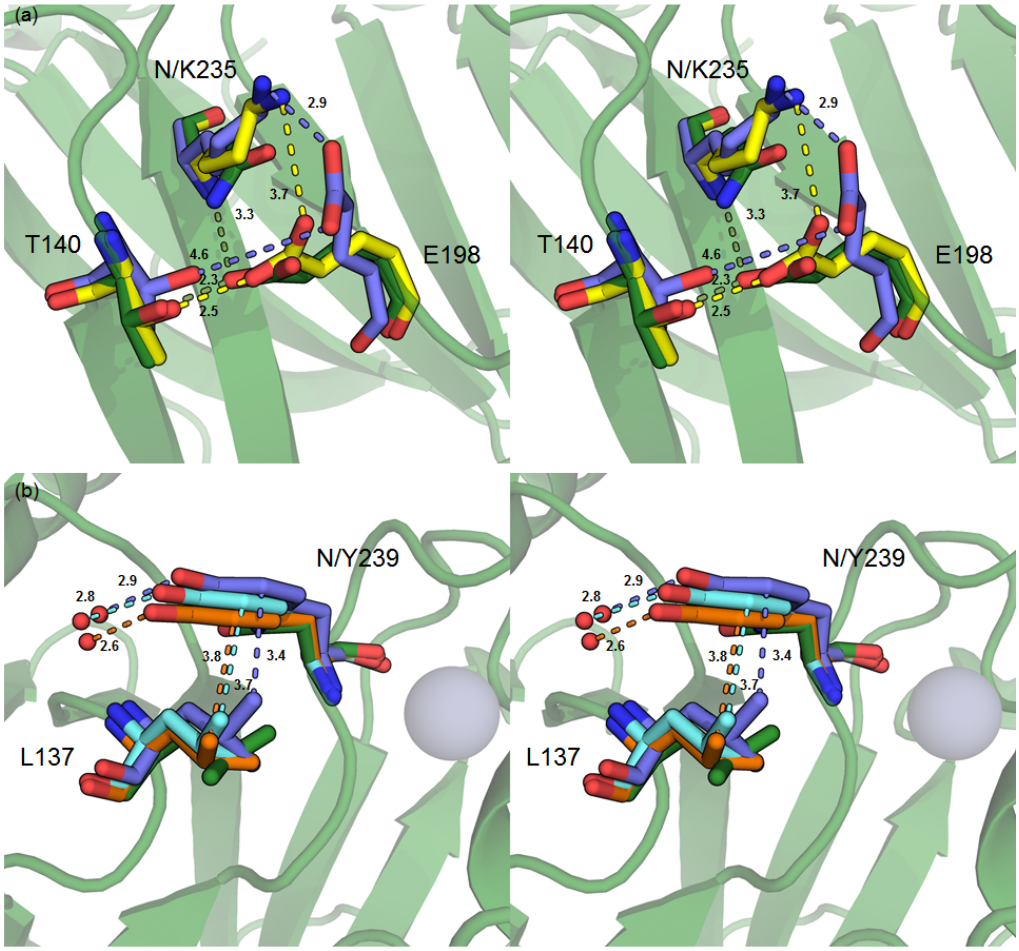

Figure 2.5. Local conformational changes at sites of suppressor mutations. Comparison of different structures, the N235K mutant (Chain B, yellow), the N239Y mutant (Chain B, orange), the rescued cancer mutant V157F/N235K/N239Y (blue), the thermostable mutant (PDB code 1UOL, Chain B, cyan) and the DNA-free wild-type p53 (PDB code 2OCJ, Chain B, green) are performed by using backbone atom superposition. Cartoon representation of DNA-free wild-type p53DBD backbone is displayed for reference. (a) Stereoview of the mutation site N235K. The suppressor mutation N2355 creates a novel salt bridge between Lys235 and Glu198. Distances for salt bridges and hydrogen bonds are indicated by dashed lines of color corresponding to respective p53 variant. (b) Stereoview of the mutation site N239Y. The suppressor mutation N239Y makes a hydrophobic contact with Leu137 and hydrogen bonding with solvent water molecules. Interatomic distances between Tyr239 and Leu137 and ordered water molecules are indicated by dashed lines of color corresponding to respective p53 variant.

Table 2.3. Data-collection and statistics for oncogenic and rescued p53 structures.

Values in parentheses are for the outer resolution shell.

	V157F	N235K	N239Y	V157F/N235K/N239Y
Data collection and processing				
Space group	$P2_1$	$P2_1$	$P2_1$	$P2_12_12$
Unit-cell parameters				
a (Å)	68.7	69.2	68.9	107.3
b (Å)	70.3	69.2	71.1	51.1
c (Å)	83.6	83.9	84.3	33.8
α (°)	90.0	90.0	90.0	90.0
β (°)	90.1	90.1	90.1	90.0
γ (°)	90.0	90.0	90.0	90.0
Monomers per asymmetric unit	4	4	4	1
Resolution range (Å)	42.35–1.50 (1.53–1.50)	53.38–2.50 (2.59–2.50)	29.11–1.85 (1.91–1.85)	46.15–2.00 (2.07–2.00)
Observed reflections	409378	98333	245716	60576
Unique reflections	122789	27431	68899	12822
Completeness (%)	96.6 (94.1)	99.2 (96.6)	98.35 (92.0)	97.3 (99.3)
$\langle I/\sigma(I)\rangle$	8.2 (2.6)	8.0 (3.5)	8.6 (2.6)	5.8 (2.6)
Multiplicity	3.33 (3.01)	3.58 (3.38)	3.57 (3.56)	4.7 (4.8)
R_{merge}† (%)	7.1 (31.3)	10.7 (28.6)	8.4 (46.9)	16.9 (47.7)
Refinement				
Protein atoms	6118	6096	6135	1564
Protein residues	777	776	776	198
Zinc ions	4	4	4	1
Water molecules	536	252	534	134
Resolution range (Å)	42.35–1.50	53.38–2.50	29.11–1.85	46.15–2.00
Twin ratio (%)	88/12	N/A	N/A	N/A
R‡ (%)	17.6	18.1	18.8	19.6
R_{free}§ (%)/% of the test set	21.0/7.3	24.7/7.3	24.4/2.9	25.6/8.0
R.m.s.d., bond lengths¶ (Å)	0.005	0.009	0.007	0.008
R.m.s.d., bond angles¶ (°)	1.0	1.2	1.1	1.1
Ramachandran plot, residues in (%)				
Core regions (%)	99.6	99.0	99.2	98.0
Additional allowed regions (%)	0.4	0.7	0.8	2.0
Generously allowed regions (%)	0.0	0.4	0.0	0.0
Disallowed regions (%)	0.0	0.0	0.0	0.0

† $R_{merge} = \sum_{hkl}\sum_i |I_i(hkl) - \langle I(hkl)\rangle| / \sum_{hkl}\sum_i I_i(hkl)$, where $I_i(hkl)$ is the mean intensity of symmetry-related reflections. ‡ $R = \sum_{hkl} \big||F_{obs}| - |F_{calc}|\big| / \sum_{hkl} |F_{obs}|$, where $|F_{obs}|$ and $|F_{calc}|$ are the observed and calculated structure-factor amplitudes, respectively. § R_{free} is calculated using part of the data that was withheld from refinement. ¶ Root-mean-square deviation.

CHAPTER 3: COMPUTATION IDENTIFICATION OF p53 BINDING POCKET

Previously published in *Nature Communications* in 2013 as: Wassman, C.D., Baronio, R., Demir, Ö., Wallentine, B.D., Chen, C.-K., Hall, L.V., Salehi, F., Lin, D.-W., Chung, B.P., Hatfield G.W., Chamberlin, A.R., Luecke, H., Lathrop, R.H., Kaiser, P., Amaro, R.E. " Computational Identification of a Transiently Open L1/S3 Pocket for p53 Cancer Mutant Reactivation" (2013) *Nature Communications* 4, article number 1407.

ABSTRACT

The tumour suppressor *p53* is the most frequently mutated gene in human cancer. Reactivation of mutant p53 by small molecules is an exciting potential cancer therapy. Although several compounds restore wild type function to mutant p53, their binding sites and mechanisms of action are elusive. Here, computational methods identified a transiently open binding pocket between loop L1 and sheet S3 of the core domain. Mutation of residue Cys124, located at the centre of the pocket, abolished *in vivo* p53 reactivation of mutant R175H by PRIMA-1, a known reactivation compound. Ensemble-based virtual screening against this newly revealed pocket selected stictic acid as a potential p53 reactivation compound. Stictic acid exhibited dose-dependent reactivation of p21 expression for mutant R175H *in vivo*, and increased thermal stability of mutants R175H and G245S *in vitro* more strongly than did PRIMA-1. These results suggest the L1/S3 pocket as a target for pharmaceutical reactivation of p53 mutants.

INTRODUCTION

Tumour suppressor protein p53 is a transcription factor that plays an important role in human cancers. It responds to various cell stress conditions, such as DNA damage, and controls pathways leading to apoptosis (programmed cell death), cellular senescence, and

cell cycle arrest, among others. Tumour initiation and maintenance depend upon inactivation of p53 pathways, which otherwise would deter uncontrolled cell growth. Consequently, *p53* is the most frequently mutated gene in human cancers. Nearly half of all human tumours have mutant *p53*. Approximately three-quarters of those tumours that have mutant *p53* are found to express full-length p53 protein with a single-residue missense mutation in the p53 DNA-binding core domain[69,70].

The resulting presence of full-length and single-point-mutated p53 protein in about one-third of all human tumours holds the promise of drugs that reactivate mutant p53 function, deter cancer cell proliferation, and shrink or kill the tumour[71]. Several p53-controlled pathways inhibit cell proliferation, and so are valid pharmaceutical targets. Studies on transgenic mice demonstrate that p53 reactivation enables tumour regression *in vivo,* even in advanced tumour cases[18,19,72-75]. Reactivation of p53 function has been demonstrated in various p53 cancer mutants by both second-site suppressor mutations[35,36,38,44,76-78] and a handful of small molecules[24-26,79-84]. The most well-studied and promising of these small molecules are PRIMA-1 and PRIMA-1^{Met}, currently in phase I/II clinical trials (APR-246). PRIMA-1 is converted into several active products[30], among them methylene quinuclidinone (MQ), that react covalently to alkylate p53 cysteine residues. This alkylation can reactivate p53 function[30], although the precise reactivation mechanism remains elusive [85].

I worked alongside the laboratories of Dr. R. H. Lathrop (Department of Computer Science, University of California, Irvine), Dr. R. E. Amaro (Department of Chemistry and Biochemistry, University of California, San Diego), and Dr. P. Kaiser (Department of Biological Chemistry, University of California, Irvine) to identify a potential binding pocket

within the p53DBD and discover a small molecule which could possibly bind within this pocket and stabilize the p53DBD. Members of the Dr. Lathrop and Dr. Amaro laboratories performed computational analysis of p53 structural models that suggests a transiently open L1/S3 binding pocket around Cys124, Cys135, and Cys141 as a possible target for reactivation of p53 mutants by small molecules. The pocket was identified through genetic mutations, all-atom molecular dynamics (MD) simulations of the p53 DNA-binding domain (DBD), computational solvent mapping of the resulting p53 structural ensemble, and ensemble-based virtual screening. Members of the Kaiser laboratory demonstrated that mutation of Cys124 to alanine abolished known $p53^{R175H}$ reactivation effects of PRIMA-1 in human Saos-2 cancer cells. Ensemble-based virtual screening[86,87] was then used to select 45 compounds with the most favourable predicted binding affinity to the L1/S3 pocket. Of these, stictic acid emerged as a compound with the ability to induce expression of p21, a gene induced by functional p53, in osteosarcoma cells expressing mutant p53. I showed that stictic acid is able to thermodynamically stabilize mutant p53 *in vitro*, which is the likely mechanism for the induced functionality of mutant p53 in osteosarcoma cells in the presence of stictic acid.

Computational identification of the L1/S3 binding pocket

Initial docking of known p53 reactivation compounds MQ, 3-methylene-2-norbornanone (NB), STIMA-1, MIRA-1, 2, 3[24-26,79-81] by members of the Dr. Lathrop and Dr. Amaro laboratories indicated preferential binding to a specific region in the mouse p53DBD crystal structure (PDB ID 3EXJ[88]), which has high sequence identity (~90%) to human p53. The corresponding region in the human p53DBD is flanked by loop L1 and strand S3, which we have termed the L1/S3 pocket. The region had been recognized by

genetic mutation studies[35,36,38,44,76-78] as highly enriched for p53 suppressor mutations including Phe113, Leu114, His115, Thr123, Leu137, and Asn235 (Fig. 3.1;), indicating that subtle structural changes in this region can reactivate p53 cancer mutants. Four of these reactivation mutation sites (Phe113, Leu114, His115, and Thr123) plus Cys124 exhibit significant or moderate NMR chemical shifts in response to binding of the p53 stabilizing peptide CDB3[89]. Three cysteines, Cys124, Cys135, and Cys141, are near the center of this putative p53 reactivation region, and covalent alkylation of a cysteine thiol group had been suggested for p53 reactivation by PRIMA-1 conversion products such as MQ and other p53 reactivation compounds[30]. In this cysteine triad, Cys124 was the most solvent-accessible, followed by Cys141 and then Cys135, in both the crystal structures and the MD simulations (Table 3.1). Initial alkylation of Cys124 had been suggested to enable alkylation of Cys141 and then Cys135[90].

In the crystal structures of the human p53 core DNA-binding domain (PDB: 1TSR[12], 2OCJ[43]), Cys124 is partially occluded and the putative L1/S3 reactivation pocket is not readily accessible to small molecules much larger than water. This occlusion in the crystal structure might seem to preclude alkylation of Cys124 in human p53. Blind docking of known p53 reactivation compounds by members of the Dr. Lathrop and Dr. Amaro laboratories onto the entire protein surface of the human p53DBD crystal structure PDB ID 1TSR chain B (1TSR-B)[12] indicated that none of the compounds bound in close proximity to any cysteine, including those in the L1/S3 pocket. However, the L1 loop can undergo a conformational switch to regulate DNA binding by an induced fit mechanism[91,92]. Nuclear magnetic resonance (NMR) studies demonstrate that Cys124 is exposed to solvent approximately 5% of the time[93]. Mass spectrometry results indicate that Cys124 and

Cys141 react preferentially with alkylating agents[90] and with glutathione[94]. Alkylating agents cause NMR chemical shifts of several residues within the L1/S3 region[90], including Leu114, His115, and Thr123, already implicated above by genetic mutations and CDB3-induced NMR chemical shifts.

Wild-type (WT) p53 is marginally stable at physiological temperature. The DNA binding domain unfolds with a half-life of around 9 min[71] and has a low melting temperature (T_m) of about 36 °C to 46 °C depending on experimental conditions[15,45,95]. All-atom explicit solvent MD simulations conducted by members the Dr. Amaro laboratory for 30 ns of $p53^{WT}$DBD and three frequent cancer mutants, $p53^{R175H}$DBD, $p53^{G245S}$DBD, and $p53^{R273H}$DBD, revealed a high degree of flexibility for the p53DBD[96] and particularly the L1/S3 region surrounding Cys124. Clustering the MD ensembles with respect to the L1/S3 pocket conformation further demonstrated the flexibility of the region (Table 3.1). In the MD ensembles of different p53 variants, average solvent accessible surface area (SASA) values of the Cys124 side chain were calculated to be in the range of 6-11 $Å^2$ (Table 1). In sharp contrast, in the p53DBD crystal structure 1TSR-B the Cys124 side chain SASA was calculated to be only 0.43 $Å^2$.

Docking into the L1/S3 pocket

Members of the Dr. Lathrop and Dr. Amaro laboratories discovered that this transiently open L1/S3 pocket forms around Cys124 due to positional and conformational changes of Ser116, Thr123, Cys124, Thr140, and especially Leu114 (Fig. 1). Three of these residues, Leu114, Thr123, and Cys124, already were implicated above. They determined five distance/dihedral angle criteria that indicated formation of an open L1/S3 pocket in about

5-8% of each simulation (Table 3.1). Fpocket [97], a program to measure the volume of a defined binding pocket (Fig. 3.1), was used by members of Dr. Lathrop and Dr. Amaro laboratories to also indicate an open L1/S3 pocket around Cys124 across several p53 variants in 5-30% of the 3,000 frames of each MD trajectory (Table 3.1). For evaluating Fpocket results, the L1/S3 pocket was considered open if its volume was larger than 150 $Å^3$, a lower bound chosen based on cancer mutant $p53^{R273H}$DBD, which exhibited the lowest average L1/S3 pocket volumes. FTMap [98], a program to identify ligand binding hot spots in proteins using organic solvent probes, predicted the L1/S3 pocket to be among the most highly occupied by the solvent probes using MD-generated conformations (Fig. 3.1). For wild-type p53 and mutant R273H MD trajectories, FTMap predicted an open L1/S3 pocket to occur, respectively, in 11 and 7 of the 15 most-populated cluster centroids. In contrast, neither Cys124 nor any other cysteine in the original PDB crystal structure 1TSR-B[12] was identified as a site where small molecules could bind using FTMap.

Six alkylating agents previously identified as capable of reactivating p53, MQ[30], NB[81], STIMA-1[26], and MIRA-1, 2, 3[25], subsequently were docked by members of the Dr. Lathrop and Dr. Amaro laboratories into the most-populated MD trajectory cluster representative that had an open L1/S3 binding pocket as defined (Table 3.1). All of these known active compounds presented low-energy predicted docking poses with the reactive methylene oriented in close proximity to the Cys124 sulfhydryl group for p53 cancer mutant $p53^{R175H}$DBD (Fig. 3.2). Reliability of the molecular docking strategy was supported by a positive control, PhiKan083[82], which docked within 1.0 Å root-mean-square-deviation (RMSD) of the reference crystal structure. The transiently open L1/S3 pocket was shared across wild type and the three p53 cancer mutants studied. Thus, several lines of evidence

provided by members of Dr. Lathrop and Dr. Amaro's laboratories suggested a transiently open binding pocket in the L1/S3 region of the human p53 protein.

Biological validation of the L1/S3 binding pocket hypothesis

Members of the Dr. Kaiser laboratory examined the role of Cys124 in the L1/S3 binding pocket by site-directed mutagenesis of Cys124 to alanine ($p53^{C124A}$). If Cys124 were a critical residue for p53 reactivation, then removal of its thiol group by this otherwise innocuous mutation would abolish the PRIMA-1 reactivation effect. For example, Cys124 might be a key attachment residue for PRIMA-1 conversion products such as MQ[30], it might initiate a Cys124-Cys141-Cys135 alkylation cascade[90], or it might form a disulphide bond that stabilized p53 in an active conformation induced by compound binding. The literature suggests that a reducing environment leads to correct p53 folding and disulphide bond formation may lead to aggregation[85]. There is no *a priori* reason to rule out any of these hypotheses.

$p53^{null}$ human osteosarcoma Saos-2 cells were engineered by members of the Dr. Kaiser laboratory to have doxycycline-inducible expression of either $p53^{WT}$ or various p53 mutants. Single clones with similar expression levels of the different p53 variants were selected for direct comparison of small molecule effects. As expected, expression of $p53^{WT}$ in Saos-2 cells halted cell proliferation whereas expression of mutant $p53^{R175H}$ had no effect on cell proliferation (Fig. 3.3). Mutation of Cys124 to alanine ($p53^{C124A}$) had little effect on otherwise wild-type p53 nor did it restore activity of $p53^{R175H}$ (R175H/C124A), indicating that the C124A mutation is largely neutral for general p53 function. Consistent with previous results[30], addition of PRIMA-1 to cells expressing inactive mutant $p53^{R175H}$ led to

p53 reactivation and subsequent inhibition of cell cycle progression. Importantly, PRIMA-1 reactivation of p53 function was blocked in the double mutant $p53^{R175H/C124A}$ (Fig. 3.3), demonstrating the potential for Cys124 in pharmacological reactivation of mutant $p53^{R175H}$ by PRIMA-1. These experimental results support the computational identification of the L1/S3 binding pocket surrounding Cys124 as significant for p53 reactivation.

Discovery of a novel p53 reactivation compound using the L1/S3 binding pocket

An ensemble-based virtual screening approach, known as the relaxed complex scheme (RCS)[86,87], was performed by members of the Dr. Amaro laboratory against the mutant $p53^{R273H}$DBD. Initially, 1,324 compounds from the NCI/DTP Open Chemical Repository Diversity Set II were virtually screened. They were docked into each of the most-populated 15 cluster centroids—altogether representing 92.5% of the entire trajectory—obtained by clustering the MD trajectory of the $p53^{R273H}$DBD cancer mutant according to the L1/S3 pocket conformation. Compounds with predicted binding affinities of -6.5 kcal/mol or better to any of the 15 centroids were chosen with a limit of 50 compounds from each centroid. The resulting 84 compounds (corresponding to ~6% of the entire NCIDS2 database) were ranked according to their population-weighted average binding affinities. The ADME properties of the compounds, as predicted by Schrodinger (QikProp, version 3.3, Schrödinger, LLC, New York, NY, 2010), were used for further filtering. Lipinski's Rule of Five and Jorgensen's Rule of Three were followed strictly, resulting in 24 compounds. Similarly, compounds from the NCI Mechanistic Set, NCI Natural Products Set, NCI COMBO Set, and NCI Oncology Approved Set (consisting of 974 compounds in total) were virtually screened and filtered for ADME properties. A more stringent ADME filter (octanol/water partition coefficient < 3) was enforced to improve compound solubility. A similar predicted

binding affinity cutoff of -6.5 kcal/mol was used, resulting in 24 additional compounds. Three were discarded because they were unavailable (NSC653010, NSC92339, and NSC653016). In total, 45 compounds were selected for biological validation.

One of these compounds, stictic acid (NSC87511), was proven to be a p53 reactivation compound by our collaborators. The best-scoring stictic acid pose when docked into the L1/S3 pockets of $p53^{WT}$DBD and mutants $p53^{R175H}$DBD, $p53^{R273H}$DBD, and $p53^{G245S}$DBD (Fig. 3.4). In order to gauge the stability of stictic acid in the L1/S3 active site, a molecular dynamics simulation was performed starting from the best-scoring docking pose of stictic acid in mutant $p53^{R175H}$DBD. The initial docking score was -6.97 and the final docking score was -7.11. This demonstrated that the p53DBD was stable and stictic acid persisted in the L1/S3 pocket throughout the entire 60 ns MD simulation.

In vivo support for stictic acid as a novel p53 reactivation compound

Stictic acid was shown by members the Dr. Kaiser laboratory to partially restore p53 activity in human Saos-2 cells expressing cancer mutant $p53^{R175H}$ (Fig. 3.5), as demonstrated by induction of the cell cycle inhibitor p21. *p21* is a canonical gene target of active p53 and a sensitive and selective output for p53 activity. Induction of p21 by stictic acid was dose-responsive. It was also dependent upon p53, because it had only a minor effect on p21 expression in cells lacking p53 (Fig. 3.5).

p53 primarily functions as a transcription factor. To more directly test the effect of stictic acid on restoring transcriptional activity of p53 mutants, members of the Dr. Kaiser laboratory generated stable cell lines harbouring reporter constructs driven by two different p53-dependent promoter elements. These elements were derived from the

promoters of the cell cycle inhibitor p21 and the pro-apoptotic gene PUMA and have previously been utilize to monitor p53 transactivation activity[99]. They compared the effect of stictic acid to that of PRIMA-1 and the recently identified allele-specific p53 reactivation compound NSC319725[84] (Fig. 3.6). All compounds modestly but significantly restored the ability of the p53 mutants $p53^{R175H}$ and $p53^{G245S}$ to express the pro-apoptotic reporter PUMA, except NSC319725, which acted in a $p53^{R175H}$-specific manner as expected[84] (Fig. 3.6a). Activation of p21 reporter transcription was more pronounced and confirmed that stictic acid is a p53 mutant reactivation compound comparable to the previously identified compound PRIMA-1.

THERMAL STABILIZATION OF REACTIVATION COMPOUNDS

RESULTS

Thermal shift assays (TSA) provide the ability to detect molecular interactions between a small molecule and a protein based on changes in the melting temperature (T_m) of the protein[100-102]. These T_m changes are taken to reflect changes in protein stability upon binding of the small molecule. I tested variants of the p53DBD (wild type, G245S, and R175H) using TSA with a range of concentrations of PRIMA-1, MQ, and stictic acid (Fig. 3.7). The T_m values in the absence of compounds for wild type, G245S, and R175H, at 4 μM, were 36.54±0.11, 33.51±0.09, and 27.89±0.11 °C, respectively. PRIMA-1 and MQ stabilized each of the p53 variants by approximately one degree or less for concentrations ranging from 10 to 80 μM, 2.5X to 20X stoichiometric ratio of compound to protein (Fig. 3.7). The greatest thermal stabilization was observed with stictic acid, up to 4.60±0.39 °C at 80 μM in mutant $p53^{R175H}$DBD. All three of these compounds demonstrated a relative dose

dependence in their ability to stabilize p53. None of these compounds had stabilizing effects on three control proteins tested, annexin A2, S100A4, and S100A10, suggesting that their interactions are specific to p53.

DISCUSSION

Despite continuous progress in cancer research and care, millions of people die annually from this disease. Therapeutic reactivation of p53 could prevent or delay many of these deaths. Here we report computer-guided identification of a transiently open L1/S3 reactivation pocket in p53 that may present a more broadly applicable region for such cancer therapies to bind. The coordinates of the human p53DBD structures with the open binding pocket conformations shown in Fig. 3.4 have been deposited in the Protein Model DataBase (PMDB)[103] by our collaborators (http://mi.caspur.it/PMDB/; PMDB ID (a) PM0078199 for $p53^{WT}$DBD; (b) PM0078200 for $p53^{R175H}$DBD; (c) PM0078201 for $p53^{G245S}$DBD; and (d) PM0078202 for $p53^{R273H}$DBD) and in SourceForge (http://sourceforge.net/projects/p53cancerrescue/, in folder "Coordinates of p53 core domain"). We anticipate that the L1/S3 reactivation region reported here will be useful to other researchers carrying out structure-based drug discovery and development of p53 reactivation drug leads.

A notable advantage of the L1/S3 pocket is that it occurs across several p53 variants, as seen in Fig. 3.4, giving hope that p53 reactivation compounds can be developed to target several p53 cancer mutants simultaneously. In contrast, for example, known compounds that target the $p53^{Y220C}$ reactivation pocket[82,83] appear to be specific to the Y220C mutant, because the pocket to which these compounds bind is only created upon mutation of

Tyr200 to cys. None of the R175H, G245S, or R273H mutations lie in the L1/S3 pocket or have direct effects on its conformation. Its generalizability is illustrated here by the result that virtual screening against one mutant, $p53^{R273H}$DBD, produced a compound that resulted in biological validation against two different mutants, $p53^{R175H}$DBD and $p53^{G245S}$DBD, and induced thermodynamic stabilization of all p53 variants studied.

Protein conformational flexibility is well-recognized as an important factor in ligand binding. A few computational drug discovery approaches attempt to accommodate protein-induced fit on ligand binding by allowing side chains to move in order to improve the fit of the ligand into the binding pocket. Very few such approaches allow the protein backbone to move to accommodate the ligand. Nevertheless, the results above provide a cautionary tale: a ligand binding pocket of medical importance may be hidden and difficult to recognize in structural databases, yet other virtual structures extracted from its conformational ensemble may support successful structure-based drug discovery. With appropriate protein conformations in hand for computational analysis, we screened only 45 compounds through biological assays to find a novel p53 reactivation compound, stictic acid.

The RCS[86,87] docking scheme clusters are based on conformations of all residues surrounding the L1/S3 pocket, not on specific conformations of particular residues. No cluster centroid produced a suitable docking pose for stictic acid docked to $p53^{G245S}$DBD (Fig. 3.4d), due to the position and rotamer state of the crucial Leu114 residue. A suitable Leu114 conformation occurred in only three or four frames of the entire 3,000-frame 30-ns trajectory (Methods, RMSD-based clustering). The sampling in MD is limited, so the fact that any suitable pocket opening events were seen at all is indication that such pockets exist at thermal equilibrium for this mutant. Indeed, three occurrences in 30 ns is

equivalent to 10^8 occurrences per second, while three occurrences in 3,000 frames is equivalent to a probability of 10^{-3}, and so the event cannot be considered rare. Instead, we see here a limitation of our current computational methods for modelling complex molecular processes.

Stictic acid remained docked after 60 ns of stable MD simulation. The rotamer state of Leu114 was critical to opening up a binding site large enough to accommodate large molecules like stictic acid. In the initial docked pose of stictic acid, there is only one direct H-bond interaction between stictic acid and the Cys124 backbone amino group, in addition to various hydrophobic interactions including Pro142 and Leu114. The hydrophobic interactions with Pro142 and Leu114 were conserved throughout the simulation. The final pose provides an elegant illustration of induced fit upon binding. Stictic acid moved deeper into the pocket, achieved a very nice shape complementarity, substantially expanded the initial network of favourable direct and water-mediated interactions, and shifted the ligand and receptor exposure patterns.

PRIMA-1 has conversion products that are more active than it is itself[30], and this may be the case for stictic acid as well. The existence of a highly active and bioavailable stictic acid decomposition product was suggested by initial experiments carried out with a stictic acid solution that had a long storage time. Such hypothetical conversion products were not present in the freshly-ordered newly-dissolved pure compound, from which the results presented here were derived.

It is unclear whether or not stictic acid requires covalent linkage to p53 for reactivation according to the general cysteine alkylation mechanism proposed by Lambert et al.[30] for

several other p53 reactivation compounds. Stictic acid may, in principle, bind covalently to nucleophilic protein side chains by acylating or alkylating nucleophilic residues such as cysteine. Likely reaction sites and modes of reactivity include the direct addition of a nucleophile (a cysteine thiol group of the protein) to either the 7-membered ring lactone carbonyl group or to the carbonyl group of the 5-membered ring lactone, resulting in acylation of the thiol and covalent attachment to the protein as the respective thioester. Alkylation is another possible mechanism, occurring via a more circuitous mechanism in which dehydration generates a reactive quinone methide-type species that can alkylate nucleophiles. An alternative dehydration pathway could produce a different methide that would result in alkylation at the corresponding benzylic position. There is no *a priori* reason to rule out any of these pathways.

In TSA experiments, pre-heated PRIMA-1 (to induce formation of conversion products) induced thermal shifts (T_m increases) that were slightly higher than for MQ. Though slight, the differences were statistically significant at higher concentrations, which is consistent with the previous evidence that MQ is not the most active conversion product of PRIMA-1[30]. These two known reactivation compounds showed significantly lower stabilizing effects on the p53 mutants tested than did stictic acid. Stictic acid is a much larger molecule than MQ. It has the potential to make more interactions within the binding pocket (compare Fig. 3.2 to Fig. 3.4), perhaps giving it a greater capacity than PRIMA-1 or MQ for stabilizing p53 cancer mutants. We cannot rule out other effects, e.g., the possibility that the low thermal shifts for PRIMA-1 may be due to its incomplete conversion into more active products, or that the low thermal shifts for MQ may be due to its highly reactive nature leading to rapid decomposition on contact with water.

Stictic acid displayed promising results in reactivating severely destabilized mutant $p53^{R175H}$ in human cancer cells. Reactivation was evident from dose-dependent and p53-dependent induction of p21 expression. Cell death was not activated by stictic acid, which may be due to insufficient reactivation of cancer mutant $p53^{R175H}$ or may indicate pathway selective restoration of p53 activity. Such probes with pathway discriminatory activity will become valuable tools for the study of p53 biology. However, reporter assays demonstrated comparable p53 reactivation by stictic acid and PRIMA-1 (Fig. 3.6), yet PRIMA-1 is a potent inducer of apoptosis in cells with mutant p53. It is possible that additional, p53-independent cytotoxic functions of PRIMA-1 or one of its degradation products[30] act synergistically with p53 reactivation to induce apoptosis. Such additive effects may not be induced by stictic acid.

Mutant $p53^{R175H}$DBD showed a greater degree of thermal stabilization in TSA by stictic acid than did wild-type or G245S. Perhaps this is because $p53^{R175H}$DBD is initially highly destabilized (a Zn region mutant, 30% folded at 37 °C[45]) while $p53^{WT}$DBD and $p53^{G245S}$DBD (a DNA region mutant, 95% folded at 37 °C [45]) are not. These results suggest that stabilization effects and reactivation outcome depend on the p53 mutation, and that thermal stabilization of the p53DBD may reactivate some p53-controlled pathways and not others in a way that depends on the ligand.

TSA *in vitro* experiments indicated direct binding of stictic acid to all p53 variants tested. *In vivo* induction of p21 expression by stictic acid showed dependence on p53-mediated pathways, because no such induction was observed in the Saos-2 parent cell lines lacking p53. Taken together, these *in vitro* and *in vivo* results indicate that stictic acid acts directly on p53.

Recently two compounds from the thiosemicarbazone family (NSC319725 and NSC319726) were identified as allele-selective reactivation compounds for cancer mutant $p53^{R175H}$ [84]. Whether these compounds directly bind to p53 and perhaps target the L1/S3 reactivation pocket identified in this study is currently unclear, but will be interesting questions to address in future experiments.

Our results demonstrate the value of integrated strategies combining genetics and computation for identification of protein regions to target, and highlight the feasibility of using molecular dynamics simulations to expose protein regions amenable to small molecule binding that otherwise may not be evident.

MATERIALS AND METHODS

Molecular dynamics simulations

Wild type p53 MD simulations were performed using crystal structure 1TSR-B[12] for the initial coordinates. Models for mutants $p53^{R273H}$DBD, $p53^{R175H}$DBD, $p53^{G245S}$DBD, and $p53^{C124A}$DBD were prepared by virtual mutation of $p53^{WT}$DBD using the AMBER10 suite[104]. The crystallographic water molecules were retained and each system was solvated in a TIP3P water box[105]. Zinc-coordinating residues were modeled using the cationic dummy atom model[106]. Protonation states of titratable residues were determined using the Whatif Web Interface[107]. Histidine, asparagine, and glutamine side chain orientations were corrected as needed using the MolProbity web server[64]. Each system was neutralized by adding chloride ions as needed. The structure files of each system consisted of about 27,260 atoms, which were prepared using the AmberFF99SB force field[108].

Each of the p53 variant systems was first relaxed using 36,000 steps of minimization followed by four consecutive restrained 250 ps molecular dynamics simulations. Thereafter, 30 ns unrestrained MD simulation was performed at 310 K and 1 atm for each system using the NAMD2.7 suite[109]. Details of the minimization and MD simulation protocol can be found in Demir et al.[96].

In order to gauge the stability of the stictic acid in the binding pocket, a 60 ns MD simulation was performed. The best-scoring docked pose of the molecule in the $p53^{R175H}$DBD L1/S3 open pocket conformation was used as the starting geometry (Fig. 3.4b). Stictic acid parameters were generated with the Antechamber module of Amber10 using the Generalized Amber Force Field (GAFF)[110,111] with RESP HF 6-31G* charges.

For each p53 variant studied, the solvent accessible surface area of the Cys124 side chain over the MD trajectory was calculated using a customized VMD[112] script.

RMSD-based clustering

Protein snapshots extracted from the simulations were clustered with respect to all heavy atoms of the L1/S3 site. For each variant, atomic coordinates were extracted at 10 ps intervals over their 30 ns MD trajectory, resulting in 3,000 virtual structures per trajectory. These 3,000 structures were superimposed with respect to all C_α atoms to remove overall translation and rotation. They were then clustered using the gromos algorithm[113,114] in the GROMACS 4.0.5 program[115] at an RMSD cut-off value of 1.65 Å, based on atomic coordinates of all atoms of those residues that had at least one atom within 10 Å of Cys124 in the minimized and equilibrated form of each p53 variant. In each cluster, the structure

with the smallest average RMSD to all the other structures in the cluster was designated as the "centroid" or "representative" structure of the cluster.

Cluster centroids exhibiting open L1/S3 pockets were identified for each p53 variant using the geometric criteria. These open centroids were used for docking stictic acid and the known p53 reactivating small molecules. In the case of $p53^{G245S}$DBD, the known small molecules were successfully docked into the cluster centroid with an identified open L1/S3 pocket. However, it was not possible to identify a cluster centroid for G245S that produced a binding pose for stictic acid (a relatively much larger molecule) in which a possible alkylation reaction with the Cys124 side chain seemed reasonable. A closer look at the $p53^{G245S}$DBD MD trajectory revealed that the position and rotamer state of Leu114 was critical for L1/S3 pocket opening. Leu114, already implicated above, exhibited a favourable conformation in only three or four frames of the entire 3,000-frame trajectory. Thus, a snapshot with an open L1/S3 pocket was extracted manually from the G245S MD trajectory and subsequently used to dock stictic acid.

In silico docking

Initial docking studies were performed using AutoDock 4.2.2. All subsequent docking studies used AutoDock Vina[116] with an exhaustiveness value of 100 and a 20 Å x 20 Å x 20 Å search space centred on the sulphur atom of Cys124. Nine different docking poses were calculated for each considered combination of a compound and a p53 variant. For initial compound scoring, population-weighted average binding affinities of the most-populated 15 cluster centroids from the $p53^{R273H}$DBD MD trajectory were calculated using the best binding affinity found by Autodock Vina for each compound. The 48 compounds selected

were re-scored using the population-weighted average binding affinities of the most-populated 30 cluster centroids. Ligand interaction diagrams were prepared using the Molecular Operating Environment (MOE) program (Chemical Computing Group Inc., Montreal, Canada).

Computational fragment-mapping using FTMap

The FTMap program[98] utilizes 16 probe molecules to identify and rank the most energetically favourable binding pockets on a protein surface. For this purpose, FTMap first performs rigid body docking of probe molecules with a fast Fourier transform method, then minimizes and rescores the docked poses. Next, it clusters them for each probe using a simple greedy algorithm, and finally locates the consensus sites of binding pockets identified by all probes.

Cell lines

Soas-2 cells were obtained from the American Type Culture Collection (ATCC, Manassas, VA). They were maintained at 37 °C in DMEM high glucose supplemented with 10% fetal bovine serum, penicillin G sodium (100 units/ml), and streptomycin (100 μg/ml).

Stable Soas-2 cell lines harbouring doxycycline-inducible $p53^{WT}$ or mutants were established by a lentivirus-based strategy[117]. Human p53 genes were cloned as SacI/PstI fragments into pEN_TmiRc3, replacing GFP and ccdB genes in the plasmid. Recombination of p53-pEN_TmiRc3 and the lentivirus vector pSlik was performed using the LR Clonase® Enzyme Mix (Invitrogen, Carlsbad, CA) according to manufacturer's instructions. Lentiviruses were generated by co-transfecting 5 μg of lentiviral vector pSlik and 5 μg of

each packaging vector (coding for Gag, Pol, Tat, Rev, and VSVG) in 90% confluent 293T cells in 10 cm plates using Lipofectamine 2000 (Invitrogen, Carlsbad, CA). Supernatants were collected 48 h after transfection and used directly to infect Soas-2 cells. 48 h after this infection, the Soas-2 cultures were switched to hygromycin B containing media. To isolate single p53-expressing clones, cells were induced with doxycycline and tested by immuno blotting. Doxycycline was used at a concentration of 1 μg/ml, hygromycin B at 50 μg/ml.

For generation of stable cell lines to measure p53-dependent activation of p21 or PUMA reporters, p21 (GAAGAAGACTGGGCATGTCT) or PUMA (CTGCAAGTCCTGACTTGTCC) response elements [99] followed by a minimal promoter (TAGAGGGTATATAATGGAAGCTCGACTTCCAG) were inserted into KpnI/XhoI cut plasmid pGL4.10 (Promega). These elements control expression of a synthetic firefly luc2 (Photinus pyralis) gene. A SV40-driven puromycin resistance cassette was inserted into the Pst1 site of pGl4.10 to enable generation of stable cell lines. The PUMA and p21 reporter vectors were transfected into Soas-2 using and single colonies resistant to 50 ug/ml puromycin were selected.

Cell viability assay

Cells were placed in 96-well plates at a density of 10,000 cells per well and incubated overnight. The next day, doxycycline (final concentration 1μg/ml) was added to induce expression of p53 for 8 h before PRIMA-1 (50 μM final concentration) or solvent was added to the cultures. PRIMA-1 was pre-heated to 100 ˚C for 10 min to promote formation of active decomposition products and then cooled before it was used in these experiments[30]. Cell viability assays were performed using CellTiter-Glo® Luminescent Cell Viability Assay

(Promega, Wisconsin, MD) according to the manufacturer's instructions. Data represent the average of four independent samples.

Western blot analysis

Approximately 500,000 cells were treated with doxycycline at a final concentration of 1 µg/ml for 8 h to induce expression of p53, then treated with stictic acid or vehicle (DMSO) at various concentrations for 48 h. For Western blot analysis, cells were lysed in 8 M Urea buffer and equal amounts of total cell lysates were resolved by SDS-PAGE (12.5% gel). Then proteins were transferred onto Immobilon transfer paper (Millipore) and probed with an anti-p21 antibody (Santa Cruz Cat#: sc-397). p21 expression was quantified using a Fuji LAS-4000 imaging system and analysed with the Multi Gauge v3 software.

PUMA and p21 reporter assay

Soas2-PUMA-luc2 or Soas2-p21-luc2 cell lines were transfected with 500 ng of CMV-renilla plasmid and 125ng of plamid carring either empty vector, $p53^{WT}$ or mutants $p53^{R175H}$ and $p53^{G245S}$ [35] using Lipofectamine 2000.. The different compounds were added 21 hours after transfection. Activation of the PUMA and p21 reporters was analysed by a luciferase assay (Dual luciferase assay system, Promega) 8 hours after the addition of compounds.

Expression and purification of p53DBD protein for wild type, G245S, and R175H

The $p53^{WT}$DBD (residues 94-312) had been previously introduced into the bacterial expression vector pSE420. Mutants $p53^{G245S}$DBD and $p53^{R175H}$DBD were generated by using a site-directed mutagenesis kit in this same vector (Invitrogen, Grand Island, NY). These vectors were transformed into *Escherichia coli* Rosetta 2 (DE3) strain, then

expressed as described[43]. Proteins were purified in a series of chromatographic steps: Q-Sepharose anion exchange column (GE Healthcare, Piscataway, NJ), SP-Sepharose cation exchange column (GE Healthcare), affinity chromatography using a HiTrap heparin Sepharose column (GE Healthcare), and gel filtration on a Superdex 200 column (GE Healthcare), followed by dialysis against 50 mM HEPES pH 7.5, 150 mM NaCl, and 0.1 mM DTT. Pure protein was concentrated by Macrosep Advance Centrifuge Devices (PALL, Port Washington, NY) to 0.22 mM and stored at -20 °C for further use. Protein concentration was determined by a Shimadzu (Columbia, MD) UV-VIS recording spectrophotometer with an extinction coefficient of 16530 cm^{-1} M^{-1} at 280 nm as calculated by the method of Gill & von Hippel[118]. All protein purification steps were monitored against 4-12% Tris-Glycine SDS-PAGE (Lonza, Basel, Switzerland) to ensure they were virtually homogeneous. All chemicals and solvents were analytical and HPLC grade, respectively.

Thermal shift assays (TSA)

Purified p53 protein (0.22 mM in 50 mM HEPES at pH 7.5, 150 mM NaCl, 0.1 mM DTT) was diluted to 4 μM final concentration in 20 mM HEPES at pH 7.5. Compounds were dissolved in DMSO to various concentrations and added to diluted protein for overnight incubation at 4 °C. An equivalent volume of DMSO was used as a control and also incubated overnight at 4 °C. PRIMA-1 in DMSO was pre-heated at 90 °C for 20 min and cooled to room temperature prior to use. Annexin A2, S100A4, and S100A10 were used as control proteins in order to rule out nonspecific interactions between compounds and p53. SyproOrange stain (Bio-Rad, Hercules, CA) at 5000X stock concentration was diluted in 20 mM HEPES at pH 7.5 and added to each well for a final 5X concentration. Each protein and compound condition was tested as replicates of 6 with 20 μL per well of a 96-well plate. TSA was

performed on $p53^{WT}$DBD and mutant $p53^{G245S}$DBD using the CFX96 Touch RT-PCR system (Bio-Rad) by increasing the temperature of the plate 0.5 °C per min from 25 °C to 52.5 °C. TSA was performed on $p53^{R175H}$DBD using the CFX96 Touch RT-PCR system by increasing the temperature of the plate 0.5 °C per min from 10 °C to 52.5 °C. Fluorescence measurements were taken once every minute during all experiments. T_m values for each well, mean T_m values, and 95% confidence intervals were calculated with the program Prism 5 (GraphPad Software, La Jolla, CA) by fitting the raw fluorescence data to a Boltzmann sigmoidal curve.

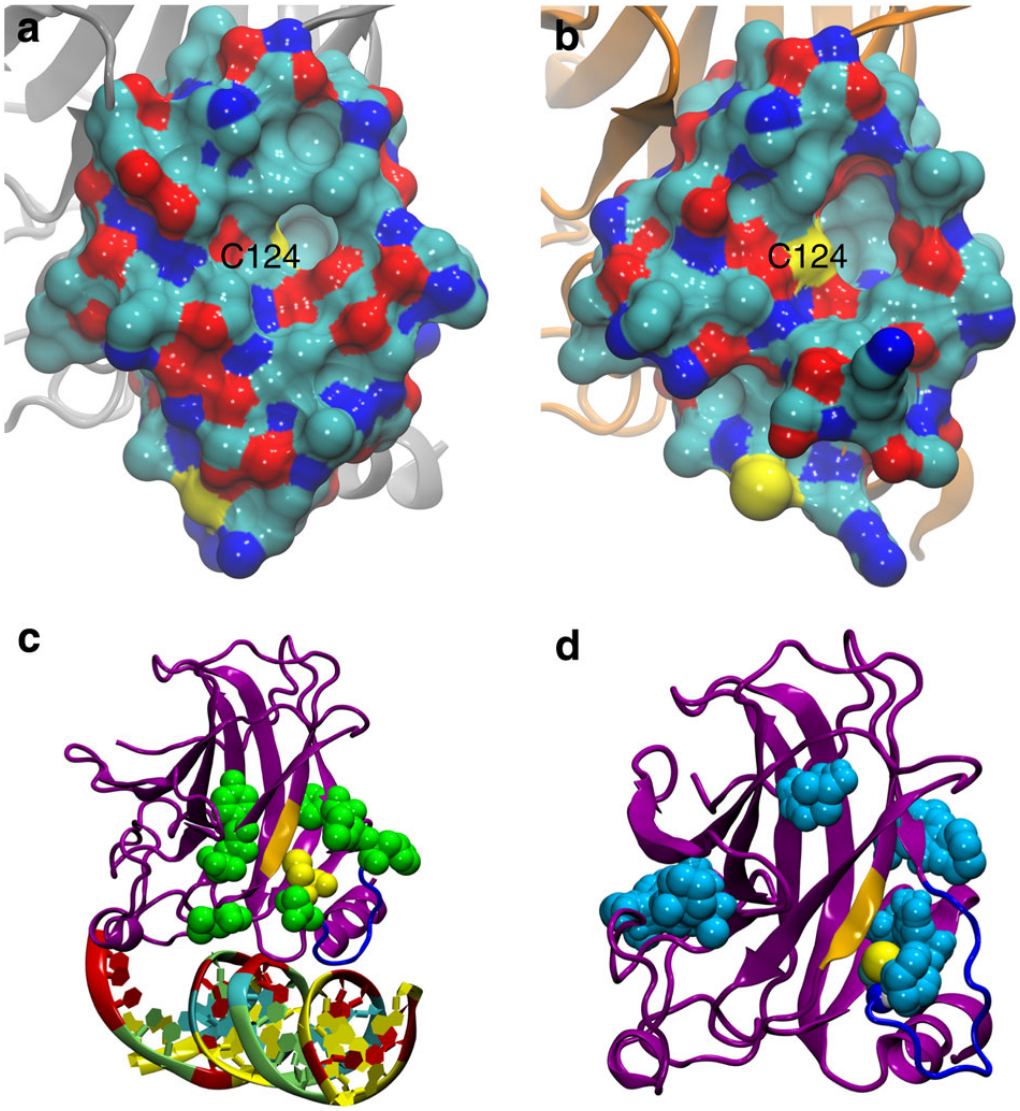

Figure 3.1. Molecular visualizations of the p53DBD (1TSR-B [12]). (a, b) All residues within 10 Å of Cys124 are shown in a surface representation coloured by atom type: cyan, C; blue, N; red, O; yellow, S. (a) Cys124 is initially occluded in the wild-type crystal structure. (b) Structure extracted from MD simulations of mutant $p53^{R273H}$DBD reveals new breathing structural topography near Cys124 within the range of normal solution dynamics. (c, d) The p53DBD is shown in magenta, loop L1 in blue, strand S3 in gold. (c) Cys124 (yellow) is surrounded by genetic mutation sites that can reactivate p53 function (green). (d) Open pockets (cyan) from FTMAP[98] for the R273H mutant. The open L1/S3 pocket surrounds Cys124 (yellow).

Table 3.1. Summary of MD simulation trajectories and open pocket occurrences.

	wt p53	R175H	G245S	R273H	C124A
Total number of clusters in trajectory	28	39	74	41	50
Open pocket as % of total trajectory by geometric criteria	6.3	7.3	6.7	5.0	5.4
Open pocket as % of total trajectory by Fpocket[43]	27.3	29.9	22.9	7.3	35.3
Avg. SASA Å^2 ± s.d. of Cys124 side chain in MD	10.93 ± 4.81	9.58 ± 4.45	6.94 ± 4.71	8.38 ± 5.84	(124Ala value) 4.45 ± 2.99
Cys124 exposure as % of MD frames with SASA > 5 Å^2	90.80	86.97	60.70	64.97	(124Ala value) 34.20
Avg. SASA Å^2 ± s.d. of Cys141 side chain in MD	0.51 ± 0.84	1.03 ± 1.27	0.56 ± 0.86	0.78 ± 1.32	1.56 ± 1.54
Cys141 exposure as % of MD frames with SASA > 5 Å^2	0.33	1.53	0.43	2.06	3.00
Avg. SASA Å^2 ± s.d. of Cys135 side chain in MD	0.17 ± 0.48	0.41 ± 0.91	0.09 ± 0.27	0.09 ± 0.34	0.20 ± 0.44
Cys135 exposure as % of MD frames with SASA > 5 Å^2	0.06	0.50	0.00	0.00	0.03

MD, molecular dynamics; SASA, solvent-accessible surface area.

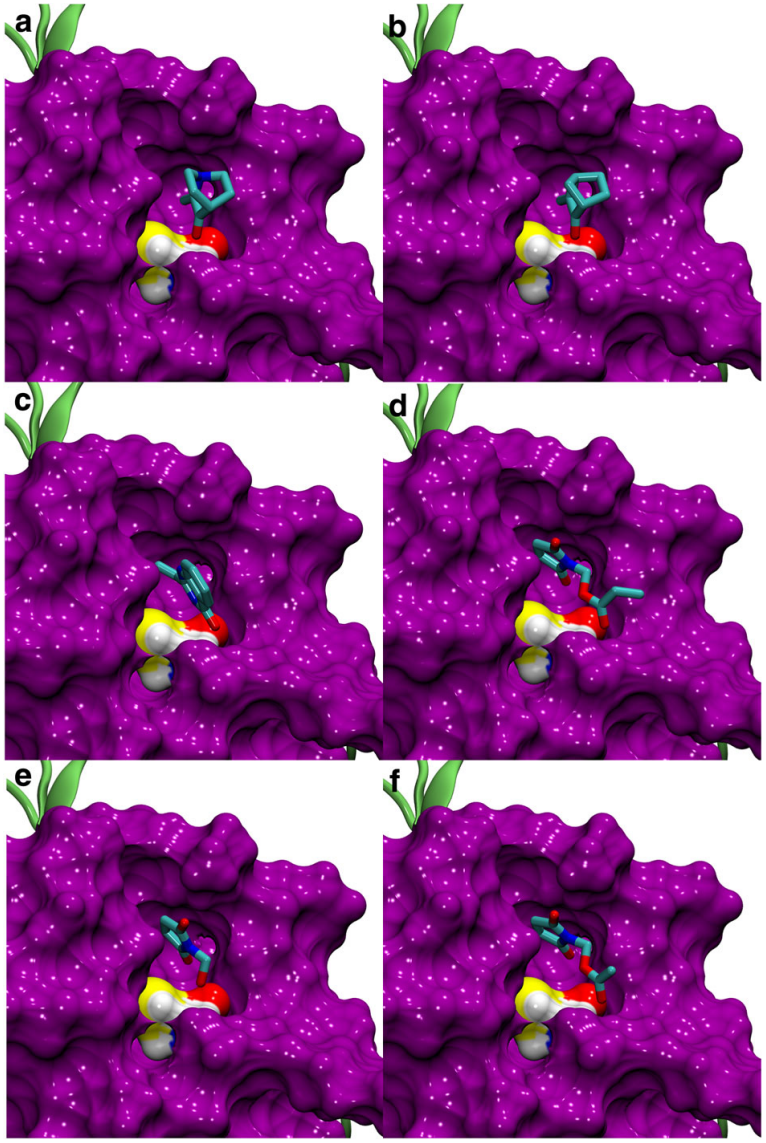

Figure 3.2. Known p53 reactivation compounds docked into the open L1/S3 pocket of p53^{R175H}DBD. (a) MQ (from PRIMA-1)[30], (b) NB[81], (c) STIMA-1[26], (d) MIRA-1[25], (e) MIRA-2[25], (f) MIRA-3[25]. Known p53 reaction compounds could dock favourably into the most-populated R175H MD trajectory cluster centroid that had an open L1/S3 pocket. All of the nine docking poses generated by Autodock Vina for each compound above scored within the published standard error of Autodock Vina docking scores [116]. In each case, the binding pose depicted above had the smallest distance between the reactive methylene of the small molecule and the Cys124 sulphydryl group. The protein surface representation is purple, except Cys124 atoms are coloured by atom type as in Figure 3.1(a, b).

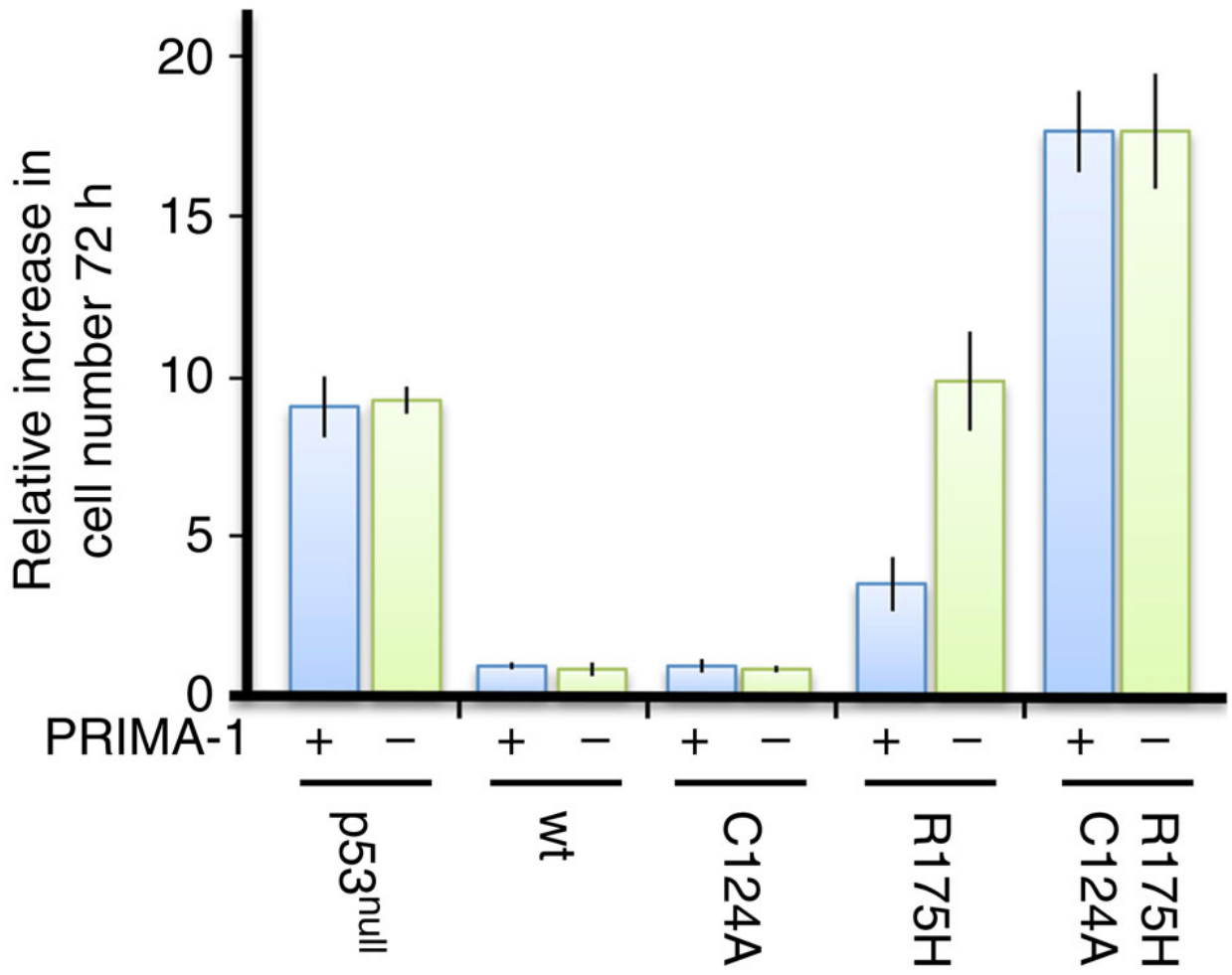

Figure 3.3. PRIMA-1 acts through cysteine 124 in p53. $p53^{null}$ Saos-2 cells expressing $p53^{WT}$, or the indicated p53 mutants, were treated with 50 μM pre-heated PRIMA-1 (blue bar) or the medium without PRIMA-1 (DMSO, green bar) for 72 h. The increase in cell number during 72 h of growth is shown. Standard deviations represent 4 independent samples.

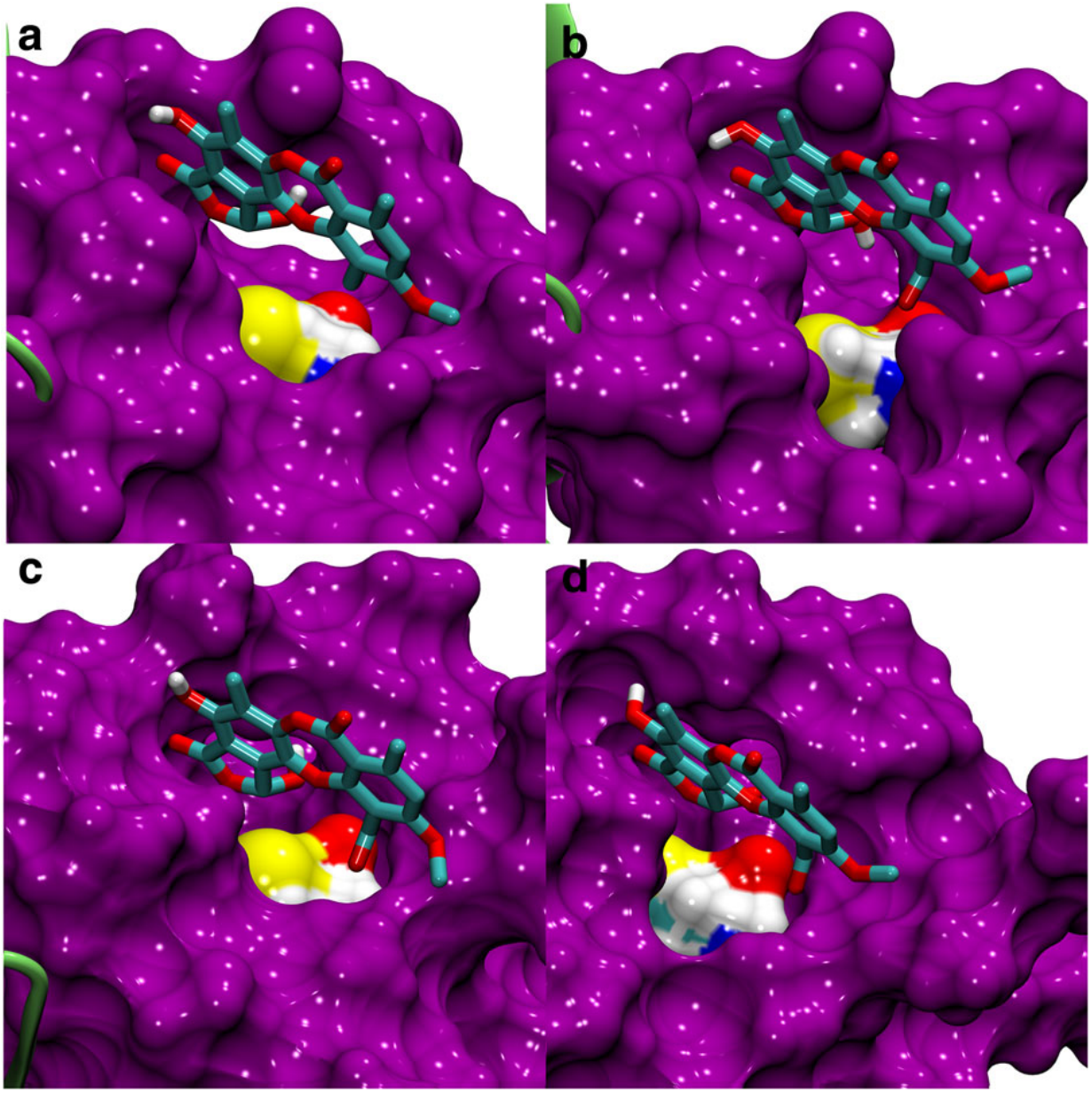

Figure 3.4. Stictic acid docked into open L1/S3 pocket of p53 variants. Stictic acid could dock favourably into the open L1/S3 pocket of MD-generated snapshots for all four p53 variants studied: (a) $p53^{WT}$DBD; (b) $p53^{R175H}$DBD; (c) $p53^{R273H}$DBD; (d) $p53^{G245S}$DBD. Only polar hydrogens of stictic acid are depicted here. Colours are as in Figure 3.2.

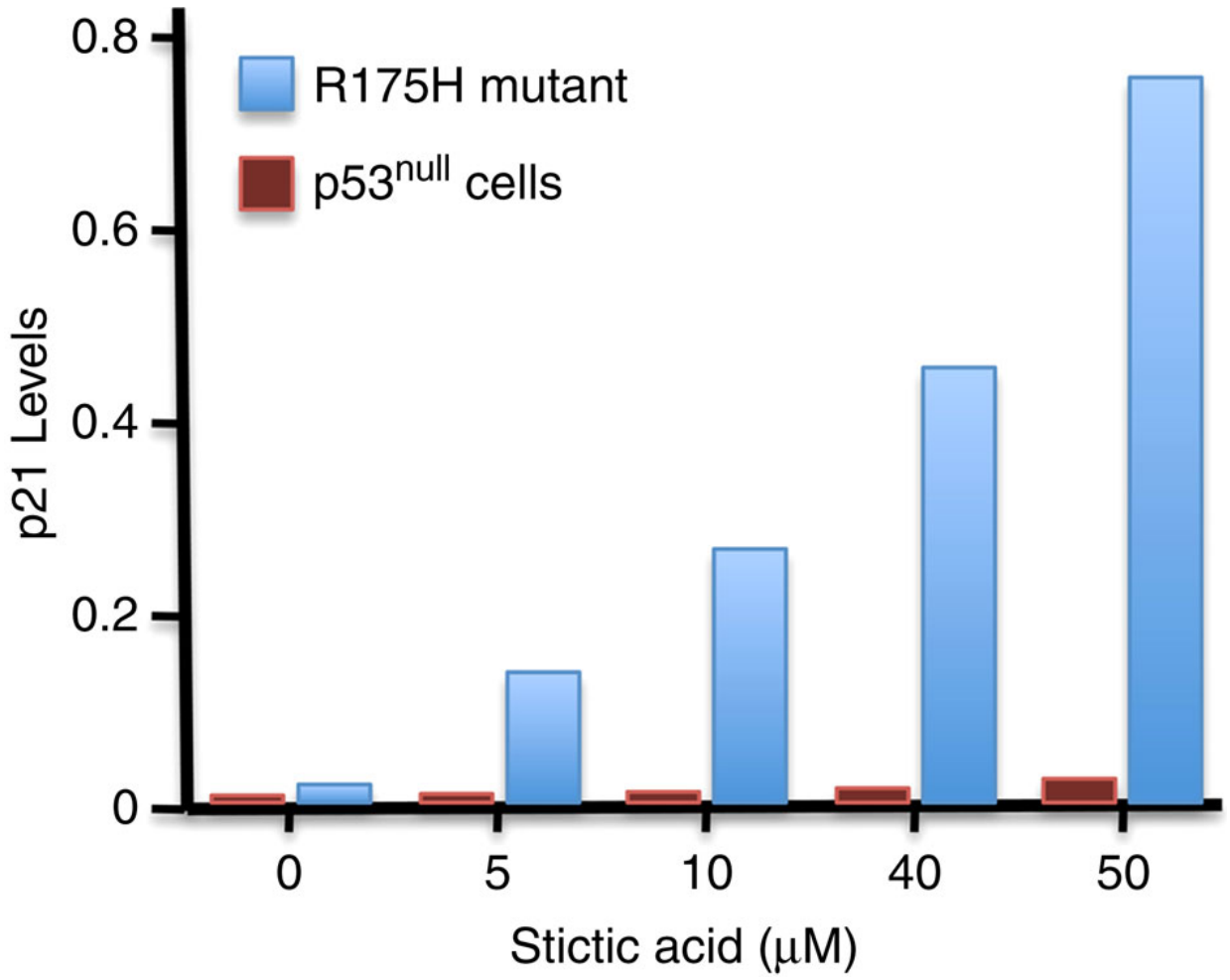

Figure 3.5. Dose-dependent p21 activation in response to stictic acid.

Saos-2 cells ($p53^{null}$) and Saos-2 cells stably expressing the cancer mutant $p53^{R175H}$ were treated with doxycycline for 8 h to induce expression of $p53^{R175H}$. Cells were then grown for 48 h in the presence of stictic acid at the concentrations indicated. p21 expression was quantified using a Fuji LAS-4000 imaging system and plotted normalized to expression of tubulin in each sample.

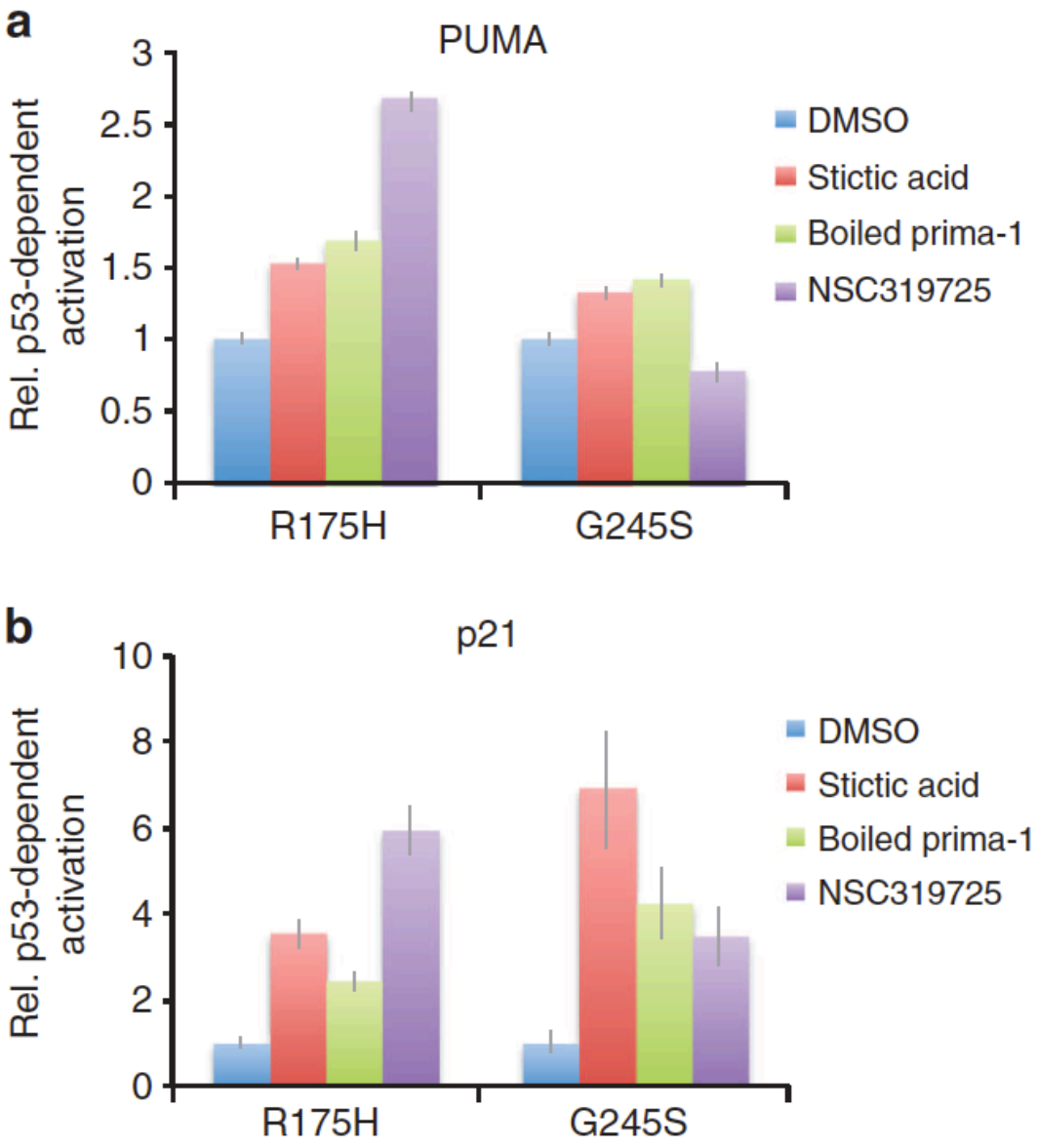

Figure 3.6. p53-dependent activation of PUMA and p21 transcription reporter by reactivation compounds. Pre-heated [30] PRIMA-1 (25µM), NSC319425 (25µM) and stictic acid (10µM) were added to stable Soas-2 ($p53^{null}$) cell lines harboring PUMA (a) or p21 (b) dependent luciferase reporter and expressing the $p53^{R175H}$ or $p53^{G245S}$ mutants as indicated. Activation of PUMA and p21transcriptional reporter was measured by luciferase activity assays. Reporter cell lines without p53 expression were processed in parallel and used for normalization to visualize p53-dependent effects. Data are represented as mean ± SD (n=4).

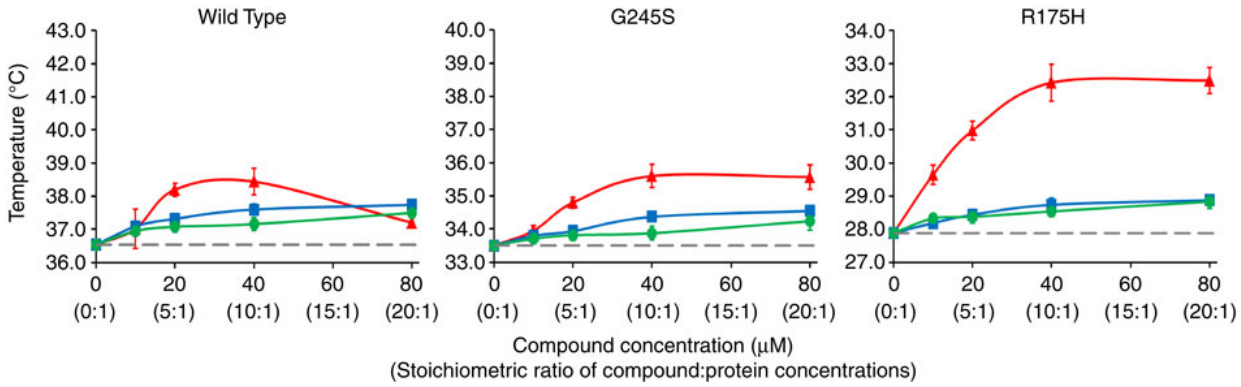

Figure 3.7. Thermal stabilization of p53 mutants by reactivation compounds.
Selected concentrations of PRIMA-1 (blue, square), MQ (green, circle), and stictic acid (red, triangle) were added to 4 μM of $p53^{WT}$DBD, $p53^{G245S}$DBD, and $p53^{R175H}$DBD protein. Thermal stabilization was measured using a thermal shift assay. Data points are plotted as the mean of sextuplet measurements, with corresponding 95% confidence intervals. Confidence interval bars not visible are smaller than the symbol used to plot the data point. PRIMA-1 and MQ stabilized each p53 variant about 1 °C or less over this range of concentrations. Stictic acid resulted in the greatest stabilization for both p53 mutants studied.

CHAPTER 4: Reactivator Identification through DNA-binding Domain Stabilization

INTRODUCTION

Studies have shown that genetically reintroducing functional p53 into cancers with *p53* mutations induces high rates of cell-cycle arrest and apoptosis as well as sensitization to traditional chemotherapies[18,20,22,119], demonstrating a therapeutic potential for restoring p53 activity. Cancer cells containing *p53* missense mutations continue to express high levels of full-length, missense p53 protein[11]. This pool of mutant p53 protein creates a significant avenue for anticancer therapeutics if a pharmaceutical can be developed that is able to restore activity to these nonfunctional p53 proteins. Several studies have identified small molecules that potentially restore wild-type (WT) function to oncogenic p53 mutants[32], including CP-31398[23], PRIMA-1MET (also known as APR246)[24,30,120], PhiKans[82], SCH529074[27], NSC319726[54], stictic acid[17] (described in Chapter 3), and MPK-09[28]. Other than the *in silico* discovery of stictic acid, most of these studies have focused on cancer cell-based approaches for small molecule discovery. Although one mutant p53-reactivating small molecule, PRIMA-1MET, had progressed to phase I/II clinical trials in Sweden[31], the clinical development of the above small molecule reactivators has been hindered by the lack of understanding of their molecular interactions and mechanism.

Because of the shortcomings of such cell-based approaches and the successes in collaboration with the validation of stictic acid, we designed an *in vitro* screen based on purified mutant p53, relying on direct small molecule/p53 interactions, to identify potential reactivating compounds. We focused our efforts on the R175H mutation (Arg175

to His), occurring in the p53 DNA-binding domain (DBD), for two reasons. First, $p53^{R175H}$ is the most common mutation in *p53*, comprising 5.0% of all missense mutations[1]. Second, R175H creates a highly destabilized p53DBD with a melting temperature (T_m) of 29 °C, about 10 °C below that of the $p53^{WT}$DBD[15,17,45]. In the $p53^{WT}$DBD, Arg175 forms a salt bridge with Asp184 within loop L2 of the zinc-binding region of the protein. The coordination of zinc is known to be important for the structural integrity and function of the domain[45,121] and reports indicate that zinc coordination is impaired in $p53^{R175H}$DBD[121]. As 80% of p53DBD mutations are conformational in nature, $p53^{R175H}$DBD is an ideal surrogate for the most common class of *p53* mutations. A small molecule that can restore thermodynamic stability to $p53^{R175H}$DBD or other p53DBD mutants that are predominantly unfolded at physiological temperature could potentially allow these mutants to regain wild-type p53 tumor suppressor functions within the cancer cell.

We employed an *in vitro* protein stability assay (TSA)[100-102] to screen 2,679 small molecules from the National Cancer Institute Developmental Therapeutics Program (NCI/DTP) for their ability to thermodynamically stabilize R175H DBD protein. Fourteen compounds stabilized $p53^{R175H}$DBD by at least 2 °C in the screen. One of these compounds, NSC635448, stabilize $p53^{R175H}$DBD by 10 °C, restoring its T_m to that of p53±DBD. When added to cancer cells harboring either $p53^{R175H}$ or $p53^{G245S}$ mutations, NSC635448 prevented cell proliferation and induced cell death in a p53-dependent manner, consistent with restoring activity to these p53 cancer mutants.

RESULTS

Small Molecule Screening

In order to identify compounds which can bind and thermodynamically stabilize the wild-type fold of the conformational cancer mutant p53^{R175H}DBD, we developed a p53±DBD-based *in vitro* screen utilizing a thermal shift assay (TSA)[100-102]. TSA is a biophysical technique capable of detecting protein-ligand interaction and stabilization through changes in protein melting temperature. The 2,679 compounds screened consisted of the four small molecule libraries available through NCI/DTP: Diversity Set II: 1,579 compounds; Approved Oncology Drugs Set II: 101 compounds; Natural Products Set II: 120 compounds; and Mechanistic Diversity Set: 879 compounds. These are the same chemical libraries used in the virtual docking screen by our collaborators (see Chapter 3). Compounds (at 20 uM) were considered for further evaluation if they raised the T_m of p53^{R175H}DBD (at 4 uM) by greater than 2 °C compared to that of the vehicle control on the same plate. 14 compounds from the screen were determined to increase the T_m of p53^{R175H}DBD by at least 2 °C, resulting in a hit rate of 0.56%.

In Vitro Validation of Screening Hits

Of these 14 compounds, 13 were available from NCI/DTP as individual samples in milligram quantities, allowing further testing to be performed. Individual samples of the 14 compounds were tested at 20 μM, 40 μM, and 80 μM concentrations for their dose-dependent thermal stabilization of 4 μM p53^{R175H}DBD (Fig. 4.1). Six of the individual samples received were not able to reproduce the stabilization of p53^{R175H}DBD by more than 2 °C at 20 μM observed in the original screen. Six of the screening hits stabilized p53^{R175H}DBD between 2 °C and 4 °C at 20 μM. NSC635448 stabilized p53^{R175H}DBD by more than 10 °C, to 43.50 ±0.07 °C at 80 μM. This addition of NSC635448 (at 40 μM or 80 μM) restores the thermodynamic stability of p53^{R175H}DBD to the level of p53^{WT}DBD.

Cellular-Based Validation of Screening Hits

The 13 hits from the *in vitro* $p53^{R175H}$DBD stabilization assay were also analyzed for their ability to reactivate the $p53^{R175H}$ mutant in cancer cells at physiological temperature. These assays utilized $p53^{null}$ ($p53^{-/-}$) human osteosarcoma Saos-2 cells as the parental line, which were engineered to stably express doxycyclin-inducible oncogenic p53 mutants[17]. Induced expression of $p53^{WT}$ in these cells prevents proliferation and induces cell death, whereas expression of $p53^{R175H}$ has no effect on cellular growth[17]. Compounds that restore activity to $p53^{R175H}$ are expected to block cell proliferation and induce cell death in $p53^{R175H}$-expressing cancer cells but should have no effect on the otherwise isogenic $p53^{null}$ Saos-2 parent cells. Briefly, a dose range of each of the 13 hits identified in the $p53^{R175H}$DBD thermal stabilization screen was first tested on the $p53^{null}$ Saos-2 cells to determine the highest dose that does not affect proliferation of Saos-2 cells (C_{max}). Next, Saos-2 cells expressing $p53^{R175H}$ and the $p53^{null}$ parental cells were cultured at the C_{max} doses of compound and cell counts were determined after 3 days. Reactivation of mutant p53 can be distinguished readily from general cytotoxic effects of compounds because general cytotoxic activity blocks cell proliferation of both $p53^{null}$ control cells and p53 mutant expressing cells. Thus selective effects of compounds on $p53^{R175H}$ cells are due to effects mediated by $p53^{R175H}$, and indicate that the compound was able to restore wild-type p53 activity. For example, PRIMA-1, the well-studied p53 reactivation compound, significantly reduced proliferation and survival to about 50% at the highest concentration that did not affect $p53^{null}$ cells (50 μM) (Fig. 4.2). Most of the *in vitro* screen-selected compounds showed minor anti-proliferative effects on $p53^{R175H}$-expressing cells (Fig. 4.2), which could be due to low cell permeability, metabolic instability in cells, or most likely because their

stabilization of $p53^{R175H}$ was not substantial enough to restore activity to the $p53^{R175H}$ protein in the cell. One of the screen-selected compounds had dramatic effects on $p53^{R175H}$-expressing cells without affecting $p53^{null}$ cells (Fig. 4.2). NCS635448 reduced cell growth by 80% at a concentration of 1 μM without affecting $p53^{null}$ cells. Significantly, NSC635448 was the only screen-identified compound that restored the T_m of $p53^{R175H}$DBD back to that of $p53^{WT}$DBD (Fig. 4.1). The remainder of our work is focused on lead compound NSC635448, which we have termed UCIPRO-001 (Universal Cancer Inhibitor p53 Reactivating Organic-metallic).

Thermal Stabilization of p53DBD by UCIPRO-001

This lead compound, UCIPRO-001, belongs to a class of chemicals known as thiosemicarbazones. The antineoplastic effects of thiosemicarbazones have been known for some time[122,123] and only very recently were thiosemicarbazones identified for their ability to target mutant p53[54]. Yu *et al.* have independently discovered the $p53^{R175H}$-reactivating thiosemicarbazones, NSC319725 and NSC319726, through a large-scale analysis of NCI drug screen data[54]. UCIPRO-001 and NSC319725 are structurally similar molecules but differ by the presence of CuBr in UCIPRO-001 (Fig. 4.3). The presence of CuBr in UCIPRO-001 is not unusual, as thiosemicarbazones contain a tridentate nitrogen-nitrogen-sulfur moiety which allows coordination of a wide variety of transition metals including copper, iron, and zinc[124], creating metal complexes. Based on the structural similarities, the fact that UCIPRO-001 is able to substantially stabilize $p53^{R175H}$DBD, and recent reports demonstrating anti-proliferative effects of NSC319725 on $p53^{R175H}$-harboring cancer cell lines[54], it was anticipated that NSC319725 might also increase the T_m of $p53^{R175H}$DBD. The thermodynamic stabilization of $p53^{R175H}$DBD (at 5 μM) by NSC319725, obtained through

NCI/DTP, was evaluated from 6.25 μM to 100 μM compound concentrations, analogous to the validation of preliminary hits from our small molecule screening (Fig 4.4). Owing to the fact that our previous results as well as that of others indicated that cysteines may be important in the binding and stabilization of the p53DBD by ligands, we included low amounts of reducing agent (0.1 mM TCEP) in the buffer for the TSA. Surprisingly, NSC319725 produced no stabilization of $p53^{R175H}$DBD across this range of concentrations. Owing to the presence of copper in UCIPRO-001, which can be coordinated by thiosemicarbazones, NSC319725 was mixed with an equimolar concentration of $Cu(II)Cl_2$ and again tested with for the stabilization of $p53^{R175H}$DBD. Upon addition of 12.5 μM or greater 2.5X molar excess or greater), NSC319725 plus $CuCl_2$ increased the T_m of $p53^{R175H}$DBD by approximately 40 °C, demonstrating stabilization at lower concentrations than UCIPRO-001. To determine whether this $p53^{R175H}$DBD stabilization was specific to NSC319725 with *copper*, NSC319725 was also tested with the addition of $Fe(II)Cl_2$ and $Zn(II)Cl_2$. NSC319725 with $FeCl_2$ did not stabilize $p53^{R175H}$DBD. Addition of NSC319725 with $ZnCl_2$ to $p53^{R175H}$DBD caused dose-dependent destabilization of the protein. The thermodynamic stability of $p53^{R175H}$DBD was also examined with $CuCl_2$, $FeCl_2$, and $ZnCl_2$ in the absence of a thiosemicarbazone. $CuCl_2$ and $ZnCl_2$ alone reduced the stability of the protein by 10 °C and $FeCl_2$ alone reduced the T_m of the protein by approximately 1 °C.

These same thermal stabilization were carried out with the analogous thiosemicarbazone NSC319726, also discovered by Yu *et al.* for its capacity to restore activity to $p53^{R175H}$ in cancer cells[54] and two other structurally similar thiosemicarbazones UCIPRO-002 (NSC335792) and UCIPRO-003 (NSC335793) obtained from NCI/DTP. All four thiosemicarbazones display similar results (Fig 4.4). The thiosemicarbazone alone has no

effect on the thermal stability of $p53^{R175H}$DBD. However upon addition of equimolar $CuCl_2$ to the thiosemicarbazone prior to addition to the protein, the copper thiosemicarbazone is able to stabilize $p53^{R175H}$DBD by 30 °C or more. The thiosemicarbazone Triapine® is thought to inhibit the enzyme ribonucleotide reductase, which is an important step in the catalysis of DNA[125,126], and is currently in clinical trials for its antitumor effects[127,128]. Triapine® increases the T_m of $p53^{R175H}$DBD by 20 °C, beyond the T_m of $p53^{WT}$DBD, albeit requiring a concentration of 50 μM to do so.

These same combinations of UCIPRO-001-like thiosemicarbazones and transition metals were also tested with $p53^{G245S}$DBD, the second most frequent conformational *p53* mutation[1], and $p53^{WT}$DBD, yielding analogous results to $p53^{R175H}$DBD (Fig. 4.4): UCIPRO-001 and copper thiosemicarbazones increased the T_m of both $p53^{G245S}$DBD and $p53^{WT}$DBD. Thiosemicarbazones alone resulted in no effect on the thermal stability of p53G245SDBD and $p53^{WT}$DBD.

Effects of UCIPRO-001 on $p53^{R175H}$ and $p53^{G245S}$ Cancer Cells

To further characterize the lead compound UCIPRO-001, we continued analysis with engineered Saos-2 cells expressing $p53^{R175H}$ or $p53^{G245S}$. Dose-response experiments showed that UCIPRO-001 reactivates both $p53^{R175H}$ and $p53^{G245S}$ mutants, although with somewhat lower efficacy towards the $p53^{G245S}$ allele (Fig. 4.5). Similar to the previously reported $p53^{R175H}$ reactivation compound NSC319725, UCIPRO-001 shows potent anti-neoplastic effects dependent on expression of the oncogenic $p53^{R175H}$ or $p53^{G245S}$ mutants. UCIPRO-001 is most effective against $p53^{R175H}$ and $p53^{G245S}$, with EC50 (concentration which effectively kills half of the cell population) values of 32.1 nM and 407 nM,

respectively. Illustrating its mutant p53-dependent activity, UCIPRO-001 is relatively less toxic to $p53^{null}$ osteosarcoma cells, with an EC50 value of 2.46 μM. UCIPRO-001 is also comparatively less toxic to healthy ($p53^{WT}$) neural progenitor cells (EC50 5.19 μM).

Role of Transition Metals in Cell-Based Reactivation of $p53^{R175H}$

Since addition of copper to NSC319725 had dramatic effects on the compound's ability to stabilize $p53^{WT}$DBD *in vitro* (Fig. 4.4), we compared NCS319725 with and without the addition of equimolar concentrations of $Cu(II)Cl_2$, $Fe(II)Cl_2$, or $Zn(II)Cl_2$ in our osteosarcoma cell-based assay (Fig. 4.6). Addition of $CuCl_2$ to NSC319725 did not dramatically enhance reactivation of $p53^{R175H}$ in cell culture after 48 hours, likely because NSC319725 chelates free copper ions in the cell or the growth medium. However, supplementation of NSC319725 with $FeCl_2$ reduced the anti-proliferative effects of NSC319725. Addition of $ZnCl_2$ to NCS319725 caused marked toxicity to both the $p53^{R175H}$ and $p53^{null}$ cell lines. Transition metal salts $CuCl_2$, $ZnCl_2$, or $FeCl_2$ alone showed no effect on $p53^{R175H}$ reactivation, suggesting that the rescue activity of UCIPRO-001, which complexes copper, is in fact due to the copper-coordinated thiosemicarbazone, not the metal ion itself.

Small Molecule Characterization

The identity and purity of UCIPRO-001 and NSC319725 obtained from NCI/DTP were evaluated using liquid chromatography mass spectrometry (LC-MS). The expected monoisotopic mass of the thiosemicarbazone UCIPRO-001 based upon the chemical structure provided by NCI/DTP is 364 Da. LC-MS demonstrated a molecular mass of only 311 Da with the presence of a copper isotope distribution. This experimental mass corresponds to the UCIPRO-001 thiosemicarbazone backbone provided by NCI/DTP with

one methyl group removed, the coordination of a copper atom, lacking bromine, with an additional sodium atom and water molecule. To confirm its identity and determine the location of the missing methyl group, the crystal structure of UCIPRO-001 was solved (Fig 4.3). This crystal structure indicated the absence of a methyl group at N4 and confirmed the presence of a coordinated copper ion. The copper moiety interacts with two bromine atoms in the crystal structure. Disparity between copper coordination in the crystal structure (two bromine atoms present) and LC-MS results (absence of bromine with addition of sodium ion and water molecule) can be attributed to the fact that UCIPRO-001 was crystallized in the absence of water but evaluated in aqueous buffer during LC-MS experimentation. Based on the presence and size of other peaks observed during LC-MS, the approximate molar purity of our UCIPRO-001 stock is 80%. For NSC319725, the expected monoisotopic mass of at 222 Da correlates with the 223 Da mass observed using LC-MS, confirming the identity of the molecule provided by NCI/DTP (Fig. 4.3). LC-MS results indicated the approximate molar purity of the NSC319725 sample to be 85%. While it is possible that the p53 stabilization and reactivation observed in the experiments were due to impurities present in the UCIPRO-001 and NSC319725 samples, we find this is unlikely since it would require similar copper binding impurities be present in both samples. To validate that NSC319725 is able to ligate copper, an equimolar concentration of $CuCl_2$ was mixed with NSC319725 to obtain its copper thiosemicarbazone form. LC-MS of NSC319725 with $CuCl_2$ resulted in an experimental mass of 325 Da with a copper isotope pattern. This mass corresponds to NSC319725 provided by NCI/DTP with a coordinated copper atom in addition to a sodium and water molecule, analogous to the LC-MS results obtained for UCIPRO-001.

DISCUSSION

Here we present the results of an *in vitro* chemical screen aimed at identifying small molecules that can restore thermodynamic stability to conformational p53 mutations, the most common type of mutation in p53 in cancers[1]. The screen was predicated on the potential of restoring activity to mutant p53 in a wide array of cancer cells by thermodynamically stabilizing mutant p53DBD. The lead compound, UCIPRO-001, raises the T_m of $p53^{R175H}$DBD and $p53^{G245S}$DBD by over 30 °C and displays anti-proliferative effects on osteosarcoma cells harboring the $p53^{R175H}$ and $p53^{G245S}$ mutations, with an IC_{50} well below 1 μM.

UCIPRO-001 appears to be a promising reactivator of oncogenic p53 mutants through stabilization of the p53DBD. The anticancer effects of certain thiosemicarbazones have been known for some time[122,123], but only recently was it reported that p53 might be an important molecular target for these compounds[54]. It is interesting that with the same aim of identifying small molecules that restore function to p53 mutants, but using an entirely different approach, we have independently discovered thiosemicarbazones for their mutant p53-reactivating properties as Yu *et al.*[54].

Following their identification of thiosemicarbazones NSC319725 and NSC319726 for targeting mutant p53, Yu *et al.* recently published work on determining the mechanism by which thiosemicarbazones restore function to mutant p53. Their model describes thiosemicarbazones as zinc metallo-chaperones which do not directly bind to mutant p53, but are believed to act by preventing zinc from binding in one or more low-affinity, disruptive, non-native zinc-binding pockets while allowing zinc to be bound at the native

high-affinity zinc coordination site[129]. This model does not fit the data presented here. Our results indicate that copper is the transition metal that confers mutant-p53 restoring activity to thiosemicarbazones and that copper thiosemicarbazones function through binding and stabilizing mutant p53DBD. Given the structural similarities between the carbon-nitrogen backbones of UCIPRO-001 (NSC635448) and NSC319725, the slightly larger thermal stability gain resulting from copper-ligated NSC319725 compared to UCIPRO-001 is likely due to the absence of the methyl group on UCIPRO-001, the presence of bromide in UCIPRO-001, or the level of impurities in each sample. The thiosemicarbazone Triapine® is currently undergoing several Phase II clinical trials for its inhibition of ribonucleotide reductase in the radiochemotherapeutic treatment of cervical cancer, has demonstrated promising tolerability and safety[128]. We find here that this thiosemicarbazone is also able to effectively stabilize p53DBD mutants. As Triapine® has been observed to be most efficacious in cervical and ovarian cancer, which have p53 mutation rates greater than 90%, some of their efficacy may be attributed to their restoration of mutant p53 function.

Importantly, the stabilization of $p53^{R175H}$DBD and $p53^{G245S}$DBD by these thiosemicarbazones translates into restoration of $p53^{R175H}$ and $p53^{G245S}$ function in cancer cells and results in anti-proliferation of cancer cells that harbor these missense mutations. Based on the results presented here, we propose a model by which thiosemicarbazones coordinate copper, bind to and thermodynamically stabilize the p53DBD. When administered to cancer cells that harbor a p53 missense mutation, where aberrant growth signals, DNA damage, and cellular stresses have activated p53 but its function is attenuated

due to mutation, the stabilization of the mutant p53DBD allows this tumor suppressor to regain sufficient function to induce cell-cycle arrest or apoptosis.

In cell culture, NSC319725 displayed anti-proliferative effects against $p53^{R175H}$- and $p53^{G245S}$-harboring osteosarcoma cells without co-administration of copper. This is likely due to the fact that copper, as well as other transition metals, is present in the media used to culture these cells, and thus media copper is likely ligated by NSC319725 when it is added to the cell culture. In cell culture, addition of copper to NSC319725 has similar efficacies towards $p53^{R175H}$ cancer cells compared to NSC319725 administered alone (Fig. 4.6). However, prior addition of zinc to NSC319725 causes it to have substantial off-target toxicities, while addition of iron to NSC319725 greatly reduces its efficacy towards $p53^{R175H}$ cancer cells. Additionally, Lovejoy *et al.* found that addition of copper-containing thiosemicarbazones markedly increases the rate at which thiosemicarbazones exert their anti-proliferative effects compared to iron-containing thiosemicarbazones or thiosemicarbazones alone[130]. Based on our results that indicate that copper is necessary for the formation of p53-stabilizing thiosemicarbazones *in vitro*, it will be important to determine whether prior incorporation of copper into the thiosemicarbazone is beneficial for *in vivo* administration.

A significant concern for many anticancer compounds, particularly given that many of these compounds are designed to interact with targets that are not exclusive to cancer cells but may be present in normal healthy cells, is their cytotoxicity. As was demonstrated here, copper thiosemicarbazones are not specific for mutant p53DBD but also bind and stabilize $p53^{WT}$DBD. The reactivity of these copper thiosemicarbazones with $p53^{WT}$ in healthy, noncancerous cells of patients is a potential concern. However, the safety profile of

thiosemicarbazones is encouraging given that thiosemicarbazones have markedly reduced cytotoxicity against normal ($p53^{WT}$) human neuronal progenitor cells compared to cancer cells(Fig. 4.5). We expect that stabilizing $p53^{WT}$ in healthy cells in the absence of p53 activation signals has minimal effects on the activity of $p53^{WT}$. Additionally, $p53^{WT}$ is maintained at very low levels in healthy cells in comparison to cancerous cells which highly express mutant p53[11].

METHODS

WT and mutant p53 DNA-binding domain (DBD)

The $p53^{WT}$DBD (residues 94-312) had been previously introduced into the bacterial expression vector pSE420[43]. Mutant $p53^{R175H}$DBD (residues 94-292) was generated by using a site-directed mutagenesis kit in this same vector (Invitrogen, Grand Island, NY). The original $p53^{R175H}$DBD-based TSA screen was carried out using proteins containing residues 94-312. Follow-up p53DBD TSA of thiosemicarbazones and metals was done using shortened p53DBD constructs containing residues 94-292 which was generated by introducing a stop codon at Glu293 using a site-directed mutagenesis kit (Invitrogen). Mutant $p53^{G245S}$DBD (residues 94-292) was generated in this same shortened by using a site-directed mutagenesis kit in this same vector (Invitrogen). These vectors were transformed into the *Escherichia coli* Rosetta 2 (DE3) strain. Cells were initially grown at 37 °C to an OD_{600} of 1.2 before the temperature was reduced to 15 °C. Expression was induced with 1 mM IPTG (isopropyl β-D-1-thiogalactopyranoside) over 40 hours, and cells were isolated by centrifugation at 6,000 g for 8 min. p53 DBD were purified as previously described[17] and stored at −80 °C until further use. Protein concentration was determined

with a Shimadzu (Columbia, MD) UV-VIS spectrophotometer using an extinction coefficient of 15,930 cm^{-1} M^{-1} at 280 nm. All protein purification steps were monitored by 4–12% Tris-Glycine SDS–PAGE (Lonza, Basel, Switzerland) to ensure they were virtually homogeneous. All chemicals and solvents used were analytical and HPLC grade, respectively.

Protein Stabilization Assay

The largest hurdle in the mutant p53 protein-based screening of $p53^{R175H}$DBD is the expression and purification of sufficient quantities of protein (about 15 mg). Its thermodynamic instability causes initial protein unfolding to begin at about 15 °C in solution[17]. Careful handling of the purified $p53^{R175H}$DBD was necessary, with all preparations being performed either on ice, or in a cold room (4 °C) if frequent sample transferring was required. Purified p53DBD (200 μM in 20 mM HEPES at pH 7.4, 0.1 mM dithiothreitol (DTT), 150 mM NaCl) was diluted to final concentration 4 μM in 20 mM HEPES at pH 7.4. Small molecules were dissolved in DMSO (dimethyl sulfoxide) to various concentrations, added to protein samples, and allowed to incubate for 30 minutes at 4 °C prior to experimentation. An equivalent volume of DMSO was used as a negative control and also incubated for 30 minutes at 4 °C. Furthermore, lysozyme was used as a control protein with identified hits to rule out nonspecific stabilization by our hit compounds. Sypro Orange stain (Bio-Rad, Hercules, CA) at 5,000X stock concentration was diluted to a final concentration of 5X. All compounds were evaluated separately for fluorescence background distribution to identify false positive results. The original TSA was performed using the CFX96 Touch RT-PCR system (Bio-Rad, Hercules, CA) with the starting temperature of 4 °C and increasing the temperature of the plate 1.0 °C per min to 54 °C.

Follow-up TSA with thiosemicarbazones and metals was performed using the CFX96 Touch RT-PCR system (Bio-Rad) with the starting temperature of 4 °C and increasing the temperature of the plate 5.0 °C per min to 90 °C. Fluorescence measurements were taken once every minute during all experiments. Melting temperature values for each well, mean T_m values, and 95% confidence intervals were calculated for the original $p53^{R175H}$DBD-based screen with the program Prism 5 (GraphPad Software, La Jolla, CA) by fitting the raw fluorescence data to a Boltzmann sigmoidal curve. Tm values for the follow-up TSA experiments were obtained through the first derivative of the melting curves using the CFX Manager software (Bio-Rad).

Liquid chromatography Mass Spectrometry (LC-MS)

Five mg each of the 14 small molecules validated as hits from the protein stabilization screen were ordered from the National Cancer Institute, Developmental Therapeutics Program (NCI/DTP) and dissolved to 200 mM in DMSO. The small molecule stocks were diluted in water from a concentrated solution in DMSO. Purities of the samples were analyzed with a Phenomenex Kinetex 2.6u C18 100A (100x2.1 mm) column (Phenomenex, Torrance, CA) on an Agilent 1100 HPLC (Agilent Technologies, Santa Clara, CA) using mobile phase A of 2% acetonitrile (v/v) with 0.2% acetic acid (v/v) and mobile phase B of 100% acetonitrile with 0.2% acetic acid (v/v). Mobile phase B was increased as a linear gradient from 2% to 95% B in 50 minutes. Tandem mass spectrometry was performed using a Waters LC/MS with an LCT premier instrument (Waters, Milford, MA).

Crystal structure of UCIPRO-001

A drop of 8 μL of 50 mM UCIPRO-001 in 50% DMSO (v/v) 50% methanol (v/v) underwent controlled evaporation over 48 hours at room temperature using EasyXtal 15-well Tool X-Seal crystal trays (Qiagen, Germantown, MD). A green crystal of approximate dimensions 0.253 x 0.192 x 0.080 mm was mounted on a glass fiber and transferred to a Bruker SMART APEX II diffractometer (Bruker, Madison, WI). The APEX2 program package (Bruker) was used to determine the unit-cell parameters and controlled data collection (15 sec/frame scan time for a sphere of diffraction data). The raw frame data were processed using SAINT (Bruker) and SADABS (Bruker) to yield the reflection data file. Subsequent calculations were carried out using the SHELXTL program (Bruker). There were no systematic absences nor any diffraction symmetry other than the Friedel condition. The centrosymmetric triclinic space group *P*1 was assigned and later determined to be correct. The structure was solved by direct methods and refined on F by full-matrix least-squares techniques. The analytical scattering factors[6] for neutral atoms were used throughout the analysis. Hydrogen atoms were included using a riding model. The sulfur was disordered and included using multiple components with partial site occupancies (90%, 10%). There was one molecule of DMSO solvent present. At convergence, wR2 = 0.1024 and Goof = 1.081 for 195 variables refined against 3975 data (0.76 Å), R1 = 0.0407 for those 3,531 data with $I > 2.0\sigma(I)$.

$$wR2 = [\Sigma[w(F_o^2-F_c^2)^2] / \Sigma[w(F_o^2)^2]]^{1/2}$$

$$R1 = \Sigma||F_o|-|F_c|| / \Sigma|F_o|$$

Goof = $S = [\Sigma[w(F_o^2-F_c^2)^2] / (n-p)]^{1/2}$ where n is the number of reflections and p is the total number of parameters refined.

The thermal ellipsoid plot is shown at the 50% probability level.

Cell lines

Soas-2 cells were obtained from the American Type Culture Collection (Manassas, VA, USA) and cultured at 37 °C in DMEM high glucose supplemented with 10% FBS, penicillin G sodium (100 units ml^{-1}), and streptomycin (100 μg ml^{-1}). Stable Soas-2 $p53^{null}$ cell lines harboring doxycycline-inducible p53 wild type or mutants were established by a lentivirus-based strategy and are described[17]. Doxycycline was used at a concentration of 1 μg ml^{-1} to induce expression of *p53* alleles. For generation of stable cell lines to measure p53-dependent activation of p21 or PUMA reporters, p21 (5′-GAAGAAGACTGGGCATGTCT-3′) or PUMA (5′-CTGCAAGTCCTGACTTGTCC-3′) response elements followed by a minimal promoter (5′-TAGAGGGTATATAATGGAAGCTCGACTTCCAG-3′) were inserted into *Kpn*I/*Xho*I cut plasmid pGL4.10 (Promega). These elements control the expression of a synthetic firefly *luc2* (*Photinus pyralis*) gene. A SV40-driven puromycin resistance cassette was inserted into the *Pst*1 site of pGl4.10 to enable generation of stable cell lines. The PUMA and p21 reporter vectors were transfected into Soas-2 cells and single colonies resistant to 50 μg ml^{-1} puromycin were selected and tested (Soas-2-PUMA-luc2 or Soas-2-p21-luc2).

Cell viability assay

Cells were cultured in 96-well plates at a density of 10,000 cells per well and incubated overnight. Doxycycline (final concentration 1 μg ml^{-1}) was added to induce the expression of p53 for 8 h before compounds were added at the indicated concentrations. Cell viability assays were performed after 3 days using CellTiter-Glo Luminescent Cell Viability Assay

(Promega, Wisconsin, MD) according to the manufacturer's instructions. Data represent the average of four independent samples.

PUMA and p21 reporter assay

Soas-2-PUMA-luc2 or Soas-2-p21-luc2 cell lines were transfected with 500 ng of cytomegalovirus-renilla plasmid and 125 ng of plasmid carrying either empty vector, WT p53 or mutant R175H using Lipofectamine 2000. The different compounds were added 21 h after transfection. Activation of the PUMA and p21 reporters was analyzed by a luciferase assay (dual luciferase assay system, Promega) 8 h after the addition of compounds.

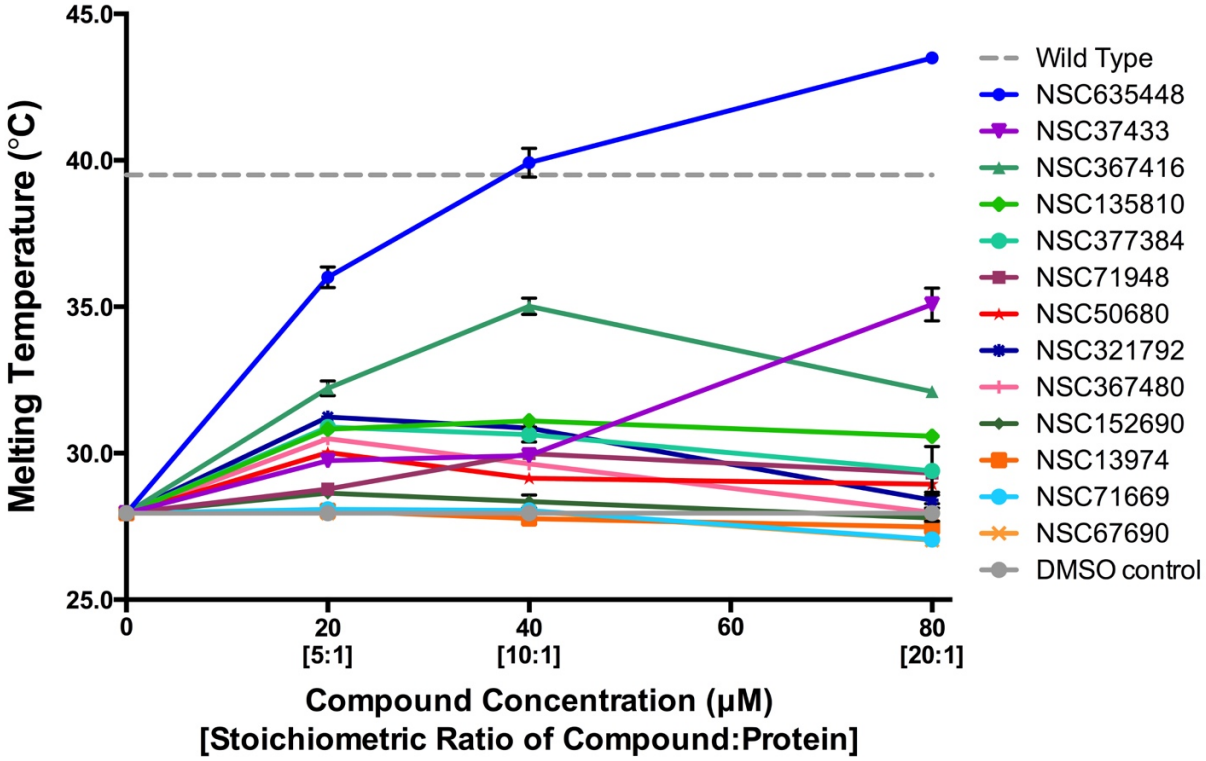

Figure 4.1. Thermal stabilization of p53^{R175H}DBD by identified screen hits. R175H DBD protein, at 4 μM, was used with compound concentrations of 20, 40, 80 μM (5:1, 10:1, and 20:1 compound:protein ratios). The dashed line at 39.5 °C represents the T_m of WT DBD.

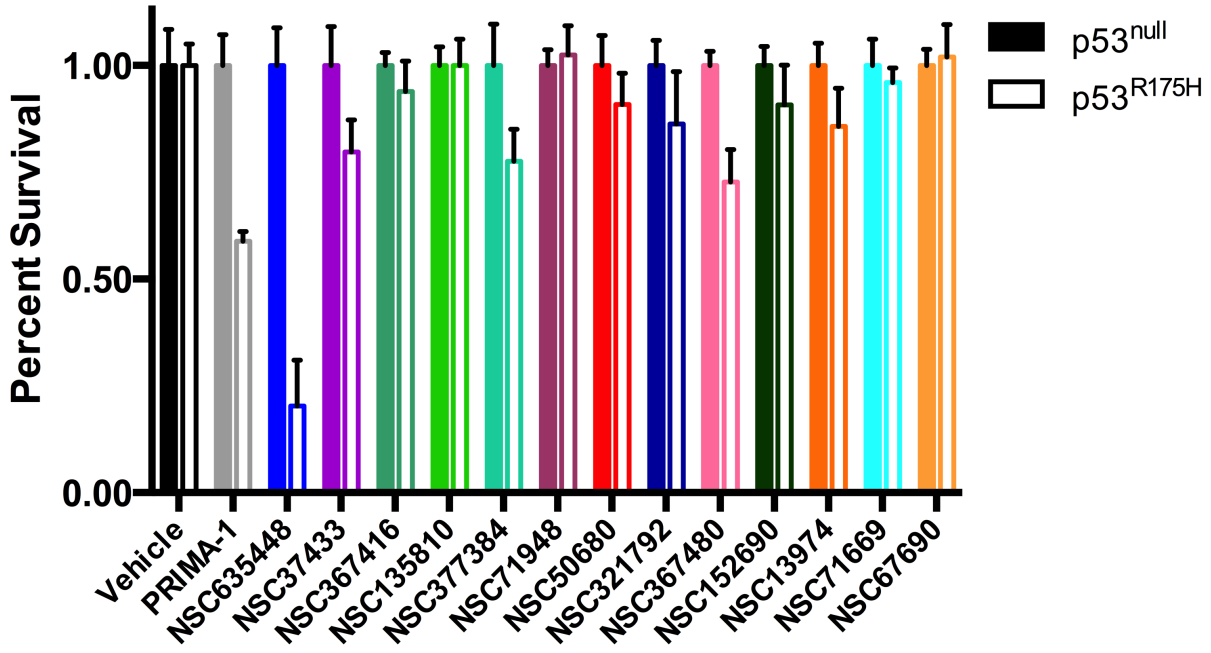

Figure 4.2. Effects of identified screening hits on the proliferation of $p53^{null}$ and $p53^{R175H}$ osteosarcoma cells. Saos-2 cells expressing no p53 ($p53^{null}$) or the cancer mutants $p53^{R175H}$, were cultured in the presence of different concentrations of thermal shift screened potential reactivation compounds for 3 days. Cell numbers were measured using the CellTiter-Glo® reagent. Results for the highest compound concentration (max. 100µM) that did not affect cell proliferation of the parental Saos-2 ($p53^{null}$) cells are shown: PRIMA-1 (50µM), NSC635448 (1 µM), NSC71948 (50µM), NSC367416 (50µM), NSC152690 (50µM), NSC377384 (50µM), NSC13974 (20µM), NSC37433 (100µM), NSC135810 (50µM), NSC321792 (50µM), NSC50680 (50µM), NSC367480 (40µM), NSC67690 (20µM), NSC71669 (10µM). Data are presented as mean with standard deviation (n= 3).

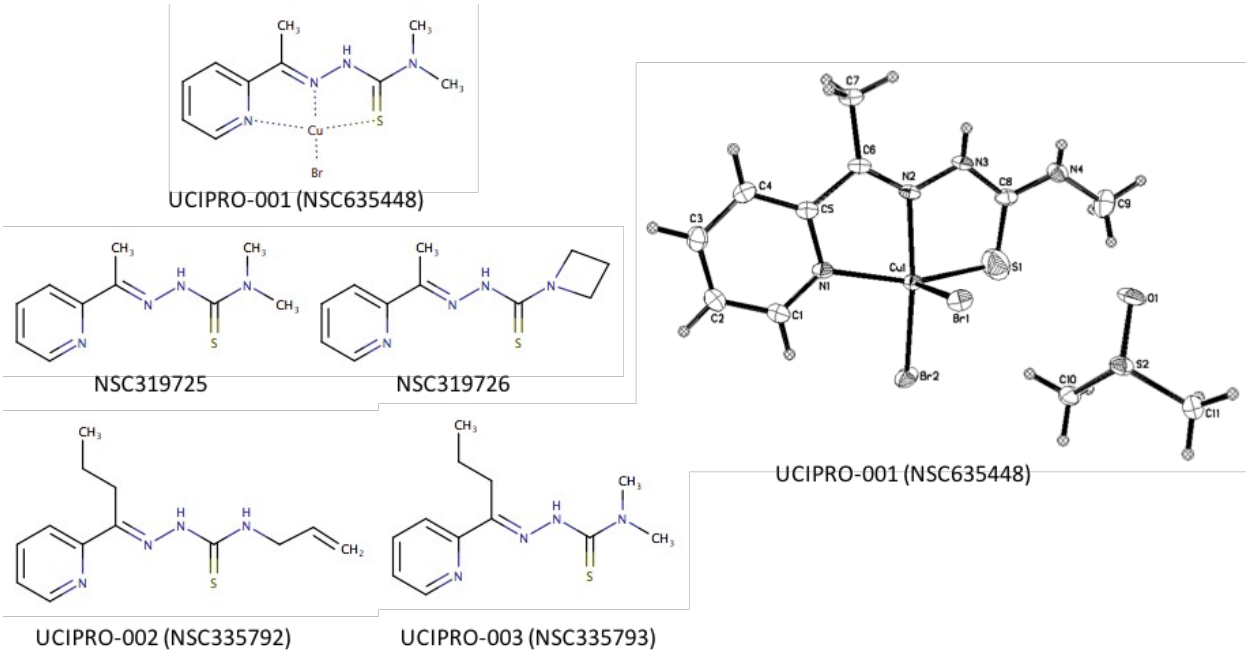

Figure 4.3. Chemical structures of thiosemicarbazones. Chemical representation (left) of UCIPRO-001 (NSC635448), NSC319725, NSC319726, UCIPRO-002 (NSC335792), and UCIPRO-003 (NSC335793). Crystal structure of UCIPRO-001 (right) with nitrogen-nitrogen-sulfur tridentate coordination of copper ion and solvent DMSO molecule. Note the difference in terminal methylation at N4 of UCIPRO-001 compared to chemical representation.

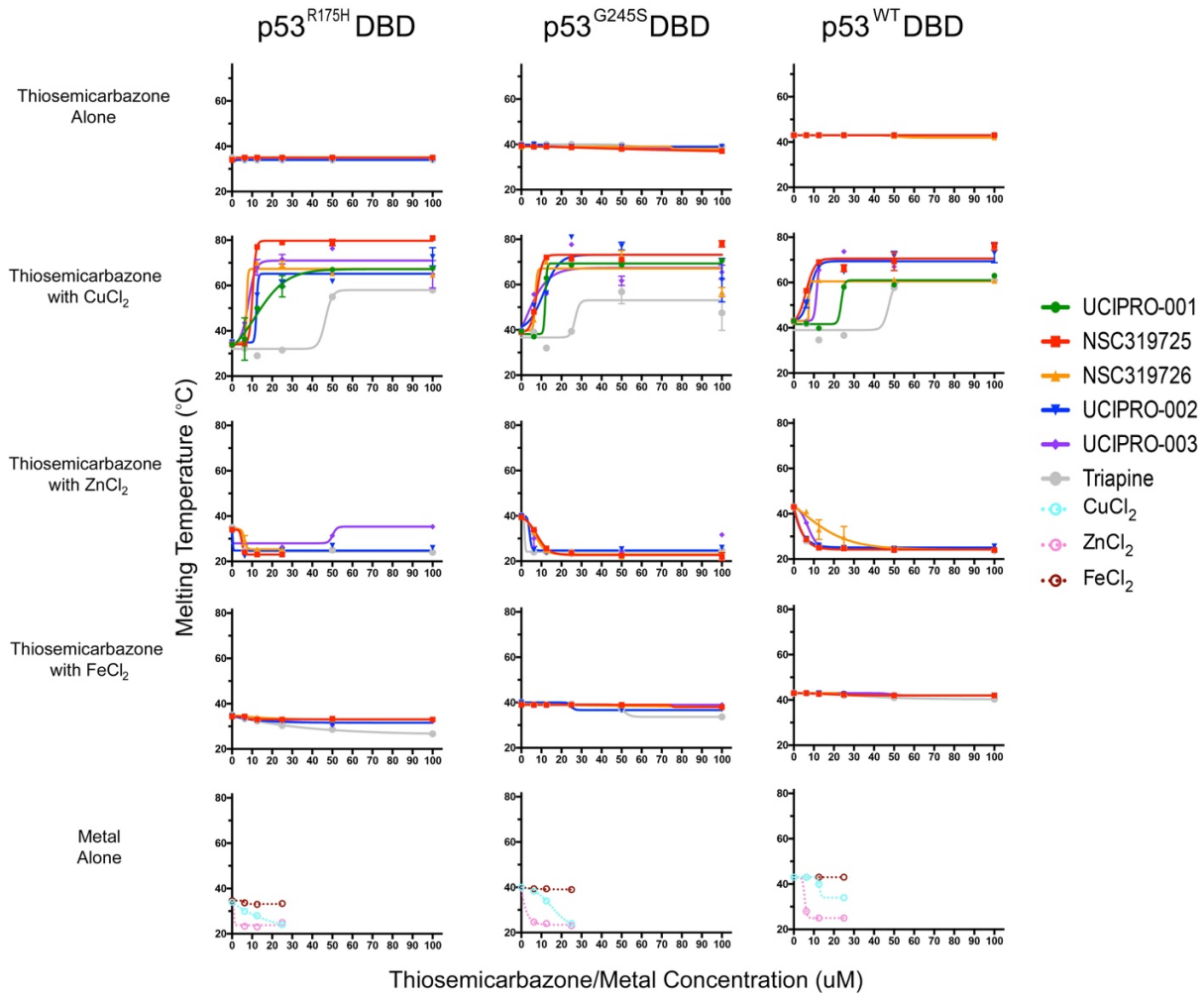

Figure 4.4. Copper thiosemicarbazones increase the thermal stability of p53. Dose-dependent effects of thiosemicarbazones, relevant metal ions, and thiosemicarbazones with metal ions on the T_m of R175H DBD, G245S DBD, and WT DBD (all 5 μM) using TSA. Compounds were tested at 6.25 μM, 12.5 μM, 25 μM, 50 μM, and 100 μM concentrations (1.25:1, 2.5:1, 5:1, 10:1, and 20:1 compound:protein ratios). Data points are plotted as the mean of triplicate measurements with corresponding standard deviation bars. T_m could not be measured for p53 variants with metal concentrations at 50 μM and above due to the unfolding of these proteins before the experiment began.

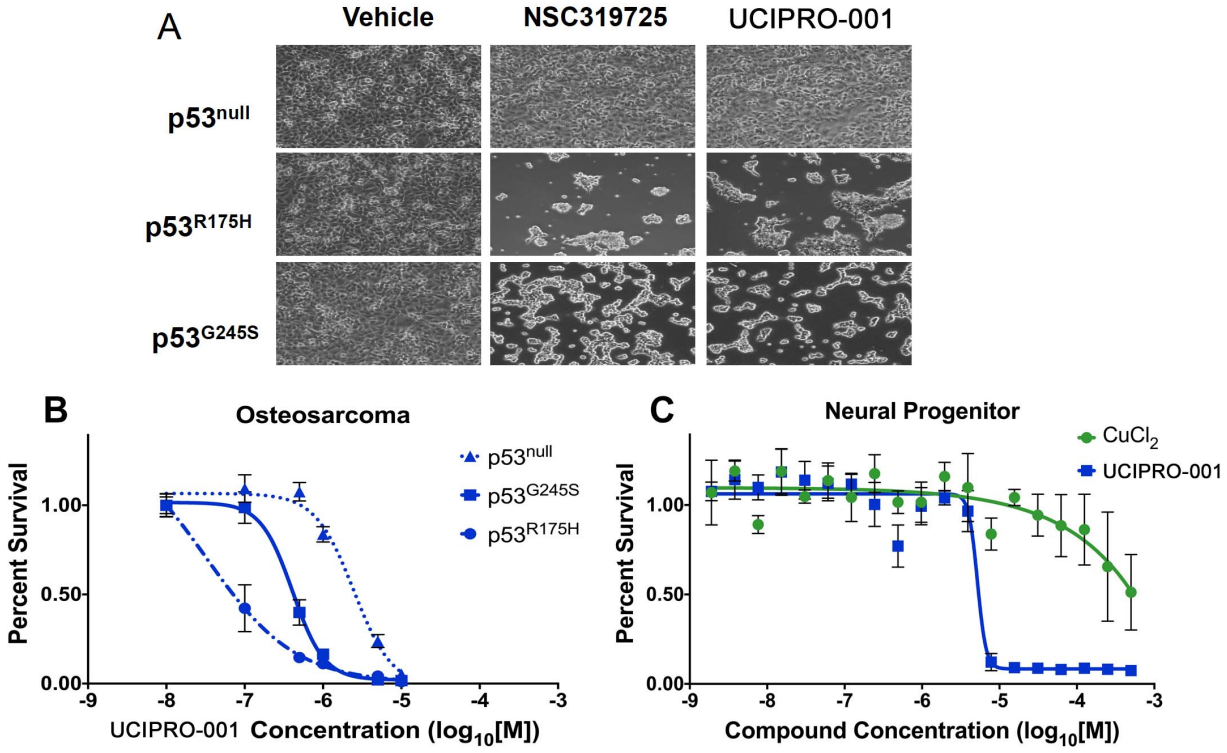

Figure 4.5. Thiosemicarbazones induce p53-dependent cell death of cancer cells. (A) Photographs of $p53^{null}$, $p53^{R175H}$, and $p53^{G245S}$ engineered Saos-2 osteosarcoma cells 72 hours after administration of vehicle, NSC319725, or NSC635448 (1 μM). (B) Dose-dependent effects of NSC635448 on $p53^{null}$, $p53^{R175H}$, and $p53^{G245S}$ engineered Saos-2 osteosarcoma cells. Cell viability was assayed (CellTiter-Glo) 72 hours after administration of NSC635448 and normalized to cell viability of vehicle-added cultures (n=4 for each dosage). (C) Dose-dependent effects of NSC635448 on healthy ($p53^{WT}$) neural progenitor cells. $CuCl_2$ control was used to determine that cytotoxicity was due copper thiosemicarbazone and not copper itself. Cell viability was assayed (CellTiter-Glo) 72 hours after administration of NSC635448 and normalized to cell viability of vehicle-added cultures (n=3 for each dosage).

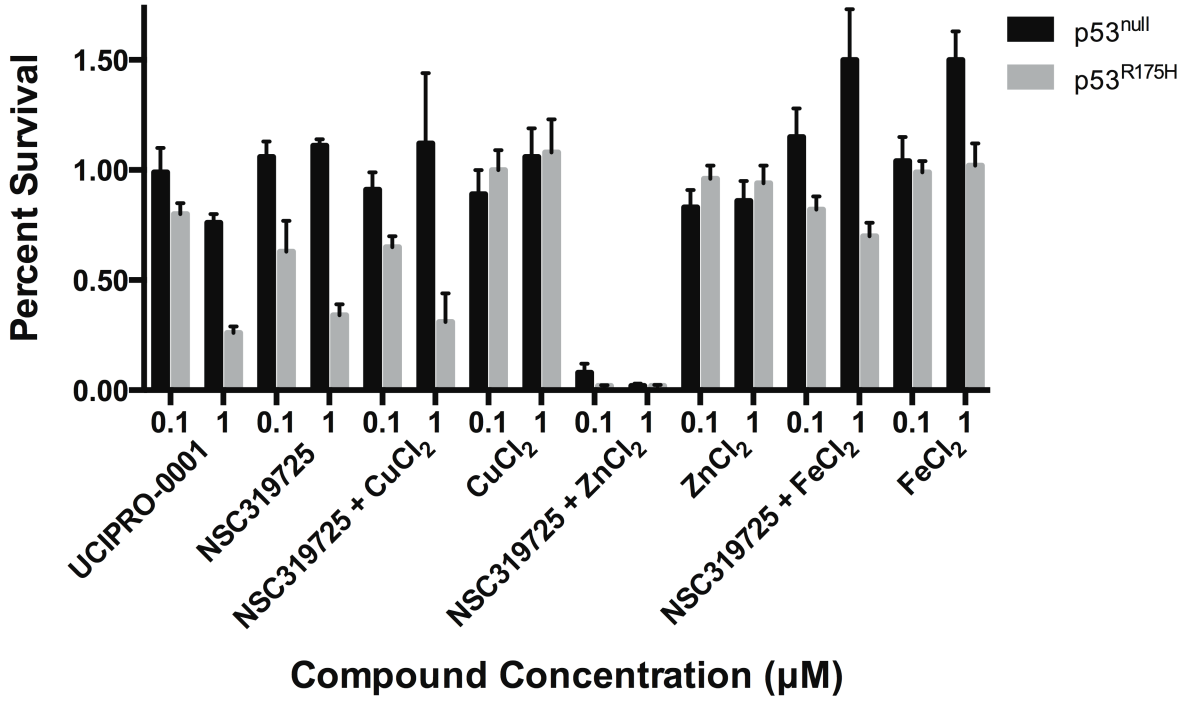

Figure 4.6. Effects of metals on thiosemicarbazone-induced cell death of cancer cells. Effects of thiosemicarbazones, relevant metal ions, and thiosemicarbazones with metal ions on proliferation of $p53^{null}$ and $p53^{R175H}$ osteosarcoma cells. Saos-2 cells ($p53^{null}$) and Saos-2 cells stably harboring $p53^{R175H}$ were treated with doxycycline for 8 h to induce expression of $p53^{R175H}$. Cells were then grown for 48 h in the presence of the different compounds at the concentrations indicated. Cell viability was measured using CellTiter-Glo® reagent.

CHAPTER 5: CONCLUSIONS AND FUTURE WORK

In my thesis work, I have been able to work with a number of research collaborators, with the overall goal of understanding *the molecular basis for restoring function to oncogenic p53 mutants*. I began by helping resolve the X-ray crystal structures of oncogenic and second-site suppressor mutations in p53DBD. Along with thermodynamic stability and DNA-binding properties of these p53DBD determined by our collaborators in the Dr. Senear laboratory, I was able to identify the mechanism by which these second-site suppressor mutations enhance the thermodynamic stability of mutant p53DBD. The hope going into the work was that understanding the structure and mechanism of these second-site suppressor mutations would reveal a method for us or others to design a small molecule to mimic this suppressor mutation. These small molecules can potentially be developed into a targeted therapeutic for clinical use. Unfortunately, these second site suppressor mutations, N235K and N239Y, occur at the solvent surface of the protein with no adjacent concavities in the protein to which a small molecule could bind and recapitulate their effects.

Our collaboration with the Dr. Lathrop, Dr. Amaro, and Dr. Kaiser laboratories realized the need to identify a cavity within the p53DBD, to which a small molecule could bind and potentially stabilize the protein. This identification of the L1/S3 binding pocket within the p53DBD, though occluded within the static crystal structures of p53DBD, held promise for a small molecule to bind and stabilize the protein. The L1/S3 region shows breathing motions, based on molecular dynamic simulations, exposing a shallow pocket containing several cysteine residues that have been implicated as the binding site for potential p53

reactivators identified by other researchers[30,90,131]. *In silico* screening of small molecules using this opened L1/S3 pocket identified several molecules which may be able to bind within it. One of these molecules, stictic acid, is able to stabilize mutant p53DBD *in vitro* and increase the expression of p21 in osteosarcoma cells expressing mutant p53. Unfortunately, stictic acid had little effect on inducing cell cycle arrest or apoptosis in these mutant p53 osteosarcoma cells. This is likely due to the fact that the 2 °C to 4 °C increase in mutant p53DBD stability, from 28 °C to 32 °C for $p53^{R175H}$DBD, observed *in vitro* is not sufficient for mutant p53 to regain substantial function within the cancer cell. Because stictic acid did not demonstrate any apoptotic potential in these mutant p53 osteosarcoma cells, our collaboration decided not to pursue it for further development as a mutant p53 reactivator.

After working on *the molecular basis for restoring function to oncogenic p53 mutants* alongside many of our collaborators for about a year, I started to realize that many of the methods that researchers, including ourselves, had used to search for small molecule reactivators of p53 were flawed. A large majority of research groups that identified small molecules which could potentially restore function to mutant p53 believed that the molecule they had discovered was restoring mutant p53 function by thermodynamically stabilizing the mutant p53 protein[17,23-28,54,82]. However, not one of these research groups used a screening assay which directly measured mutant p53 protein stability. They used fairly indirect measurements of p53 function restoration including measurement of cell death in cancer cells harboring mutant p53, increased DNA binding affinity of mutant p53, or simulated binding of the molecule to p53 *in silico*. I realized that the best screening technique for discovering small molecules able to restore stability to mutant p53 would be

one that directly assesses whether a small molecule can stabilize purified mutant p53 protein *in vitro*. With this idea in mind, we screened the approximately 2,700 compounds available through the NCI/DTP chemical screening library for their capacity to thermodynamically stabilize $p53^{R175H}$DBD. Interestingly, the *virtual* NCI/DTP chemical screening library used by members of the Dr. Lathrop and Dr. Amaro laboratories to screen for molecules which could bind to the L1/S3 pocket *in silico* contains the same molecules as the chemical NCI/DTP library that we screened with our thermal shift assay. This demonstrates the effectiveness of biochemical-based screens for discovering small molecules with certain properties compared to computational screens. Although computation screens are convenient, being able to be performed at little cost in a short amount of time, they don't seem to replicate real world chemistry well enough to be implemented for chemical screening in a large number of applications. The biochemical screen, particularly those in which the desired effect of the compound is directly measured in the assay, are of considerable usefulness in identifying compounds with novel purposes. UCIPRO-001, the molecule we discovered through this screening assay, shows very promising results in its ability to stabilize mutant p53 *in vitro* and induce cellular death of cancer cells expressing mutant p53.

Based on these promising results, we have recruited several new research collaborators to join us in the preclinical studying of the UCIPRO class and its ability to restore function to mutant p53. The laboratory of Dr. C. Vanderwal (Department of Chemistry, University of California, Irvine) is currently synthesizing analogs of UCIPRO-001. These copper thiosemicarbazone analogs will be evaluated for their capacity to stabilize $p53^{R175H}$DBD using our TSA. Our lab is currently working to determie the site on

the p53DBD to which copper thiosemicarbazones bind. Knowing the molecular interactions between copper thiosemicarbazones and p53DBD is important for two reasons. (1) It helps confirm that copper thiosemicarbazones bind directly to p53DBD. (2) It allows us and our collaborators to rationally design future generations of copper thiosemicarbazones, optimizing the interactions between the copper thiosemicarbazone and p53DBD. I am using a combination of structural biology (X-ray crystallography) and mutational analysis to pinpoint the binding site. Our lab is also working out the extent to which mutant p53DBD regains its DNA-binding and protein binding activity at near physiological temperature upon the binding of copper thiosemicarbazones *in vitro*. Dr. M. A. Digman (Department of Biomedical Engineering, University of California, Irvine) and her laboratory are examining the DNA-binding properties of mutant p53 upon addition of copper thiosemicarbazones in cell culture. To do so, mutant p53 is tagged with the fluorescent eGFP protein, allowing the movement, location, concentration, and oligomerization of p53 to be tracked, with tetramerization of mutant p53 indicating that the protein is functionally bound to DNA[51].

It will also be crucial to understand which of the vast number of oncogenic p53 mutations can be reactivated with copper thiosemicarbazones. Here, I show functional restoration of the two most common conformational *p53* mutations, $p53^{R175H}$ and $p53^{G245S}$, by copper thiosemicarbazones. Yu *et al.* have demonstrated the efficacy of thiosemicarbazones toward cancer cells harboring the conformational mutations $p53^{R175H}$, $p53^{C242S}$, $p53^{C242F}$, $p53^{C176F}$, $p53^{G245S}$, $p53^{C238S}$ [54,129]. They determined that these thiosemicarbazones were less efficacious against cancer cells harboring DNA-contact mutations $p53^{R248W}$ and $p53^{R273H}$, and showed very little efficacy towards the cancer cells

containing the conformational mutation $p53^{R249M}$ [54,129]. To this end, we have partnered with Dr. R. D. Damoiseaux (Molecular Shared Screening Facility, University of California, Los Angeles), to test the efficacy of several copper thiosemicarbazones on cancer cells with a variety of *p53* mutations. To understand the efficacy of thiosemicarbazones *in vivo*, the laboratory of Dr. A. Boiko (Department of Molecular Biology and Biochemistry, University of California, Irvine) will be evaluating the efficacy of copper thiosemicarbazones as a monotherapy in the clearing of mutant p53 xenograft tumors (human cancer-derived tumor) in mice. Although many questions remain, our work here demonstrates the potential for developing copper thiosemicarbazones into a therapeutic that can restore the function of mutant p53 in the vast number of patients with cancers harboring these mutations.

REFERENCES

1. Petitjean, A. et al. Impact of mutant p53 functional properties on TP53 mutation patterns and tumor phenotype: lessons from recent developments in the IARC TP53 database. *Hum Mutat* **28**, 622-9 (2007).
2. Levine, A.J. p53, the cellular gatekeeper for growth and division. *Cell* **88**, 323-31 (1997).
3. Cerami, E. et al. The cBio cancer genomics portal: an open platform for exploring multidimensional cancer genomics data. *Cancer Discov* **2**, 401-4 (2012).
4. Gao, J. et al. Integrative analysis of complex cancer genomics and clinical profiles using the cBioPortal. *Sci Signal* **6**, pl1 (2013).
5. Kandoth, C. et al. Mutational landscape and significance across 12 major cancer types. *Nature* **502**, 333-9 (2013).
6. Levine, A.J. & Oren, M. The first 30 years of p53: growing ever more complex. *Nat Rev Cancer* **9**, 749-58 (2009).
7. Kruse, J.P. & Gu, W. Modes of p53 regulation. *Cell* **137**, 609-22 (2009).
8. Green, D.R. & Kroemer, G. Cytoplasmic functions of the tumour suppressor p53. *Nature* **458**, 1127-30 (2009).
9. Lowe, S.W., Ruley, H.E., Jacks, T. & Housman, D.E. p53-dependent apoptosis modulates the cytotoxicity of anticancer agents. *Cell* **74**, 957-67 (1993).
10. Fan, S. et al. p53 gene mutations are associated with decreased sensitivity of human lymphoma cells to DNA damaging agents. *Cancer Res* **54**, 5824-30 (1994).
11. Soussi, T., Legros, Y., Lubin, R., Ory, K. & Schlichtholz, B. Multifactorial analysis of p53 alteration in human cancer: a review. *Int J Cancer* **57**, 1-9 (1994).
12. Cho, Y., Gorina, S., Jeffrey, P.D. & Pavletich, N.P. Crystal structure of a p53 tumor suppressor-DNA complex: understanding tumorigenic mutations. *Science* **265**, 346-55 (1994).
13. Pietsch, E.C. et al. Oligomerization of BAK by p53 utilizes conserved residues of the p53 DNA binding domain. *J Biol Chem* **283**, 21294-304 (2008).
14. Petros, A.M., Gunasekera, A., Xu, N., Olejniczak, E.T. & Fesik, S.W. Defining the p53 DNA-binding domain/Bcl-x(L)-binding interface using NMR. *FEBS Lett* **559**, 171-4 (2004).
15. Bullock, A.N. et al. Thermodynamic stability of wild-type and mutant p53 core domain. *Proc Natl Acad Sci U S A* **94**, 14338-42 (1997).
16. Ang, H.C., Joerger, A.C., Mayer, S. & Fersht, A.R. Effects of common cancer mutations on stability and DNA binding of full-length p53 compared with isolated core domains. *J Biol Chem* **281**, 21934-41 (2006).
17. Wassman, C.D. et al. Computational identification of a transiently open L1/S3 pocket for reactivation of mutant p53. *Nat Commun* **4**, 1407 (2013).
18. Ventura, A. et al. Restoration of p53 function leads to tumour regression in vivo. *Nature* **445**, 661-5 (2007).
19. Martins, C.P., Brown-Swigart, L. & Evan, G.I. Modeling the therapeutic efficacy of p53 restoration in tumors. *Cell* **127**, 1323-34 (2006).
20. Fujiwara, T. et al. Induction of chemosensitivity in human lung cancer cells in vivo by adenovirus-mediated transfer of the wild-type p53 gene. *Cancer Res* **54**, 2287-91 (1994).
21. Spitz, F.R. et al. Adenoviral-mediated wild-type p53 gene expression sensitizes colorectal cancer cells to ionizing radiation. *Clin Cancer Res* **2**, 1665-71 (1996).
22. Yang, B., Eshleman, J.R., Berger, N.A. & Markowitz, S.D. Wild-type p53 protein potentiates cytotoxicity of therapeutic agents in human colon cancer cells. *Clin Cancer Res* **2**, 1649-57 (1996).
23. Foster, B.A., Coffey, H.A., Morin, M.J. & Rastinejad, F. Pharmacological rescue of mutant p53 conformation and function. *Science* **286**, 2507-10 (1999).
24. Bykov, V.J. et al. Restoration of the tumor suppressor function to mutant p53 by a low-molecular-weight compound. *Nat Med* **8**, 282-8 (2002).
25. Bykov, V.J. et al. Reactivation of mutant p53 and induction of apoptosis in human tumor cells by maleimide analogs. *J Biol Chem* **280**, 30384-91 (2005).
26. Zache, N. et al. Mutant p53 targeting by the low molecular weight compound STIMA-1. *Mol Oncol* **2**, 70-80 (2008).
27. Demma, M. et al. SCH529074, a small molecule activator of mutant p53, which binds p53 DNA binding domain (DBD), restores growth-suppressive function to mutant p53 and interrupts HDM2-mediated ubiquitination of wild type p53. *J Biol Chem* **285**, 10198-212 (2010).

28. Metri, P.K., Naz, S., Kondaiah, P. & Prasad, K.R. MPK-09, a Small Molecule Inspired from Bioactive Styryllactone Restores the Wild-Type Function of Mutant p53. *ACS Chem Biol* (2013).
29. Rippin, T.M. et al. Characterization of the p53-rescue drug CP-31398 in vitro and in living cells. *Oncogene* **21**, 2119-29 (2002).
30. Lambert, J.M. et al. PRIMA-1 reactivates mutant p53 by covalent binding to the core domain. *Cancer Cell* **15**, 376-88 (2009).
31. Lehmann, S. et al. Targeting p53 in vivo: a first-in-human study with p53-targeting compound APR-246 in refractory hematologic malignancies and prostate cancer. *J Clin Oncol* **30**, 3633-9 (2012).
32. Yu, X., Narayanan, S., Vazquez, A. & Carpizo, D.R. Small molecule compounds targeting the p53 pathway: are we finally making progress? *Apoptosis* **19**, 1055-68 (2014).
33. Barretina, J. et al. The Cancer Cell Line Encyclopedia enables predictive modelling of anticancer drug sensitivity. *Nature* **483**, 603-7 (2012).
34. Reinhold, W.C. et al. CellMiner: a web-based suite of genomic and pharmacologic tools to explore transcript and drug patterns in the NCI-60 cell line set. *Cancer Res* **72**, 3499-511 (2012).
35. Brachmann, R.K., Yu, K., Eby, Y., Pavletich, N.P. & Boeke, J.D. Genetic selection of intragenic suppressor mutations that reverse the effect of common p53 cancer mutations. *Embo J* **17**, 1847-59 (1998).
36. Wieczorek, A.M., Waterman, J.L., Waterman, M.J. & Halazonetis, T.D. Structure-based rescue of common tumor-derived p53 mutants. *Nat Med* **2**, 1143-6 (1996).
37. Joerger, A.C., Ang, H.C., Veprintsev, D.B., Blair, C.M. & Fersht, A.R. Structures of p53 cancer mutants and mechanism of rescue by second-site suppressor mutations. *J Biol Chem* **280**, 16030-7 (2005).
38. Baroni, T.E. et al. A global suppressor motif for p53 cancer mutants. *Proc Natl Acad Sci U S A* **101**, 4930-5 (2004).
39. Brachmann, R.K. p53 mutants: the achilles' heel of human cancers? *Cell Cycle* **3**, 1030-4 (2004).
40. Wang, W., Rastinejad, F. & El-Deiry, W.S. Restoring p53-dependent tumor suppression. *Cancer Biol Ther* **2**, S55-63 (2003).
41. Nikolova, P.V., Henckel, J., Lane, D.P. & Fersht, A.R. Semirational design of active tumor suppressor p53 DNA binding domain with enhanced stability. *Proc Natl Acad Sci U S A* **95**, 14675-80 (1998).
42. Joerger, A.C., Allen, M.D. & Fersht, A.R. Crystal structure of a superstable mutant of human p53 core domain. Insights into the mechanism of rescuing oncogenic mutations. *J Biol Chem* **279**, 1291-6 (2004).
43. Wang, Y., Rosengarth, A. & Luecke, H. Structure of the human p53 core domain in the absence of DNA. *Acta Crystallogr D Biol Crystallogr* **63**, 276-81 (2007).
44. Danziger, S.A., Zeng, J., Wang, Y., Brachmann, R.K. & Lathrop, R.H. Choosing where to look next in a mutation sequence space: Active Learning of informative p53 cancer rescue mutants. *Bioinformatics* **23**, i104-i114 (2007).
45. Bullock, A.N., Henckel, J. & Fersht, A.R. Quantitative analysis of residual folding and DNA binding in mutant p53 core domain: definition of mutant states for rescue in cancer therapy. *Oncogene* **19**, 1245-56 (2000).
46. Nikolova, P.V., Wong, K.B., DeDecker, B., Henckel, J. & Fersht, A.R. Mechanism of rescue of common p53 cancer mutations by second-site suppressor mutations. *Embo J* **19**, 370-8 (2000).
47. McLure, K.G. & Lee, P.W. How p53 binds DNA as a tetramer. *Embo J* **17**, 3342-50 (1998).
48. Melero, R. et al. Electron microscopy studies on the quaternary structure of p53 reveal different binding modes for p53 tetramers in complex with DNA. *Proc Natl Acad Sci U S A* **108**, 557-62 (2011).
49. Aramayo, R. et al. Quaternary structure of the specific p53-DNA complex reveals the mechanism of p53 mutant dominance. *Nucleic Acids Res* **39**, 8960-71 (2011).
50. Rippin, T.M., Freund, S.M., Veprintsev, D.B. & Fersht, A.R. Recognition of DNA by p53 core domain and location of intermolecular contacts of cooperative binding. *J Mol Biol* **319**, 351-8 (2002).
51. Weinberg, R.L., Veprintsev, D.B. & Fersht, A.R. Cooperative binding of tetrameric p53 to DNA. *J Mol Biol* **341**, 1145-59 (2004).
52. Suad, O. et al. Structural basis of restoring sequence-specific DNA binding and transactivation to mutant p53 by suppressor mutations. *J Mol Biol* **385**, 249-65 (2009).
53. Joerger, A.C., Ang, H.C. & Fersht, A.R. Structural basis for understanding oncogenic p53 mutations and designing rescue drugs. *Proc Natl Acad Sci U S A* **103**, 15056-61 (2006).
54. Yu, X., Vazquez, A., Levine, A.J. & Carpizo, D.R. Allele-specific p53 mutant reactivation. *Cancer Cell* **21**, 614-25 (2012).
55. Pflugrath, J.W. The finer things in X-ray diffraction data collection. *Acta Crystallogr D Biol Crystallogr* **55**, 1718-25 (1999).

56. Brunger, A.T. et al. Crystallography & NMR system: A new software suite for macromolecular structure determination. *Acta Crystallogr D Biol Crystallogr* **54**, 905-21 (1998).
57. Storoni, L.C., McCoy, A.J. & Read, R.J. Likelihood-enhanced fast rotation functions. *Acta Crystallogr D Biol Crystallogr* **60**, 432-8 (2004).
58. Jones, T.A., Zou, J.Y., Cowan, S.W. & Kjeldgaard. Improved methods for building protein models in electron density maps and the location of errors in these models. *Acta Crystallogr A* **47 (Pt 2)**, 110-9 (1991).
59. Emsley, P. & Cowtan, K. Coot: model-building tools for molecular graphics. *Acta Crystallogr D Biol Crystallogr* **60**, 2126-32 (2004).
60. Evans, P. Scaling and assessment of data quality. *Acta Crystallogr D Biol Crystallogr* **62**, 72-82 (2006).
61. Adams, P.D. et al. PHENIX: a comprehensive Python-based system for macromolecular structure solution. *Acta Crystallogr D Biol Crystallogr* **66**, 213-21 (2010).
62. Afonine, P.V. et al. Towards automated crystallographic structure refinement with phenix.refine. *Acta Crystallogr D Biol Crystallogr* **68**, 352-67 (2012).
63. Laskowski, R.A., Rullmannn, J.A., MacArthur, M.W., Kaptein, R. & Thornton, J.M. AQUA and PROCHECK-NMR: programs for checking the quality of protein structures solved by NMR. *J Biomol NMR* **8**, 477-86 (1996).
64. Chen, V.B. et al. MolProbity: all-atom structure validation for macromolecular crystallography. *Acta Crystallogr D Biol Crystallogr* **66**, 12-21 (2010).
65. Krissinel, E. & Henrick, K. Secondary-structure matching (SSM), a new tool for fast protein structure alignment in three dimensions. *Acta Crystallogr D Biol Crystallogr* **60**, 2256-68 (2004).
66. Pace, C.N. Determination and analysis of urea and guanidine hydrochloride denaturation curves. *Methods Enzymol* **131**, 266-80 (1986).
67. Tretyachenko-Ladokhina, V., Cocco, M.J. & Senear, D.F. Flexibility and adaptability in binding of E. coli cytidine repressor to different operators suggests a role in differential gene regulation. *J Mol Biol* **362**, 271-86 (2006).
68. Senear, D.F. & Brenowitz, M. Determination of binding constants for cooperative site-specific protein-DNA interactions using the gel mobility-shift assay. *J Biol Chem* **266**, 13661-71 (1991).
69. Olivier, M. et al. The IARC TP53 database: new online mutation analysis and recommendations to users. *Hum Mutat* **19**, 607-14 (2002).
70. Soussi, T. & Beroud, C. Assessing TP53 status in human tumours to evaluate clinical outcome. *Nat Rev Cancer* **1**, 233-40 (2001).
71. Joerger, A.C. & Fersht, A.R. The tumor suppressor p53: from structures to drug discovery. *Cold Spring Harb Perspect Biol* **2**, a000919 (2010).
72. Selivanova, G. & Wiman, K.G. Reactivation of mutant p53: molecular mechanisms and therapeutic potential. *Oncogene* **26**, 2243-54 (2007).
73. Sharpless, N.E. & DePinho, R.A. Cancer biology: gone but not forgotten. *Nature* **445**, 606-7 (2007).
74. Wiman, K.G. Restoration of wild-type p53 function in human tumors: strategies for efficient cancer therapy. *Adv Cancer Res* **97**, 321-38 (2007).
75. Xue, W. et al. Senescence and tumour clearance is triggered by p53 restoration in murine liver carcinomas. *Nature* **445**, 656-60 (2007).
76. Baronio, R. et al. All-codon scanning identifies p53 cancer rescue mutations. *Nucleic Acids Res* **38**, 7079-88 (2010).
77. Danziger, S.A. et al. Predicting positive p53 cancer rescue regions using Most Informative Positive (MIP) active learning. *PLoS Comput Biol* **5**, e1000498 (2009).
78. Danziger, S.A. et al. Functional census of mutation sequence spaces: the example of p53 cancer rescue mutants. *IEEE/ACM Trans Comput Biol Bioinform* **3**, 114-25 (2006).
79. Bykov, V.J., Issaeva, N., Selivanova, G. & Wiman, K.G. Mutant p53-dependent growth suppression distinguishes PRIMA-1 from known anticancer drugs: a statistical analysis of information in the National Cancer Institute database. *Carcinogenesis* **23**, 2011-8 (2002).
80. North, S., Pluquet, O., Maurici, D., El-Ghissassi, F. & Hainaut, P. Restoration of wild-type conformation and activity of a temperature-sensitive mutant of p53 (p53(V272M)) by the cytoprotective aminothiol WR1065 in the esophageal cancer cell line TE-1. *Mol Carcinog* **33**, 181-8 (2002).
81. Reddy, N.L., Hill, J., Ye, L., Fernandes, P.B. & Stout, D.M. Identification and structure-activity relationship studies of 3-methylene-2-norbornanone as potent anti-proliferative agents presumably working through p53 mediated apoptosis. *Bioorg Med Chem Lett* **14**, 5645-9 (2004).

82. Boeckler, F.M. et al. Targeted rescue of a destabilized mutant of p53 by an in silico screened drug. *Proc Natl Acad Sci U S A* **105**, 10360-5 (2008).
83. Wilcken, R. et al. Halogen-Enriched Fragment Libraries as Leads for Drug Rescue of Mutant p53. *J Am Chem Soc* **134**, 6810-8 (2012).
84. Yu, X., Vazquez, A., Levine, A.J. & Carpizo, D.R. Allele-Specific p53 Mutant Reactivation. *Cancer Cell* **21**, 614-625 (2012).
85. Wiman, K.G. Pharmacological reactivation of mutant p53: from protein structure to the cancer patient. *Oncogene* **29**, 4245-52 (2010).
86. Amaro, R.E., Baron, R. & McCammon, J.A. An improved relaxed complex scheme for receptor flexibility in computer-aided drug design. *J Comput Aided Mol Des* **22**, 693-705 (2008).
87. Cheng, L.S. et al. Ensemble-based virtual screening reveals potential novel antiviral compounds for avian influenza neuraminidase. *J Med Chem* **51**, 3878-94 (2008).
88. Malecka, K.A., Ho, W.C. & Marmorstein, R. Crystal structure of a p53 core tetramer bound to DNA. *Oncogene* **28**, 325-33 (2009).
89. Friedler, A. et al. A peptide that binds and stabilizes p53 core domain: chaperone strategy for rescue of oncogenic mutants. *Proc Natl Acad Sci U S A* **99**, 937-42 (2002).
90. Kaar, J.L. et al. Stabilization of mutant p53 via alkylation of cysteines and effects on DNA binding. *Protein Sci* **19**, 2267-78 (2010).
91. Emamzadah, S., Tropia, L. & Halazonetis, T.D. Crystal structure of a multidomain human p53 tetramer bound to the natural CDKN1A (p21) p53-response element. *Mol Cancer Res* **9**, 1493-9 (2011).
92. Petty, T.J. et al. An induced fit mechanism regulates p53 DNA binding kinetics to confer sequence specificity. *EMBO J* **30**, 2167-76 (2011).
93. Canadillas, J.M. et al. Solution structure of p53 core domain: structural basis for its instability. *Proc Natl Acad Sci U S A* **103**, 2109-14 (2006).
94. Velu, C.S., Niture, S.K., Doneanu, C.E., Pattabiraman, N. & Srivenugopal, K.S. Human p53 is inhibited by glutathionylation of cysteines present in the proximal DNA-binding domain during oxidative stress. *Biochemistry* **46**, 7765-80 (2007).
95. Natan, E. et al. Interaction of the p53 DNA-binding domain with its n-terminal extension modulates the stability of the p53 tetramer. *J Mol Biol* **409**, 358-68 (2011).
96. Demir, O. et al. Ensemble-based computational approach discriminates functional activity of p53 cancer and rescue mutants. *PLoS Comput Biol* **7**, e1002238 (2011).
97. Le Guilloux, V., Schmidtke, P. & Tuffery, P. Fpocket: an open source platform for ligand pocket detection. *BMC Bioinformatics* **10**, 168 (2009).
98. Brenke, R. et al. Fragment-based identification of druggable 'hot spots' of proteins using Fourier domain correlation techniques. *Bioinformatics* **25**, 621-7 (2009).
99. Goh, A.M. et al. Using targeted transgenic reporter mice to study promoter-specific p53 transcriptional activity. *Proc Natl Acad Sci U S A* **109**, 1685-90 (2012).
100. Vedadi, M. et al. Chemical screening methods to identify ligands that promote protein stability, protein crystallization, and structure determination. *Proc Natl Acad Sci U S A* **103**, 15835-40 (2006).
101. Lo, M.C. et al. Evaluation of fluorescence-based thermal shift assays for hit identification in drug discovery. *Anal Biochem* **332**, 153-9 (2004).
102. Niesen, F.H., Berglund, H. & Vedadi, M. The use of differential scanning fluorimetry to detect ligand interactions that promote protein stability. *Nat Protoc* **2**, 2212-21 (2007).
103. Castrignano, T., De Meo, P.D., Cozzetto, D., Talamo, I.G. & Tramontano, A. The PMDB Protein Model Database. *Nucleic Acids Res* **34**, D306-9 (2006).
104. Case, D.A. et al. AMBER 10. (University of California, San Francisco, 2008).
105. Jorgensen, W.L., Chandrasekhar, J., Madura, J.D., Impey, R.W. & Klein, M.L. Comparison of simple potential functions for simulating liquid water. *J. Chem. Phys.* **79**, 926-935 (1983).
106. Pang, Y.-P. Novel Zinc Protein Molecular Dynamics Simulations: Steps Toward Antiangiogenesis for Cancer Treatment. *J. Mol. Model.* **5**, 196-202 (1999).
107. Rodriguez, R., Chinea, G., Lopez, N., Pons, T. & Vriend, G. Homology modeling, model and software evaluation: three related resources. *Bioinformatics* **14**, 523-8 (1998).
108. Hornak, V. et al. Comparison of multiple Amber force fields and development of improved protein backbone parameters. *Proteins* **65**, 712-25 (2006).
109. Phillips, J.C. et al. Scalable molecular dynamics with NAMD. *J Comput Chem* **26**, 1781-802 (2005).

110. Wang, J., Wang, W., Kollman, P.A. & Case, D.A. Automatic atom type and bond type perception in molecular mechanical calculations. *J Mol Graph Model* **25**, 247-60 (2006).
111. Wang, J., Wolf, R.M., Caldwell, J.W., Kollman, P.A. & Case, D.A. Development and testing of a general amber force field. *J Comput Chem* **25**, 1157-74 (2004).
112. Humphrey, W., Dalke, A. & Schulten, K. VMD: visual molecular dynamics. *J Mol Graph* **14**, 33-8, 27-8 (1996).
113. Baron, R. & McCammon, J.A. Dynamics, hydration, and motional averaging of a loop-gated artificial protein cavity: the W191G mutant of cytochrome c peroxidase in water as revealed by molecular dynamics simulations. *Biochemistry* **46**, 10629-42 (2007).
114. Daura, X. et al. Peptide Folding: When Simulation Meets Experiment. *Angewandte Chemie International Edition* **38**, 236–240 (1999).
115. Hess, B., Kutzner, C., Spoel, D.v.d. & Lindahl, E. GROMACS 4: Algorithms for Highly Efficient, Load-Balanced, and Scalable Molecular Simulation. *J. Chem. Theory Comput.* **4**, 435–447 (2008).
116. Trott, O. & Olson, A.J. AutoDock Vina: improving the speed and accuracy of docking with a new scoring function, efficient optimization, and multithreading. *J Comput Chem* **31**, 455-61 (2010).
117. Stegmeier, F., Hu, G., Rickles, R.J., Hannon, G.J. & Elledge, S.J. A lentiviral microRNA-based system for single-copy polymerase II-regulated RNA interference in mammalian cells. *Proc Natl Acad Sci U S A* **102**, 13212-7 (2005).
118. Gill, S.C. & von Hippel, P.H. Calculation of protein extinction coefficients from amino acid sequence data. *Anal Biochem* **182**, 319-26 (1989).
119. Martins, C.P., Brown-Swigart, L. & Evan, G.I. Modeling the Therapeutic Efficacy of p53 Restoration in Tumors. *Cell* **127**, 1323-1334 (2006).
120. Bykov, V.J. et al. PRIMA-1(MET) synergizes with cisplatin to induce tumor cell apoptosis. *Oncogene* **24**, 3484-91 (2005).
121. Palecek, E., Ostatna, V., Cernocka, H., Joerger, A.C. & Fersht, A.R. Electrocatalytic monitoring of metal binding and mutation-induced conformational changes in p53 at picomole level. *J Am Chem Soc* **133**, 7190-6 (2011).
122. Brockman, R.W., Thomson, J.R., Bell, M.J. & Skipper, H.E. Observations on the antileukemic activity of pyridine-2-carboxaldehyde thiosemicarbazone and thiocarbohydrazone. *Cancer Res* **16**, 167-70 (1956).
123. Yu, Y. et al. Thiosemicarbazones from the old to new: iron chelators that are more than just ribonucleotide reductase inhibitors. *J Med Chem* **52**, 5271-94 (2009).
124. Bernhardt, P.V. et al. Iron chelators of the dipyridylketone thiosemicarbazone class: precomplexation and transmetalation effects on anticancer activity. *J Med Chem* **52**, 407-15 (2009).
125. Finch, R.A. et al. Triapine (3-aminopyridine-2-carboxaldehyde- thiosemicarbazone): A potent inhibitor of ribonucleotide reductase activity with broad spectrum antitumor activity. *Biochem Pharmacol* **59**, 983-91 (2000).
126. Shao, J. et al. In vitro characterization of enzymatic properties and inhibition of the p53R2 subunit of human ribonucleotide reductase. *Cancer Res* **64**, 1-6 (2004).
127. Chao, J. et al. A phase I and pharmacokinetic study of oral 3-aminopyridine-2-carboxaldehyde thiosemicarbazone (3-AP, NSC #663249) in the treatment of advanced-stage solid cancers: a California Cancer Consortium Study. *Cancer Chemother Pharmacol* **69**, 835-43 (2012).
128. Kunos, C.A. et al. Radiochemotherapy plus 3-aminopyridine-2-carboxaldehyde thiosemicarbazone (3-AP, NSC #663249) in advanced-stage cervical and vaginal cancers. *Gynecol Oncol* **130**, 75-80 (2013).
129. Yu, X. et al. Small molecule restoration of wildtype structure and function of mutant p53 using a novel zinc-metallochaperone based mechanism. *Oncotarget* **5**, 8879-92 (2014).
130. Lovejoy, D.B. et al. Antitumor activity of metal-chelating compound Dp44mT is mediated by formation of a redox-active copper complex that accumulates in lysosomes. *Cancer Res* **71**, 5871-80 (2011).
131. Scotcher, J. et al. Identification of two reactive cysteine residues in the tumor suppressor protein p53 using top-down FTICR mass spectrometry. *J Am Soc Mass Spectrom* **22**, 888-97 (2011).